A Study of Multiple Asteroid Flyby Mission Design: An Approach Using Optimal Control

by

Bruno Victorino Sarli

In Partial Fulfillment of the Requirements
for the Degree of
Doctor of Engineering

Department of Space and Astronautical Science
School of Physical Sciences
The Graduate University for Advanced Studies
2015

A Study of Multiple Asteroid Flyby Mission Design: An Approach Using Optimal Control

by

Bruno Victorino Sarli

This doctoral thesis has been examined by a Committee of the Department of Space and Astronautical Science as follows:

Dr. Shin-ichiro Sakai	Chairman, Thesis Committee	SOKENDAI & ISAS/JAXA
Dr. Yasuhiro Kawakatsu	Thesis Supervisor	SOKENDAI & ISAS/JAXA
Dr. Makoto Yosikawa	Member, Thesis Committee	SOKENDAI & ISAS/JAXA
Dr. Yuichi Tsuda	Member, Thesis Committee	SOKENDAI & ISAS/JAXA
Dr. Ryu Funase	Member, Thesis Committee	University of Tokyo

SOKENDAI

Acknowledgments

I would like to thank my supervisor, Prof. Dr. Yasuhiro Kawakatsu, for his direction, assistance and guidance. All the recommendations, ideas and suggestions have been invaluable for the development of this work. I also wish to thank Dr. Stefano Campagnola for sharing his experience and opinions during the research.

A special thanks go to Prof. Dr. Ikkoh Funaki for his invaluable support during these three years, Prof. Dr. Hideo Matsuhara who welcomed me in his department of Space and Astronautical Sciences, and Ms. Ruriko Kinoshita for her assistance and kindness. I would also like to thank my committee members, Prof. Dr. Makoto Yosikawa, Prof. Dr. Ryu Funase, Prof. Dr. Shin-ichiro Sakai, Prof. Dr. Yuichi Tsuda for serving as my committee members even at hardship.

I would like to express my gratitude to my colleagues and friends who were always present sharing ideas and experiences.

Most importantly, many thanks to my family for the support they provided me through my entire life. Without their love and encouragement, I would not have finished this thesis.

"The understanding of the origin and evolution of the solar system is one of the major scientific goals of space research. The important data in this respect are the physical and chemical properties of the solar system at the time of its formation. Bodies of the size of the Moon and planets have necessarily undergone substantial evolution in the last 4.5 billion years and these evolutionary processes have altered much of the initial record of their formation. However, smaller bodies-asteroids, comets, and meteorites-probably contain a less altered record of the early history of the solar system."

Homer E. Newell
Associate Administrator National Aeronautics and Space Administration

Abstract

Over the years the missions to asteroids have enhanced our knowledge on many aspects of these bodies. Such a growing interest on them is due to many reasons from purely scientific, such as, understanding the formation mechanisms of our solar system, to more mundane, like planetary protection and mining rare materials. So far asteroid related mission have involved rendezvous, touchdowns and sample returns. However, asteroid flyby missions present unique aspects, such as: cost effectiveness, low fuel usage (e.g. EPOXI and Stardust-NExT missions), and flexible that makes it more effective (e.g. Galileo and Rosetta missions).

This work focuses on the study of multiple asteroid flyby missions developing methods and tools to design deepspace trajectories for these missions based on optimal control. The multiple asteroid flyby trajectory design is challenging in many aspects, but believed to be very relevant and in line with the 2013 Global Exploration Roadmap. In order to achieve the final goal, the research is developed in three large areas of space trajectory, which comprehend the fundamentals of the design used in space missions: trajectory design by ballistic arcs, trajectory design by impulsive maneuvers, and trajectory design by low-thrust maneuvers. In here, the ballistic area is used to identify the problem minimums and as basis for the impulsive area, with and both designing main trajectories that are latter used as reference in the low-thrust area to add a secondary a objective, midcourse flyby, to the mission.

In the first area an asteroid mission of scientific interest is analyzed design main trajectories the allow a broader understanding of the problem and defining the basic concepts to be used later. A B-type Near-Earth Asteroid, (3200) Phaethon, parent body of the Geminid meteor shower, and asteroids (155140) 2005 UD and (225416) 1999 YC, likely fragments originating from Phaethon, collectively known as the Phaethon-Geminid complex. A mission to this group could provide key information on their origins and solve fundamental issues in thermal and dynamical evolution of comet-asteroid transition bodies. This study assesses the feasibility of a multiple flyby mission for Phaethon, 2005 UD and 1999 YC by a small-class mission. The objective is to design a multiple flyby mission based on ballistic transfers combined with gravity assisted maneuvers that fly by some or all members of the Phaethon-Geminid Complex. The results showed periodic launch opportunities to all three asteroids with the best case for Phaethon requiring less than 1 km/s of Earth excess velocity. No direct transfer can be made to 1999 YC with less than 4 km/s. However, with a gravity assist maneuver at Mars, an Earth-Mars-1999 YC transfer requires less than 3 km/s. It is also found that, with a maximum of 3 km/s, there is not a single transfer that connects all asteroids. However, launch windows in the years 2026 and 2027 allow a flyby of Phaethon and later 2005 UD by conducting an Earth gravity assist maneuver.

The second area presents a method of impulsive trajectory optimization based on the well known Primer Vector theory, a gradient based method. Since the gradient allows the optimization in the vicinity of the initial estimation, it is important to take into account the analysis made in the first area so this part can be applied in a region of interest. In this work the Primer Vector theory is modified to accommodate weights in the cost function. This change arises from the need of a fast and accurate

analysis obtained with an indirect method that takes into account the velocity increment used for departure from the planet and, particularly for flyby missions, the disregard of the last rendezvous impulse. A detailed derivation of the weighted cost function and its gradient is presented, followed by a discussion on the values of the weights specifically for flyby and rendezvous missions. To test the optimization method, realistic test cases are selected and their results compared against a trajectory using the solution of the Lambert problem and optimization by a nonlinear programming solver. The proposed method showed a faster design with a lower costs than the other two methods.

The third area is the design of low-thrust trajectories with a midcourse asteroid flyby using as a reference the trajectories designed in areas one and two. Recently, with new trajectory design techniques and use of low-thrust propulsion systems, missions have become more efficient and cheaper with respect to propellant. As a way to increase the mission's value and scientific return, secondary targets close to the main trajectory are often added with a small change in the transfer trajectory. As a result of their large number, importance and facility to perform a flyby, asteroids are commonly used as such targets. Once again the Primer Vector theory is used to define the direction and magnitude of the thrust for a minimum fuel consumption problem. The design of a low-thrust trajectory with a midcourse asteroid flyby is not only challenging for the low-thrust problem solution, but also with respect to the selection of a target and its flyby point. Currently more than 700,000 minor bodies have been identified, which generates a very large number of possible flyby points. This work uses a combination of reachability, reference orbit, and linear theory to select appropriate candidates, drastically reducing the simulation time, to be later included in the main trajectory and optimized.

Contents

List of Figures

List of Tables

Chapter 1
Introduction

The interest in asteroids has largely increased over the years, not only in the scientific community but also in the space agencies. The scientists believe that, asteroids can provide many answers to the formation's mechanisms of our solar system; as asteroids may maintain their original composition for billions of years due to its orbit and history. Moreover, it is also hypothesized that life was originated and came to Earth by these celestial bodies. The space agencies are also interested as some of these bodies are easily reachable, not only by unmanned spacecrafts but in the case of the NEOs, Near-Earth Orbit, manned missions are possible requiring low propellant expenditure. The study of asteroidal missions is also necessary from the planetary protection point of view, as some of those may pose a threat to life on the planet either by a direct impact or a near passage. Finally, the economical exploration of asteroid and the development of technologies for mining it may be of great interest for governments and private companies, due to the fact, that these bodies can be a natural resource of material that are rarely found on the Earth's surface.

So far asteroid related mission have involved rendezvous, touchdowns and sample returns; however, asteroid flyby missions have had little application so far. Nevertheless, flyby missions present some unique aspects, such as:

- A flyby mission is cost effective in contrast with rendezvous missions (NEAR) and sample return missions (Hayabusa). The cost does not only mean saving money but also with respect to the energy. Flyby missions do not orbit the asteroid; therefore, there is no need of extra propellant in order to match the relative velocity.

- A flyby mission is more effective due to its flexibility as proved in the recent results from the missions EPOXI and Stardust-NExT of NASA. Both missions were extended and given a new objective, this was possible because the new mission involved a study performed during a flyby.

- Finally, an asteroid flyby mission is attractive from two aspects: first, as an auxiliary mission to the main mission, like in Galileo and Rosetta, and, second, as a dedicated low-cost multiple asteroids flyby mission.

The research proposed here will focus on one of the mission's main points for its success, the spaceflight dynamics or astrodynamics focusing on the asteroid flyby type of mission. The design of a trajectory to an asteroid is challenging due to large number of candidates, types of propulsion system and amount of fuel available. This research plan comes to directly address and support The Global Exploration Roadmap [ISECG 2013] developed space agencies participating in the International Space Exploration Coordination Group (ISECG) in the Autumn of 2013. On the roadmap it was decided that the future space exploration will focus on small but frequent exploration missions to the solar system. In this context, the asteroid flyby is of paramount importance because, due to its large number and scientific importance, it allows the addition of secondary targets to the mission's main trajectory.

Up to this day there is only a few asteroid dedicated missions; however, past missions, e.g. Galileo and Rosetta, took advantage of the proximity of the main trajectory to an asteroid to add it as a secondary objective. By performing a small change on the original trajectory, an asteroid flyby was obtained increasing the mission's importance and scientific return at the cost of a small propellant addition. Studies have been done in this topic but no systematic or efficient way to design it has been developed. In conclusion, the present situation favors this theme and the development of a systematic and efficient plan to design flyby missions will have a big impact in modeling the future of the deep space exploration.

1.1 Objective

The final goal is to obtain a new method, fast and comprehensive, for finding a trajectory to the main target that flyby one or more secondary targets in the middle of the transfer while minimizing the amount of fuel used. A comprehensive design of a low-thrust multiple flyby mission has many challenging aspects, such as target selection, reference trajectory design, and the low-thrust optimization. In other words, this study presents a method for trajectory design based on optimal control for the case of a mission using low-thrust propulsion system considering midcourse constraints. The objective is to perform the smallest possible change on the main trajectory to allow a flyby on a neighboring asteroid while maintaining the initial and final conditions, required for achieving the main mission objective.

In order to achieve the final goal the research has been developed in steps, with the first two focus on the design and of the main trajectory, identifying the best trajectories to be taken into account for the next step, and the definition of important theories. The final step, using low-thrust, takes the main trajectory as a reference and adds a midcourse flyby to it. Next section presents in more details each steps of the research, from this point on refereed as area, Fig. 1.1 presents the structure of the thesis' objective related to the areas studied.

1.2 Study Areas of Trajectory Design

The main objective is to investigate the space flight dynamics of an asteroid flyby mission, developing methods and theories that can be applied in the design of real missions. These tools and methods focus on the three main types of trajectories: ballistic, impulsive and low-thrust. The natural flow of the research is associated to each type of trajectory, making the three trajectory design areas explored in this study:

- Trajectory design by ballistic arcs;

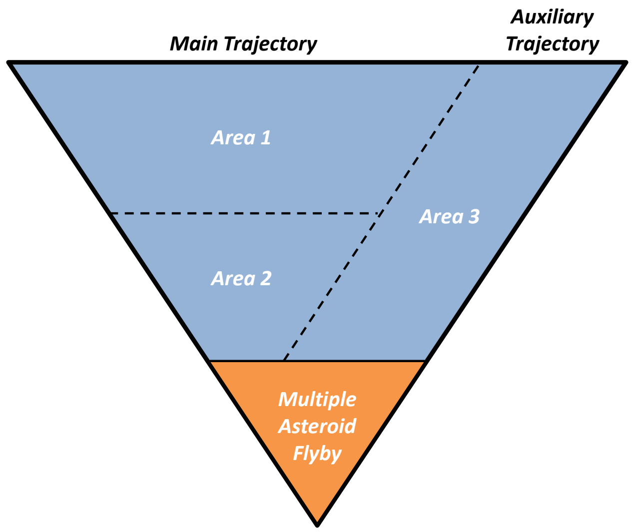

Figure 1.1: Thesis objective structure.

- Trajectory design by impulsive maneuvers; and
- Trajectory design by low-thrust maneuvers.

In the first two areas, theories and methods are developed to design the main mission's trajectory, primary mission target, while the theories and methods developed in area 3 use the main trajectory as a reference to find possible midcourse asteroid flybys within the mission constraints. Area 1, although dealing with a concept previously explored and largely used, presents a new method to connect ballistic arcs and gravity assist maneuvers. Area 2, uses the basic concepts derived on area 1 and optimal control to modify an existing theory to better accommodate the physical aspects of the mission. Nevertheless, each of the transfer arcs design in the two previous areas still accommodate only one target (multiple arcs, of course, accommodate multiple targets). Therefore, to enhance each arc allowing, not only the main, but also secondary targets, the main trajectory design on areas 1 and 2 is taken into account in area 3 as reference to add an additional mission target, a midcourse flyby. This area includes not only the design of the trajectory but also a method to perform the midcourse target selection. By applying the process described above, a trajectory can be designed in a systematic way with not only the main objective, but also with additional targets. Obtaining, in this way, a multiple target trajectory efficiently and allowing the designer a better understanding and assessment of the problem.

1.2.1 Ballistic Trajectory Design

The ballistic part comprehends the selection of an optimal flyby sequence of asteroids from an extensive database taking into account ballistic transfers departing from Earth utilizing the solution of the Lambert problem with the use of gravity assisted maneuvers. This approach allows the identification of a global minimum and a better understand of the problem as a whole. This step uses a extensive search to find all the problem minimums, in a ballistic environment, that are necessary for the following steps since they rely on gradient base methods that can only locally optimize the problem. This part was applied to a mission proposal to the asteroids (3200) Phaethon, (155140) 2005 UD and (225416) 1999 YC, it successfully obtained several possible trajectories that allow the study of the asteroids; in special a single ballistic trajectory that flyby Phaethon and latter 2005 UD by performing an Earth gravity assist and a trajectory that reaches 1999 YC with a low fuel usage by making a Mars gravity assist that previously was not possible with direct Earth transfer.

1.2.2 Impulsive Trajectory Design

Once the problem as a whole is understood and the global and local minimums are identified, a second step involves adding an impulsive maneuver, which comprehends the instantaneous velocity change using chemical propulsion, somewhere during the transfer. The impulse is used to alter the trajectory in order to place the spacecraft in a different orbit which can provide more encounter opportunities or the use of less propellant for the same flyby sequence. The problem of where to deliver the impulse is broad with no close form; therefore, more sophisticated mathematical theories are implemented such as the primer vector theory. This part was used in developing a modified version of the primer vector theory which includes a more profound assessment of how and where impulses are provided. This constitutes an important step for the next area not only because, as the previous one, designs the main trajectory, but also lays the basis of the Primer Vector theory and the linear theory used extensively on the next area. Among the results, this part shows faster and more accurate results than the traditional nonlinear programing solvers normally used in this type of analysis.

1.2.3 Low-Thrust Trajectory Design

By having the less energetic trajectories and flyby sequences identified not only with respect to the ballistic transfer but also identifying the most profitable point for an impulsive maneuver, the last step consists in the implementation of the latest propulsion system that makes use of a low-thrust propeller, which is based in an electric propulsion system. At this point the impulses can be replaced by propelled arcs which will once more require the development of a analysis in order to identify the best transfer trajectories. The use of low-thrust propulsion is gaining more attention over the year due to the fact that new missions are successfully using these propellers and with this are able to save propellant mass, increase the mission value by adding more science opportunities and reducing risks. Taking the advantages provided by the low-thrust propulsion system, a midcourse flyby is accommodated near the main trajectory enhancing and adding new value for the mission. Due to their large number, importance and facility to perform a flyby, asteroids are commonly used as such targets. Nevertheless, these advantages come with a great complexity in the mission design, trajectory and asteroid selection, that needs to be overcome with new analyses techniques, which in this case is based on the optimal control theory derived primer vector. The optimal control defines the necessary conditions for the control parameters to minimize the defined cost and the transversality conditions obtaining an optimal initial, final and midcourse conditions. The asteroid selection process combined with the indirect method for optimization obtains trajectories with midcourse flybys faster and with a better understand of the selection and posterior trajectory design than the typical brute force approaches.

1.3 Contributions of the Research

This research aims to solve the asteroid flyby problem using a fast and accurate evaluation, an important point in the space exploration scenario. The asteroid flyby trajectory design can be very extensive and time demanding, it is usually done by what is generally called brute force method or extensive search, in which each possible case is evaluated individually with simulations that usually take a long time. Therefore, to obtain a fast solution that provides better understanding of the problem is of great importance.

The solution method proposed here provides fast solution with a better understanding of the dynamics and constraints involved, permitting a more profound evaluation of the problem. This method is derived using optimal control theory with the addition of midcourse constraints that results in a simple and effective analytical solution for the control functions and path conditions. With this new approach, this problem can be solved in a shorter time.

A few previous researches have addressed this issue before, however, the complications of such study are generally avoided by having powerful computers and a large amount of time for simulations. However, as these type of missions are mainly possible due to electric propulsion system and the Global Exploration Roadmap clamming for more frequent missions, time may no longer be available for such long simulations.

1.4 Thesis Roadmap

Represented in the next diagram is the roadmap of this thesis, which outlines the relation between the chapters an areas they comprehend.

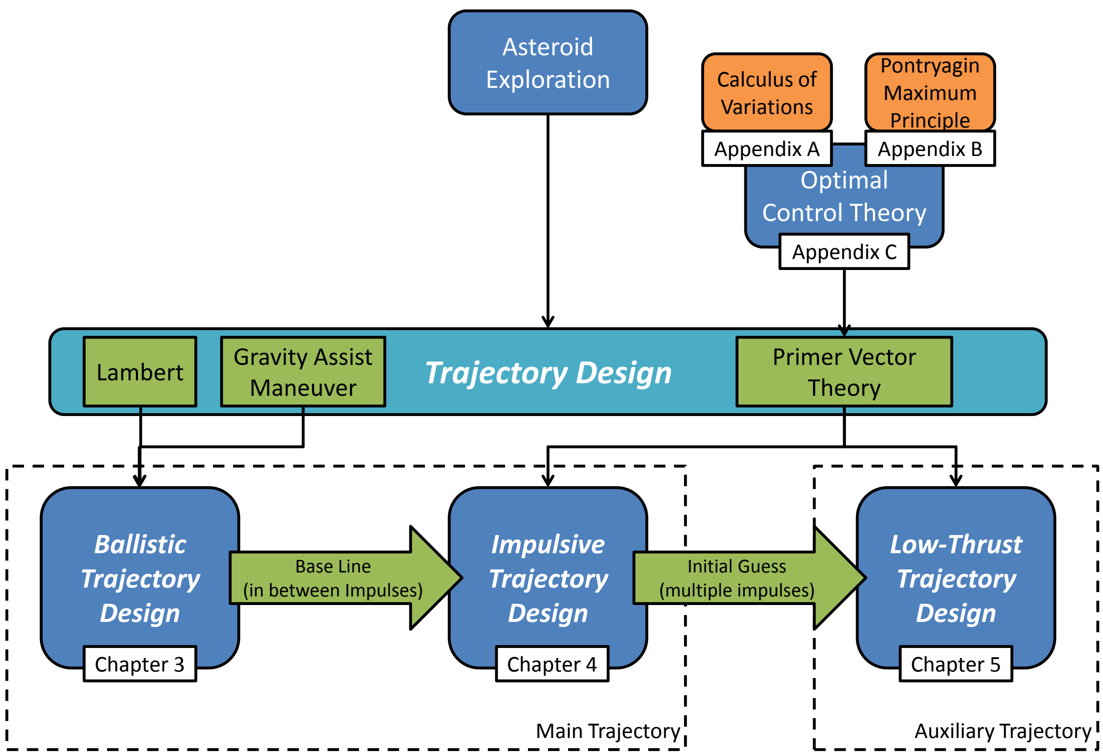

Figure 1.2: Thesis roadmap diagram.

CHAPTER 2

Bibliographic Revision

This chapter presents a bibliographic revision of the most significant works used in this thesis divided into Books and Articles. Some of the main databases of bibliographic information presented here are originated from the American Institute of Aeronautics and Astronautics, with emphasis on the Journal of Guidance, Control, and Dynamics, and The International Astronautical Federation.

A complete list of all the bibliography used in this work can be found in the Bibliography chapter, which also includes the publication details. Specifics of each theory and its application to the research can be found on the methodology description at each appropriate chapter.

2.1 Books

[Battin 1999], Introduction to the Mathematics and Methods of Astrodynamics. Presents the basic theories and methods of basic astrodynamics used throughout this document. Some of the most important to be pointed out are the different solution methods for the Lamber problem, calculation of the orbit linearized dynamics, and basic applications for the linear theory on trajectory design.

[Vallado 2007], Fundamental of Astrodynamics and Applications. Similarly to [Battin 1999], this book is used here for the basis of the astrodynamics theories. Once again, the most important contribution to be pointed out is the different solution methods for the Lamber problem and the magnitude assessment of secondary order effects.

[Kirk 2004], Optimal Control Theory: An Introduction. Describe all the basic concepts of the optimal control applied to trajectory design. The book derives the optimal control using both the Calculus of Variations and Pontryagin's Maximum Principle. Among the different scenario derivations, the midcourse condition in an optimal problem is of special interest for this work.

[Lawden 1963], Optimal Trajectories for Space Navigation. As one of the most important books describing the basis of optimal control applied to space trajectories, it presents the first derivation of the Primer Vector Theory used here for impulsive and low-thrust maneuvers. In fact, the author, Derek F. Lawden, created the name primer vector in this publication as an allusion to the burning of cordite by means of a primer charge used in the World War II artillery.

[Conway 2010], Spacecraft Trajectory Optimization. Presents a summary of the different techniques for impulsive and low-thrust trajectory design using indirect, direct, and heuristic methods. The book also presents the basic derivation of the primer vector theory and its application for impulsive trajectory design. Also important, the book present a derivation of spacecraft trajectory optimization using direct transcription and nonlinear programming, which is here used for comparison against the indirect method.

[Pontryagin 1987], Mathematical Theory of Optimal Processes. This book present a collection of the works of Lev Semyonovich Pontryagin a Russian mathematician. The most significant part of this book for this work is the derivation of Pontryagin's Maximum Principle. This principle is used on the definition of the optimal thrust control on the trajectories using low-thrust propulsion system.

2.2 Articles

[Lion 1968], Primer Vector on Fixed-Time Impulsive Trajectories. Develops the Primer Vector Theory applied to an impulsive trajectory. In this work it is shown how the primer vector behaves if the trajectory is optimal and how it can be used to determine if the trajectory can be improved by means of a midcourse impulse. The derived theory also provide the necessary conditions for when an additional impulse improves the trajectory. Also, derived are the necessary conditions to improve the trajectories with a initial or final coast orbit.

[Jezewski 1968], Efficient Method for Calculating Optimal Free-Space N-Impulsive Trajectories. Developed in this work and efficient method to compute an N-impulsive optimal trajectory by combining the findings of the previous works of [Lawden 1963], primer vector, and [Lion 1968], gradient vector, combined with a conjugate gradient iterator.

[Jezewski 1971], Inequality Constraints in Primer-Optimal, N-Impulse Solutions. This article details the process to evaluate, with a penalty function approach, a differential cost function with inequality constraints. In this way generating a completely general, two-body, N-impulsive, optimal trajectory for a set of constraints.

[Russell 2007], Primer Vector Theory Applied to Global Low-Thrust Trade Studies. Performs a general low-thrust trade analysis using a tool based on a global search with local indirect method solutions. This article develops an efficient propagator with an implicit "bang-bang" thrusting structure. It also includes a detailed derivation of the standard adjoint control transformation providing additional physical insight and control over the costates that define the thrust profile.

[Ranieri 2005], Optimization of Round-Trip, Time-Constrained, Finite-Burn Trajectories via and Indirect Method. Here the primer vector theory is used in the trajectory optimization study between two orbits in the two-body problem. The trajectory is assumed time-constrained, performing a round-trip with finite burn. The developed method solves a multi-point boundary value problem with two discontinuities in the controls corresponding to the arrival at and the departure from the target.

[Senent 2005], Low-Thrust Variable Specific Impulse Transfers and Guidance to Unstable Periodic Orbits. This article studies the primer vector applied to a spacecraft using a power-limited, variable-specific-impulse propulsion system. The transfer trajectory is designed in the circular restricted three-body environment from near the primary to an arbitrary orbit. The indirect method coupled with an adjoint control transformation yields a robust and efficient solution method to construct these transfers.

[Petropoulos 2008], Low-Thrust Transfers using Primer Vector Theory and a Second-Order Penalty Method. In this work the authors derive the penalty functions' first and second derivatives utilizing principles of static-dynamic control and dynamic programming. This work deals with low-thrust propulsion systems with fix and variable specific impulse with a mapping of derivatives across switching times.

CHAPTER 3

Ballistic Trajectory Design

3.1 Introduction

The Near-Earth Asteroid (3200) Phaethon, the parent of the Geminid meteor shower, is a 5 km diameter, B-type asteroid. Unlike most meteor showers parent bodies (usually comets), Phaethon is dynamically an asteroid with little cometary features, except near its perihelion suggesting a comet-asteroid transition body [Jewitt 2010, Jewitt 2013]. The observed sodium depletion in Geminid meteoroids suggests that its origins are a partial melting of the parent Phaethon, rather than from sodium loss by solar heating [Kasuga 2009]. Asteroids (155140) 2005 UD, B-type, and (225416) 1999 YC, C-type, are likely fragments that originated from Phaethon [Ohtsuka 2008] and are collectively know as the Phaethon-Geminid Complex (PGC) [Ohtsuka 2006]. Furthermore, the main-belt B-type asteroid Pallas has been also suggested to be characteristically linked with Phaethon [de León 2010]. The sodium depletion of the Geminid meteoroid observed near the perihelion and the chemical heterogeneity among the PGC members suggest that Phaethon may consists of primitive cometary materials and locally melted differentiated materials. Yet, the nature of Phaethon remains an open question, making the PGC critical mission targets to understand the surface, internal composition, and origin of comet-asteroid transition bodies, as well as, providing key information on the thermal and dynamical evolution of primitive asteroids in the solar system. Because of its scientific importance, Phaethon was a target candidate for NASA's Deep Impact [Blume 2005] and OSIRIS-REx missions [Lauretta 2012]. A space mission to PGC can provide information on three dimensional physical and chemical characteristics of the PGC parent body. The data obtained with such a mission is a key to understand the origins of Phaethon and PGC, and to solve fundamental issues in solar system sciences.

The intent of this paper is to investigate the possibility of a multiple flyby mission that facilitates the study of Phaethon, 2005 UD and 1999 YC; designing trajectories that fly by some or all the target asteroids. Mission concepts exclusive to Phaeton have already been explored [Padevet 1986, Kasuga 2006]; however, this work focus on the study of the "Phaethon family". Despite the fact that multiple asteroid missions have already been proposed [Perozzi 2001], missions to a predefined set of asteroid targets are more challenging because it is not possible to assure a design with a reasonable energy before obtaining the result. As a result, very few missions have been executed to a predefined set of asteroid targets, e.g. the Contour mission [Cochran 2006], and no multiple flyby mission specific to the Phaethon family has been proposed, to the best of the authors' knowledge. Due to the asteroids' orbital properties, large relative velocities are generated at the time of encounters making rendezvous or sample return missions to more than one of these asteroids costly with respect to the Δv needed to cancel the excess velocity upon arrival, as will be seen further in the analysis. Therefore, only a flyby strategy is considered in this work. The objective is to obtain practical ballistic transfers that fly by two or, perhaps, all three asteroids without relying on any deterministic intermediate maneuvers. Considering specific arrival times, single transfers that connect three or more points on different orbits are rare and, by adding a constraint on the maximum excess velocity to escape the first body, these orbits usually do not exist. To allow for multiple encounters, considering the constraints adopted, gravity assist maneuvers (GAM) can provide a feasible solution; in this case, Earth and Mars GAM are taken into account.

The mission characteristics and constraints adopt in this work are based in a small-class mission, such as, the DESTINY mission [Kawakatsu 2012]. This work is also considered to be a preliminary assessment of one of the mission's extension proposal. Based on this, midcourse maneuvers are not included since for a small-class deep space mission the amount of propellant available is limited and, as the Earth escape velocity is mainly provided by the launch vehicle, ballistic trajectories are generally preferred. Specifically for the DESTINY extended mission, propellant for deep space maneuvers will no longer be available during this phase.

In section 3.2, the objective of the study is discussed, highlighting some aspects predefined by system engineering requirements. Section 3.3 describes the tools and theories used to analyze the problem, such as target body orbital data, ballistic trajectory transfers, and gravity assists maneuvers. Finally, section 3.4 presents the results for the flybys using ballistic and GAM transfers, followed by section 3.5 that presents the conclusion of this work.

3.2 Mission Design Framework

A primary driver behind multiple flyby missions is the desire to gather the most diverse data possible. However, the orbital geometry of the asteroids considered in this work (Fig. 3.1) combined with a low departure velocity leads to a requirement for large relative velocities for an arrival spacecraft departing from Earth. This requirement makes rendezvous and sample return missions infeasible due to the large amount of fuel necessary to negate the large relative velocity on arrival. Therefore, a flyby study is ideal for this mission, and may potentially lead to saving propellant and time.

From the infinite number of transfers that connect two points on an orbit, only a finite number (depending on the number of revolutions) of orbits will result in a transfer with a given time of flight (ToF). The ToF in this case is necessary to ensure the correct phasing upon reaching the asteroid at the arrival point. Considering a mission time frame and a maximum excess velocity, these infinite number of solutions may be reduced to a few feasible departure dates. The addition of another flyby objective that also contains a time constraint will, in most cases, reduce these solutions to be few or non-existent. Due to these limitations, a multiple-flyby objective can rarely be achieved. The solution for this problem, which does not rely on providing extra Δv or more complicated mechanisms, is to make use of a GAM that facilitates the desired change in the transfer orbit with some degree of flexibility.

This research makes use of a series of simple ballistic transfers combined with GAMs. This approach is very robust, allowing a global search analysis of minimum energy trajectories for the three asteroid targets, making it very suitable for the preliminary steps of this mission design. System design requirements are also taken into account, including a maximum transfer time of 2 years, considering a mission time frame in the 2020s, and a maximum Earth hyperbolic escape speed (v_∞) of 3 km/s. The latter condition is derived from the DESTINY mission [Kawakatsu 2012], which relies on a small launcher similar to the architecture assumed in this paper. Another point for using such a small v_∞ is based in the fact that future small-class deep space mission are expected to be launched in low-Earth orbit piggyback on a main spacecraft; and due to limited amount of propellant available, the v_∞ achieved at Earth's escape is small.

This study was initiated by evaluating the launch windows for each asteroid. With the analysis of the resulting transfers and their orbital resonances with the Earth, it is possible to devise a strategy that changes the original trajectory and re-targets the spacecraft to reach a second flyby using a GAM at Earth. These results provided an interesting possibility that inspired the study of a GAM at Mars as a way to lengthen the launch window and introduce more flexibility into the mission architecture.

3.3 Assumptions for the Analysis

Using NASA's Horizon system, the positions and velocities of Earth, Mars, Phaethon, 2005 UD and 1999 YC with respect to the solar system's barycenter were obtained for the mission timeline (with a time step of 1 day). The orbits, with respect to the ecliptic, are shown in Fig. 3.1, showing clearly the large inclination of the asteroids' orbits with their descending and ascending nodes represented by O and $*$, respectively. Table 3.1 shows the asteroids' mean orbital properties.

Table 3.1: Mean orbital elements in J2000

	Earth	(3200) Phaethon	(155140) 2005 UD	(225416) 1999 YC	Mars
Semi-major axis [A.U.]	1.00000011	1.2711714	1.2748781	1.4217526	1.52366231
Eccentricity	0.01671022	0.8898360	0.8722251	0.8305044	0.09341233
Inclination [deg]	0.00005	22.23998	28.67657	38.21391	1.85061
Argument of the perihelion [deg]	102.94719	322.14372	217.5137	156.38307	336.04084
Right ascension of the ascending node [deg]	-11.26064	265.26523	207.57680	64.80592	49.57854
Period [years]	0.99838	1.4705	1.4504	1.6958	1.8746

By specifying the departure and arrival dates, the initial and final positions for the transfer are defined using the Horizon database, with the ToF being the difference between the departure and arrival dates. The transfer trajectory can be then calculated by solving Lambert's problem. In this work, the method chosen to solve Lambert's problem is the Universal variable method [Battin 1999, Vallado 2007, Wagner 2011, Shen 2003, Arora 2010]. The upper bound on the ToF for each transfer is 2 years, which constrains the solutions to zero, one or two heliocentric revolutions. Low energy transfers departing from Earth do not deviate significantly from Earth's orbit, which takes about

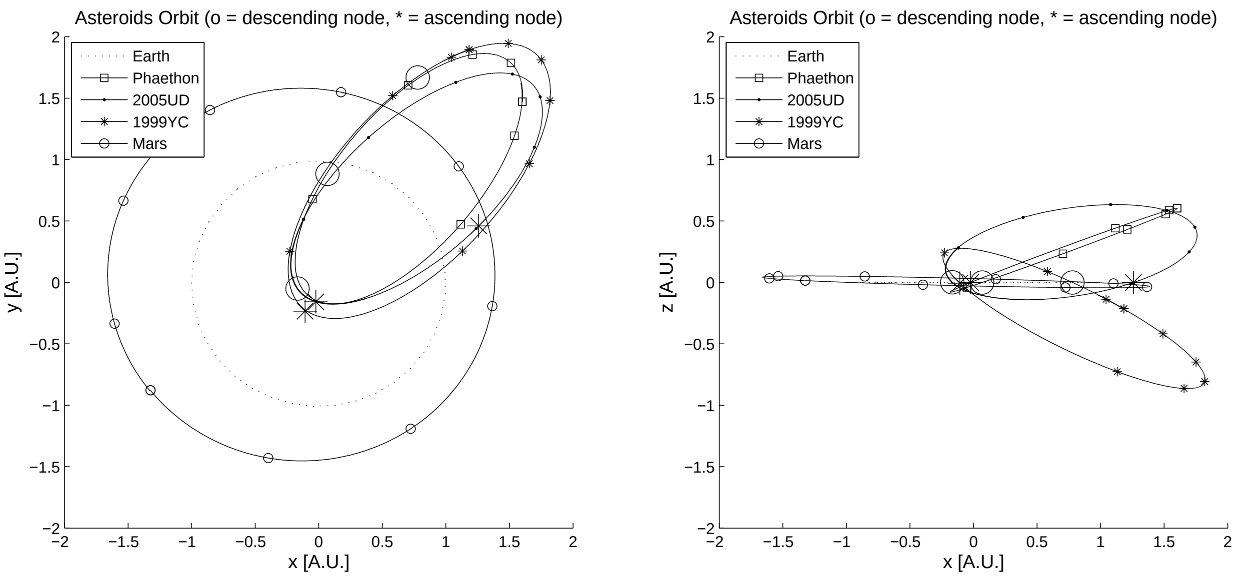

(a) X-Y plane

(b) X-Z plane

Figure 3.1: Bodies orbit with respect to the ecliptic (astronomical unit, A.U.).

1 year for each revolution around the Sun. Therefore, solutions that use 3 or more heliocentric revolutions would take more than the 2 year limit.

Finally, GAMs at Earth and Mars are also taken into account. This type of maneuver is not considered at the asteroids because their gravity is not strong enough to perform a significant change on the spacecraft's heliocentric velocity vector.

For January 1, 2020 through December 31, 2029, the trajectory of each asteroid is discretized into 3653 points (1 day time step) meaning that each Lambert problem between two bodies has to be solved 13344409 times (3653^2). In order to improve the total computational time and speed, all Lambert solutions are stored in a large database from which the feasible transfers and potential points for a GAM are taken. The evaluation of feasible single transfers from the database is accomplished by simply selecting transfers with less than the maximum v_∞ and ToF. A trajectory that includes a GAM is generated by selecting two Lambert arcs that meet at the GAM point. These arcs are required to have the same magnitude of arrival and departure v_∞ at the GAM point in the zero sphere of influence patched conics model. This constraint requires more work to precisely match the v_∞ because the discretized nature of the Lambert trajectories does not guarantee exact GAM v_∞ matching. The GAM matching algorithm is depicted in Fig. 3.2, where the GAM date is selected by having on the GAM day two results containing the target v_∞ in between, one result for the arrival transfer and one result for the departure transfer. These two pairs of transfers (two for arrival and two for departure) at the GAM point have to be obtained by two consecutive departure days for the first arc (before GAM) and two consecutive arrival days for the second arc (after GAM). Once

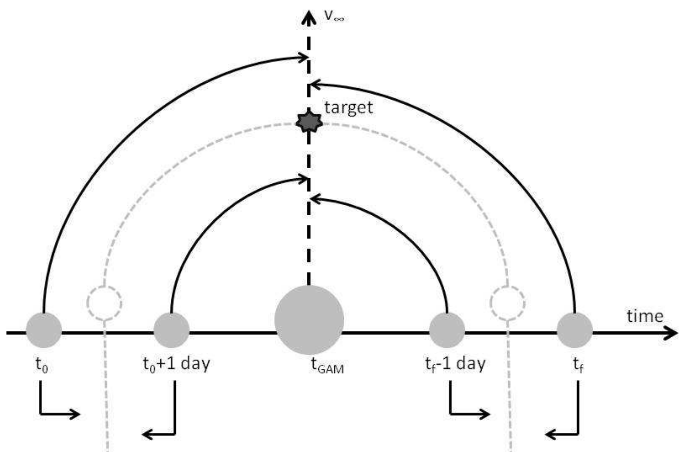

Figure 3.2: GAM matching algorithm.

the initial and final dates of the two transfers dates are selected from the database a grid search is performed between in order to obtain an exact match for the GAM's v_∞. With the GAM trajectory constructed, the final step is to check if the required change in the velocity vector can be performed at or above a defined minimal altitude. The minimal altitudes assumed are 1000 km for Earth, considering the operations of low-Earth orbit satellites, and 500 km for Mars, considering Mars' atmosphere. The maneuver distance from the planet can be calculated as

$$\mathrm{r_p} = \frac{\mu}{\mathrm{v}_\infty^2}\left[\sin\left(\frac{\phi}{2}\right)^{-1} - 1\right] \tag{3.1}$$

where, v_∞ [km/s] is the hyperbolic arrival velocity, ϕ $[\mathrm{rad}]$ is the arrival-departure velocity angle, μ $[\mathrm{km^3 s^{-2}}]$ is the planet's gravitational parameter and $\mathrm{r_p}$ [km] is the hyperbolic orbit's radius of perigee.

3.4 Flyby Mission to the Phaethon-Geminid Complex

In the following subsections, the trajectory design for potential asteroid flyby trajectories is performed. Initially, a simple Earth-to-asteroid transfer is assessed, and this transfer is later used to construct a GAM at Earth to perform a second asteroid flyby. At the end of this section, GAMs at Mars are also evaluated in order to construct new asteroid connections.

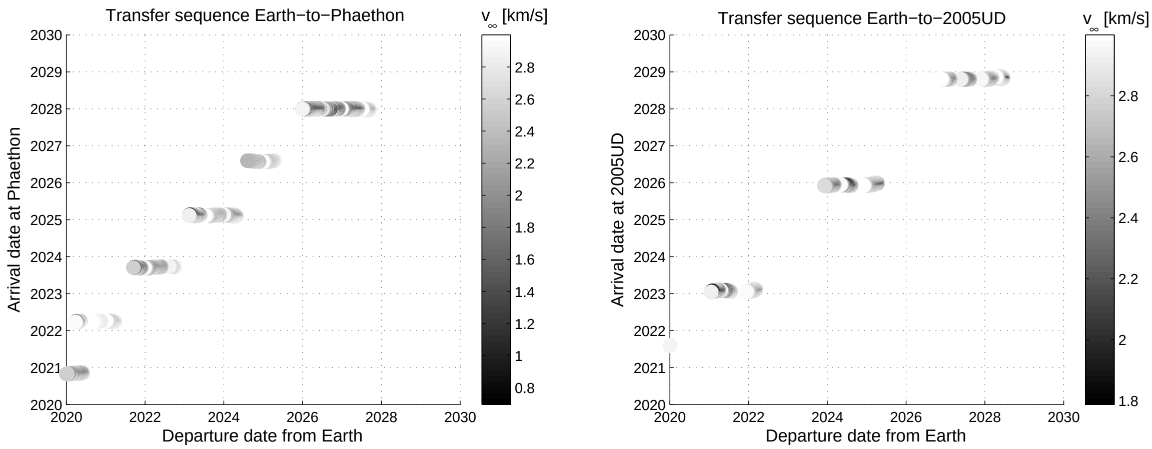

(a) Target - Phaethon

(b) Target - 2005 UD

Figure 3.3: Launch window for orbits with a maximum v_∞ of 3 km/s.

3.4.1 Earth-to-Asteroid Transfer

From the Lambert solution database, the launch window for the possible transfers from Earth to Phaethon, 2005 UD and 1999 YC is obtained taking into account only those transfers that require a maximum v_∞ of 3 km/s and maximum transfer time of 2 years. Figs. 3.3a, 3.3b and 3.4a show the departure date with respect to the arrival date and the shading of the points represent the v_∞ required at Earth's hyperbolic escape. The transfer to 1999 YC does not present any solution for $v_\infty \leq 3$ km/s; therefore, the results in Fig. 3.4a are shown with a higher values for v_∞ for comparison (as an example, a limiting value of 5 km/s is use to make easier to observe the plot)

For the Earth-to-Phaethon transfers (Fig. 3.3a) it is notable that Phaethon can be reached with a periodicity of approximately 1.5 years, which is close to the body's synodic period with respect to Earth. Fig. 3.5 depicts the lowest v_∞ Earth-Phaethon transfer, less than 1 km/s, in the X-Y plane. 2005 UD also presents periodic launch opportunities. However, in general, these transfers require more v_∞ than Phaethon's transfers due to the orbit's higher inclination, as outlined in Tab. 3.1. Moreover, 2005 UD lacks the low v_∞ transfer opportunities during some years; at these dates the transfers require slightly more than 3 km/s, due to the orbit's higher inclination, as can be seen in Fig. 3.4b where the graph shows solution for larger v_∞ (as an example, a limiting value of 5 km/s is use to make easier to observe the plot).

The relative flyby velocities for the Phaethon and 2005 UD transfers (Figs. 3.6a and 3.6b) show mean values of around 30-35 km/s. These large relative velocities arise from the low departure v_∞ which leads to a large relative velocity upon arrival (common for this type of mission). These velocities during the scientific data acquisition phase need to be taken into account during the planning of encounter operations.

The flyby velocities present above are high relative to those for previous and current aster-

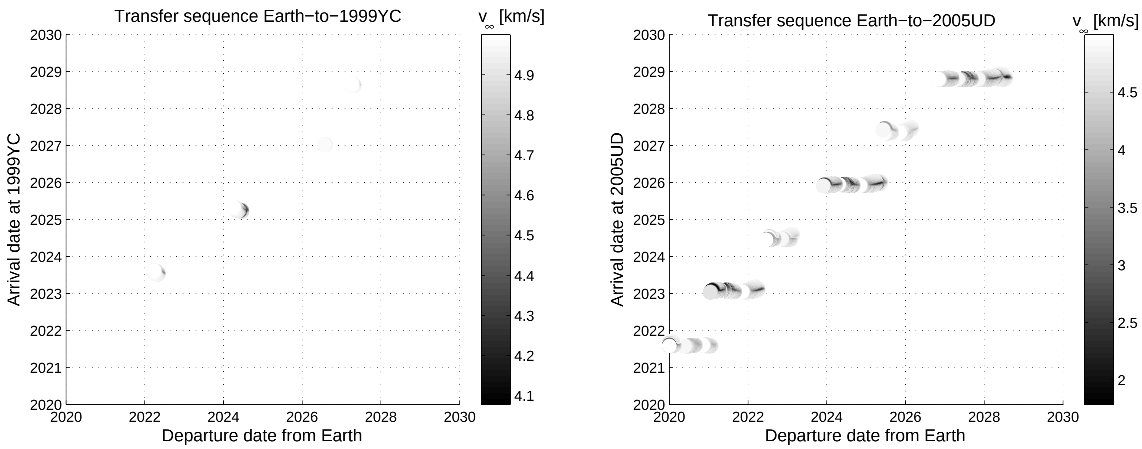

(a) Target - 1999 YC

(b) Target - 2005 UD

Figure 3.4: Launch window for orbits with a maximum v_∞ of 5 km/s.

oids/comets mission, such as, NEAR-Shoemaker: 9.93 km/s; Stardust: 6.1 km/s; Rosetta: 8.6-15.0 km/s. These missions had their main targets selected mainly based on technical feasibility for each mission purpose. In contrast, this study focuses on a science-driven mission with the target asteroids chosen based on their scientific importance, comet–asteroid transition body. In fact, Giotto, Vega, and four other spacecraft flew by the comet Halley in 1985-1986 with a relative velocity of 76 km/s. These were science (target) driven and technically challenging missions, similar to a Phaethon-Geminid Complex mission. Giotto was equipped with a time-of-flight mass spectrometry (ToF-MS) to make use of the high relative velocity. A similar ToF-MS design to that used on the Cassini mission, an updated model of Giotto ToF-MS, would be use in a mission described in this work, as well as, a high definition TV (HDTV) camera to observe the surface and possible dust ejection from the asteroids. The HDTV camera would be assembled in gimbaled platform to properly point to the target. The strategy of such mission is to flyby the target with a limited number of science instruments, ToF-MS to get chemical composition of dust particle around the asteroid by in-situ analyses and HDTV camera, to observe the surface geology and possible heterogeneity of surface reflectance, namely chemical and physical nature of the surface materials.

The arrival points at asteroids Phaethon and 2005 UD are far apart due to the large difference in their node location (Figs. 3.1 and 3.7). The fact that the transfer trajectories to Phaethon and 2005 UD are considerably different means that the possibility to fly by both asteroids with a single transfer is very small. Transfers from Earth to 1999 YC (Fig. 3.4a) require a larger v_∞ than the other two transfers, with a v_∞ of 4 km/s for the lowest energy transfer. As shown in Fig. 3.7, transfers using less v_∞ are located near the point where 1999 YC crosses the ecliptic plane, which is located beyond the orbit of Mars. The fact that the node crossing is beyond Mars' orbit results in the highly energetic trajectories shown. Transfers to points closer to Earth require much more v_∞ for changing the orbit plane.

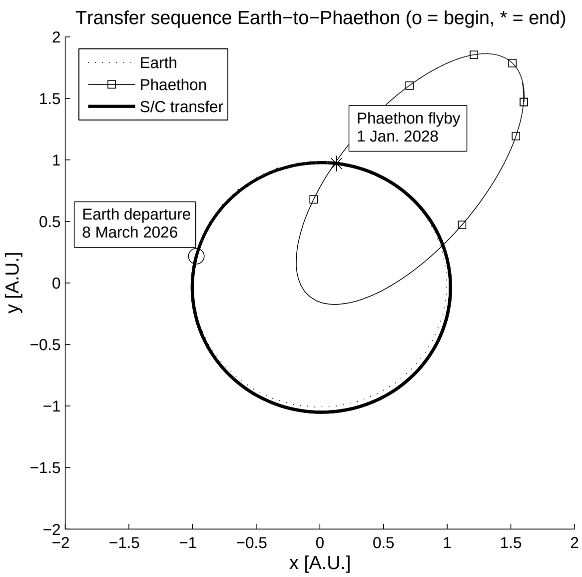

Figure 3.5: Lowest energy transfer Earth-Phaethon, X-Y view (spacecraft, S/C).

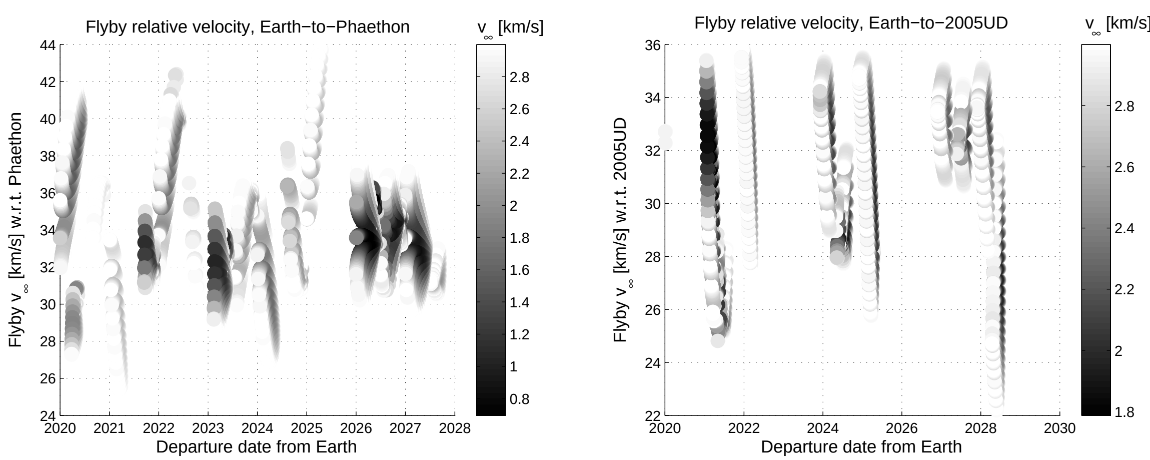

(a) Earth-Phaethon (b) Earth-2005 UD

Figure 3.6: Relative velocity at the flyby (with respect to, w.r.t.).

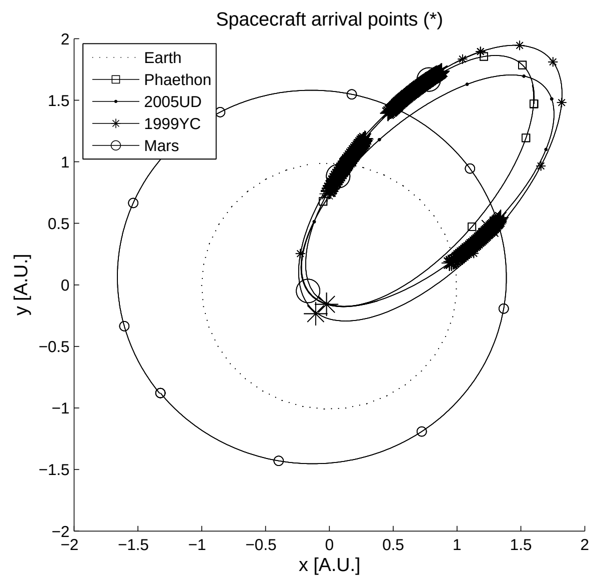

Figure 3.7: Earth-asteroid transfers with respect to the ecliptic, X-Y view.

In order to access two or more of the asteroids in one mission, a large maneuver needs to be made to change the transfer orbit. In this case, the use of on-board propulsion is impractical due to the large Δv required for maneuvering. As mentioned before, a practical solution is to make use of a GAM to perform the necessary heliocentric velocity change. With this concept in mind, the following strategies can be considered: first, enter into resonance with Earth's orbit, and re-encounter Earth after the first flyby to perform a GAM that changes the velocity vector and places the spacecraft on a new transfer orbit that allows it to fly by another asteroid. Second, transfer to Mars and perform a GAM that places the spacecraft in a new transfer orbit that flies by two asteroids.

3.4.2 Earth-Asteroid-Earth-Asteroid Transfer

Following the single Earth-to-asteroid transfer, this section investigates the possibility of an Earth-asteroid-Earth-asteroid transfer where the second Earth flyby consists of a GAM that connects the two previously separated Earth-to-asteroid transfers. The motivation for this type of analysis comes from the fact that, due to the asteroids' orbit shapes and periods, there is not a single transfer with a sufficiently small Earth departure v_∞ that connects Phaethon and 2005 UD, as presented in the previous section. Nevertheless, it is noticeable that many of the transfers are resonant with Earth, which allows for the required re-encounter.

Figure 3.8 present the transfer orbit period from Earth to each respective asteroid as well as the resonances with respect to Earth. The resonance is calculated as the orbit period of Earth divided by the orbit period of the spacecraft, the values shown are constrained by the closest values to the mission timeline. The horizontal axis shows the Earth's departure date and the vertical axis presents

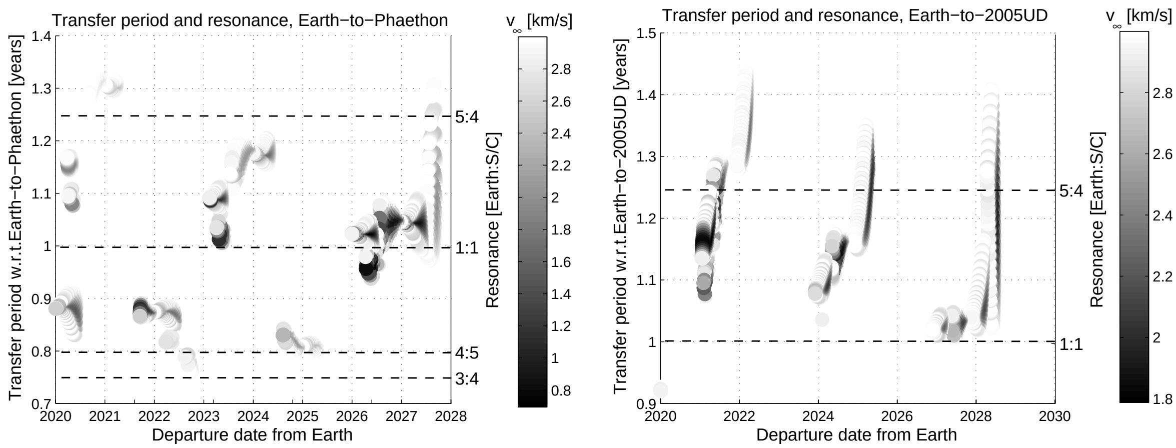

(a) Earth-Phaethon

(b) Earth-2005 UD

Figure 3.8: Transfer orbit resonances.

the transfer period on the left and the resonances on the right. Each point represents the same value for the v_∞ at Earth departure as used previously. As 1999 YC cannot be accessed with less than 3 km/s, it is not possible to reach it with an Earth GAM since the flyby maneuver will simply change the direction of the v_∞ vector and not its magnitude.

From Fig. 3.8a, it is apparent that there are 3 distinct resonance ratios with possible transfers: 1:1 (from April 2026 to September 2026 and April 2027 to September 2027): 5:4 (from July 2027 to September 2027) and 4:5 (from October 2024 to January 2025 and March 2025 to May 2025). The results for Earth-to-2005 UD in Fig. 3.8b show resonances with Earth at 5:4 (from March 2021 to June 2021 and January 2025 to April 2025 and March 2028 to July 2028). Tables 3.2 and 3.3 show the results for the Earth-Phaethon and Earth-2005 UD transfers, respectively.

Table 3.2: Earth-to-Phaethon transfer resonant points (Fig. 3.8a)

Trajectory resonance ratio	Earth departure dates (solution range)	Heliocentric revolutions	Resonant period	Phaethon flyby dates (solution range)	Possible Earth GAM dates (solution range)
1:1	Apr.2026-Sept.2026	1	1 year	Dec.2027-Jan.2028	Apr.2028-Sept.2028 Apr.2029-Sept.2029
	Apr.2027-Sept.2027	0		Dec.2027-Jan.2028	Apr.2028-Sept.2028 Apr.2029-Sept.2029
5:4	Jul.2027-Sept.2027	0	4 years	Dec.2027-Jan.2028	Jul.2031-Sept.2031
4:5	Oct.2024-Jan.2025	1	5 years	Jul.2026-Aug.2026	Oct.2029-Jan.2030
	Mar.2025-May.2025	1		Jul.2026-Aug.2026	Mar.2030-May.2030

With the results presented for Earth-to-Phaethon transfer, it is possible to find a suitable date connection to the Earth-to-2005 UD transfer within the mission timeline. The date connection can

Table 3.3: Earth-to-2005 UD transfer resonant points (Fig. 3.8b)

Trajectory resonance ratio	Earth departure dates (solution range)	Heliocentric revolutions	Resonant period	2005 UD flyby dates (solution range)	Possible Earth GAM dates(solution range)
5:4	Mar.2021-Jun.2021	1	4 years	Jan.2023-Feb.2023	Mar.2025-Jul.2025
	Jan.2025-Apr.2025	0		Nov.2025-Jan.2026	Jan.2029-Apr.2029
	Mar.2028-Jul.2028	0		Oct.2028-Nov.2028	Mar.2032-Jun.2032

be made by matching the Earth departure date of the Earth-to-2005 UD transfer (Fig. 3.3b) with an Earth-to-Phaethon orbit that has the same Earth return date (last column of table 3.2); the velocity connection at the GAM will be done at a later step. For the Earth-to-Phaethon leg, the results show possible GAMs for the years 2028 and 2029, and the Earth-to-2005 UD orbit resonance generates a possible Earth GAM in 2025 and 2029.

For the connection Earth-Phaethon-Earth-2005 UD, the possible Earth GAM dates found in Table 3.2 that generate suitable connection with the Earth-to-2005 UD transfer are for the year 2029. For the connection Earth-2005 UD-Earth-Phaethon, possible dates were found in 2025; however, this sequence has a total time of flight greater than 4 years, making the Earth-Phaethon-Earth-2005 UD sequence preferable.

Consequently, the possibility of Earth-Phaethon-Earth-2005 UD transfer is studied here, and the GAM matching procedure is used to analyze if the connection is in fact possible. The resulting trajectories are shown in Table 3.4 depicting each event, and demonstrating that the sequence connection by means of a GAM is indeed possible. For certain points the Earth-to-2005 UD transfer is close to a 4:5 resonance with 2005 UD, which indicates that a second flyby opportunity occurs again in 5 years. The altitude of the gravity assist maneuver, with respect to Earth's surface, ranges from 62,000 to 86,000 km, indicating that the maneuver is feasible in a patched-conics sense taking into account a minimum altitude of 1000 km.

Table 3.4: Possible Earth-Phaethon-Earth-2005 UD transfer

Trajectory event	Possible date	v_∞ [km/s]	Orbit resonance	Maneuver altitude [10^4 km]
Earth launch	Apr.2026-Sept.2026	1.25-3.00	1:1	
	Apr.2027-Sept.2027	1.25-3.00	1:1	
Phaethon flyby	Dec.2027-Jan.2028	33.25-34.5	close to 2:3	
Earth gravity assist maneuver	Mar.2028-Jul.2028	1.25-3.00	1:1	6.2-8.6
2005 UD flyby	Oct.2028-Nov.2028	24.0-30.0	close to 4:5	

Fig. 3.9 presents the lowest v_∞ transfer with an Earth departure on May 11, 2026, Phaethon flyby on January 4, 2028, Earth gravity assist on May 29, 2028 and 2005 UD flyby on November 1,

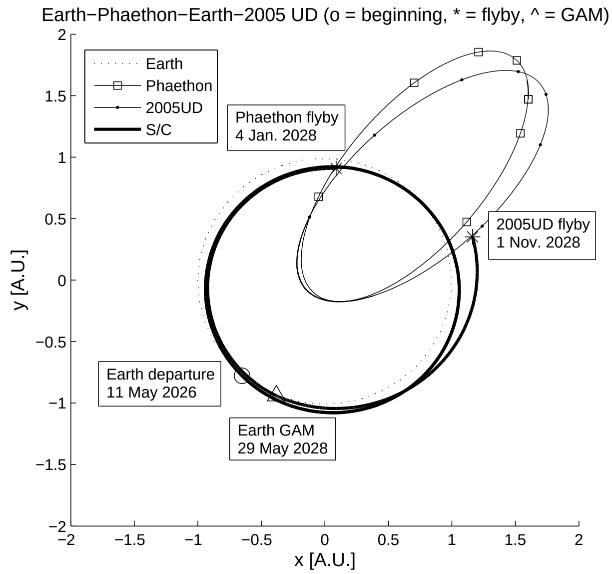

Figure 3.9: Lowest energy transfer Earth-Phaethon-Earth-2005 UD, X-Y view.

2028.

3.4.3 Earth-Mars-Asteroid Transfer

In this section, the possibility of a GAM at Mars is investigated. This maneuver at Mars can occur after a direct departure from Earth, which may improve the launch possibilities and access to the asteroids with less v_∞, or after a GAM at Earth. This approach may present a possibility for a third asteroid flyby following the result presented in section 3.4.2.

Following a similar procedure to the one used in section 3.4.2, but without the need to consider the orbital period of the transfer orbits, the sequence Earth-Mars-asteroid is constructed and the resulting possible trajectories are constrained by a maximum Earth escape velocity of 3 km/s, 2 year duration, and a minimum altitude for the gravity assist of 500 km above a spherical Martian surface. As a result, the sequences for Phaethon and 2005 UD do not produce better transfers than before, and take longer to arrive and require a higher v_∞ than a direct transfer from Earth. However, the Mars GAM produces viable results for performing a flyby of 1999 YC. The results are shown in Table 3.5.

Even though the launch window for Earth is relatively short, the results show a possibility to access 1999 YC that is not possible with a direct Earth transfer with less than 4 km/s. None of the results present a viable resonance with Mars, which precludes the possibility of a second asteroid flyby by means of another GAM at Mars. The launch window is too short to allow for a connection with the resonant orbits calculated in Tables 3.2 and 3.3. Therefore, an Earth-to-Mars transfer after the first Earth-asteroid flyby is not possible either considering the mission time frame.

Table 3.5: Possible Earth-Mars-1999 YC transfer

Trajectory event	Possible date range	v_∞ [km/s]	Orbit resonance	Maneuver altitude [10^2 km]
Earth departure	Mar.2026-Apr.2026	2.88-3.00	None feasible	
Mars gravity assist maneuver	Jan.2028-Feb.2028	4.50-4.81	None feasible	8.6-18
1999 YC flyby	Aug.2028-Sept.2028	21.1-21.5	None feasible	

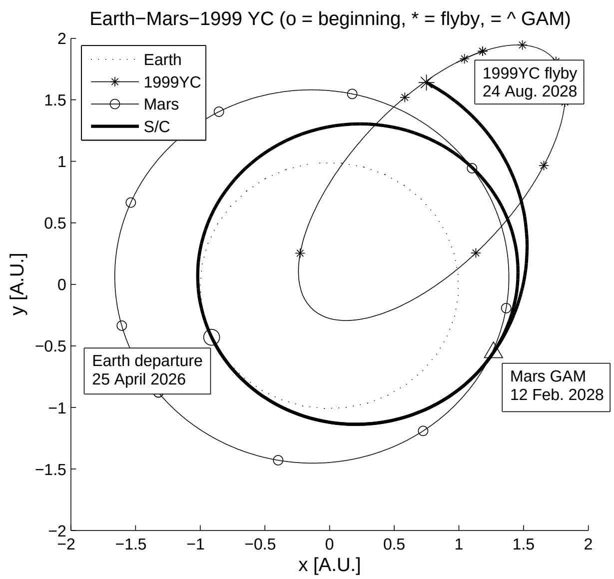

Figure 3.10: Lowest energy transfer Earth-Mars-1999 YC, X-Y view.

Fig. 3.10 presents the lowest v_∞ transfer with an Earth departure on April 15, 2026, Mars gravity assist on February 12, 2028 and 1999 YC flyby on August 24, 2028.

3.4.4 Tentative Earth-Venus-Asteroid Transfer

Gravity assist maneuvers at Venus were also explored using the same concept and procedure as applied in the Mars case. However, the results generated low-energy trajectories only to Phaethon and 2005 UD that, as in the case for Mars, are longer and require more v_∞ than a direct transfer from Earth on the same date. Therefore, no further investigation was made for trajectories using GAM at Venus.

3.5 Conclusion

By using a patched-conics model and performing a grid search of transfer possibilities with Lambert targeting, many flyby missions for asteroids in the Phaethon-Geminid Complex are cataloged and described considering the constraints adopted for a small-class mission. The results show periodic launch opportunities to all three asteroids, with a minimum launch v_∞ of 1 km/s to the asteroid Phaethon. Considering a maximum hyperbolic excess velocity of 3 km/s, direct ballistic trajectories to Phaethon and 2005 UD can be achieved; however, direct transfers to 1999 YC cannot be accomplished with a v_∞ of less than 4 km/s. In order to accomplish multiple asteroid flybys transfers with the constrains considered, it was found that a 1:1 resonant transfer with Earth provides a feasible low-energy option by making use of a gravity assist maneuver at either Earth or Mars. A launch window between 2026 and 2027 facilitates a ballistic flyby of both Phaethon and 2005 UD. By incorporating a gravity assist maneuver at Mars, new transfer possibilities are found. For Phaethon and 2005 UD, these transfers are longer and require more v_∞ than a direct transfer from Earth at the same dates, but an Earth-Mars-1999 YC transfer presents possible access to 1999 YC with an Earth departure v_∞ of less than 3 km/s.

CHAPTER 4

Impulsive Trajectory Design

4.1 Introduction

Over the years, missions to asteroids have enhanced our knowledge on many aspects of these bodies. Such a growing interest in them is due to many reasons which can go from purely scientific, such as understanding the formation mechanisms and composition of our early solar system, to more tangible matters like planetary protection and the possibility of mining rare materials. Particularly, flyby missions present some interesting aspects which are not found in any other types of mission. For example, flyby missions are: cost effective, cheaper with respect to the use of propellant, and flexible. On the other hand, rendezvous missions allow a much more detailed and long analysis of the target providing, in many cases, a more profound understanding of its long term behavior and physical evolution.

The framework of the proposed problem consists of generating a trajectory composed of impulses that allow a more cost effective transfer. The initial guess for the trajectory optimization is a Lambert solution from the initial point to the desired target, which generates a two-impulse transfer solution. The methodology used to generate the final optimal trajectory is then based on an optimization that calculates the best location and time for a midcourse impulse respecting its initial and final positions as well as the transfer time.

The process that generates the optimal transfer consists of adding a midcourse impulse using the primer vector theory (PVT), an indirect method of trajectory optimization based on impulsive maneuvers. Initially developed by Derek Frank Lawden in 1963 [Lawden 1963] and later complemented with the works of Lion & Handelsman, 1968 [Lion 1968], Jezewiski & Rozendaal, 1968 [Jezewski 1968], and Jezewski & Faust, 1971 [Jezewski 1971], the PVT provides time and position for adding a midcourse thrust impulse that minimizes the cost. Most importantly, the PVT evaluates the optimality of the result by analyzing the evolution of the primer vector's magnitude, which indicates if another midcourse impulse will further decrease the trajectory's cost. In the context of space missions, a low cost transfer requires, among other things, a minimum velocity increment at an orbit close to the planet to generate an hyperbolic excess velocity and minimum fuel usage for deep space maneuvers; both requirements can be expressed in terms of a velocity increment, $\Delta \mathrm{v}$. Therefore, it would make the optimization more robust if the cost could be associated with these two parameters. One way to associate the cost with the specific characteristics of how and where the $\Delta \mathrm{v}$ is apply is to modify the cost function to accommodate weights that are set to reflect these characteristics. In this work, the classical cost used in the PVT is modified to better accommodate the transfer by applying weights in the cost function's elements and its gradient. Preliminary work on this topic was made by the authors in [Sarli 2013] only for flyby cases and in this paper the theory is revisited and completed to include different types of missions. The method proposed in this work will be referred to as the weighted method.

As an application example, the design of a flyby trajectory to the main asteroid of the Phaethon Geminid Complex (PGC), 3200 Phaethon, is performed. Among the many possible targets for a flyby mission, the study of the Geminid meteor shower can be of special interest since it may hold the answers to fundamental questions about the early solar system. Perhaps the most important asteroid related to the Geminid is 3200 Phaethon, a B-type asteroid which is believed to be the parent of the complex. Such is the importance of the PGC that Phaethon was a target candidate for NASA's Deep Impact [Blume 2005] and OSIRIS-Rex missions [Lauretta 2012]. Another flyby application example explored is the preliminary asteroid selection of the PROCYON mission [Funase 2014, Ozaki 2014] to be launched on November 2014 piggyback on Hayabusa-2. The mission consists in demonstrating a micro-spacecraft bus system for deep space exploration and asteroid close flyby observation. And for the rendezvous example, an encounter trajectory is calculated to the near-Earth asteroid 25143 Itokawa, the target of Hayabusa mission. The MUSES-C or Hayabusa, re-named after launch, was a Japanese rendezvous and sample return mission, launched in May 2003, famous for having been the first to return an asteroid sample to Earth for analysis on June 2010. In this work, the transfer design is based on impulsive thrusts rather than the ionic propulsion used to originally design the Japanese mission.

Section 4.2 presents a background of the classical linearization method used on the transfer trajectory and a short historical background of the primer vector theory with its most important equations. Section 4.3 provides a derivation for the novel method of a weighted cost function and its gradient, showing the differences in the necessary conditions for optimality between the weighted and the classical methods. Section 4.4 presents possible values for the weights particularly for the single asteroid flyby and rendezvous cases. Section 4.5 deals with the Phaethon flyby, the PROCYON asteroid selection, and the Itokawa rendezvous test cases, comparing the results with the Lambert solution and a direct method optimization. Finally, section 4.6 presents the conclusions derived from the previous chapters.

4.2 Classical Theory

4.2.1 Linearization

The linearization of the orbit is necessary to calculate the evolution of the primer vector and some variables of interest. A perturbed trajectory is evaluate in three points of interest: beginning, a generic midcourse and the end, these points are denote respectively by the subscripts o, m and f. Figure 4.1 presents these points, as well as, the initial velocity perturbation, $\delta\mathbf{v}_\mathrm{o}$, final velocity perturbation, $\delta\mathbf{v}_\mathrm{f}$, the midcourse position perturbation, $\delta\mathbf{r}_\mathrm{m}$, and the perturbed velocities before, $\delta\mathbf{v}_\mathrm{m}^-$, and after, $\delta\mathbf{v}_\mathrm{m}^+$, it. The state transition matrix for a generic elliptical orbit can be obtained from the work of Glandorf [Glandorf 1969], among others, which bases the linearization in an inverse-square gravitational field. Having the state transition matrix, $\boldsymbol{\Phi}$, the perturbations can be derived in the linear system caused by a position displacement $\delta\mathbf{r}_\mathrm{m}$ at the point m, however, maintaining the

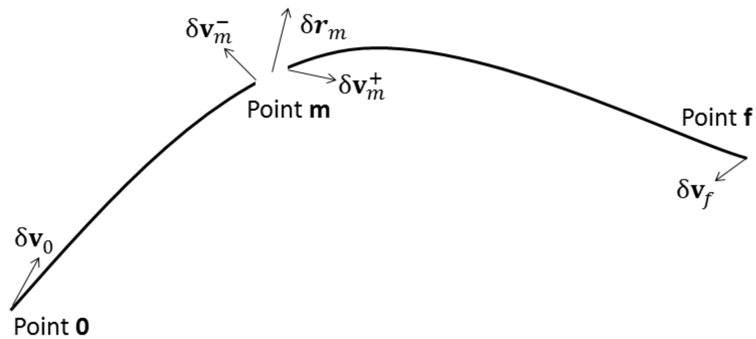

Figure 4.1: Trajectory representation

initial and final points the same, $\delta\mathbf{r}_\mathrm{o} = 0$ and $\delta\mathbf{r}_\mathrm{f} = 0$.

$$\begin{bmatrix} \delta\mathbf{r}_\mathrm{m} \\ \delta\mathbf{v}_\mathrm{m}^- \end{bmatrix} = \mathbf{\Phi}_\mathrm{mo} \begin{bmatrix} \delta\mathbf{r}_\mathrm{o} \\ \delta\mathbf{v}_\mathrm{o} \end{bmatrix}; \quad \begin{bmatrix} \delta\mathbf{r}_\mathrm{f} \\ \delta\mathbf{v}_\mathrm{f} \end{bmatrix} = \mathbf{\Phi}_\mathrm{fm} \begin{bmatrix} \delta\mathbf{r}_\mathrm{m} \\ \delta\mathbf{v}_\mathrm{m}^+ \end{bmatrix} \tag{4.1}$$

Where, $\mathbf{\Phi}_\mathrm{mo}$ is the state transition matrix from the beginning until the midcourse, $\mathbf{\Phi}_\mathrm{mo} = \mathbf{\Phi}(\mathrm{t_m}, \mathrm{t_o})$, and $\mathbf{\Phi}_\mathrm{fm}$ is from m until *f*. From Eq. (4.1) the velocity variations at all points are obtained. For clarification the matrix $\mathbf{\Phi}$ is subdivided as $\mathbf{\Phi} = \begin{bmatrix} \mathbf{M} & \mathbf{N} \\ \mathbf{S} & \mathbf{T} \end{bmatrix}$,

$$\begin{cases} \delta\mathbf{v}_\mathrm{o} = \mathbf{N}_\mathrm{mo}^{-1}\delta\mathbf{r}_\mathrm{m} \\ \delta\mathbf{v}_\mathrm{m}^- = \mathbf{T}_\mathrm{mo}\mathbf{N}_\mathrm{mo}^{-1}\delta\mathbf{r}_\mathrm{m} \\ \delta\mathbf{v}_\mathrm{f} = (\mathbf{S}_\mathrm{fm} - \mathbf{T}_\mathrm{fm}\mathbf{N}_\mathrm{fm}^{-1}\mathbf{M}_\mathrm{fm})\delta\mathbf{r}_\mathrm{m} \\ \delta\mathbf{v}_\mathrm{m}^+ = -\mathbf{N}_\mathrm{fm}^{-1}\mathbf{M}_\mathrm{fm}\delta\mathbf{r}_\mathrm{m} \end{cases} \tag{4.2}$$

Finally, the difference between the velocities at the point *m*, $\Delta\mathbf{v}_\mathrm{m}$, can be calculate as $\Delta\mathbf{v}_\mathrm{m} = \mathbf{v}_\mathrm{m}^+ - \mathbf{v}_\mathrm{m}^- = \mathbf{v}_\mathrm{m} + \delta\mathbf{v}_\mathrm{m}^+ - (\mathbf{v}_\mathrm{m} + \delta\mathbf{v}_\mathrm{m}^-)$, which making use of Eq. (4.2) results in

$$\Delta\mathbf{v}_\mathrm{m} = -\left(\mathbf{N}_\mathrm{fm}^{-1}\mathbf{M}_\mathrm{fm} + \mathbf{T}_\mathrm{mo}\mathbf{N}_\mathrm{mo}^{-1}\right)\delta\mathbf{r}_\mathrm{m} \tag{4.3}$$

4.2.2 Primer Vector Theory

The primer vector theory is an indirect method of trajectory optimization, determining the necessary conditions and sufficient conditions for optimality. Particularly for impulsive trajectories, the primer vector provides information on if the trajectory's cost can be decreased by a midcourse impulse by analyzing its magnitude, as well as, the optimal direction, time and position of this impulse.

In 1963 Lawden [Lawden 1963] gave birth to the theory and the term primer vector by defining the necessary conditions for an optimal impulsive trajectory, by examining the limiting conditions on an optimal finite thrust solution. Such conditions are known as Lawden's necessary conditions for an optimal impulsive trajectory. His results, then, specify the conditions that must be satisfied by the primer vector and its derivative on a trajectory that is considered optimal.

Following the work of Lawden, Lion & Handelsman [Lion 1968] developed in 1968 a criterion that improves a reference impulsive trajectory, in this way, reducing the cost. This was achieved by developing a gradient of the cost function with respect to the intermediate position vector and time. This provides the condition under which an additional midcourse impulse or final coast would improve the solution. Based on this method, the minimum cost of an N-impulsive maneuver can be calculated.

Jezewski & Rozendal [Jezewski 1968] in 1968 developed a method to compute a two-body optimal trajectory composed of N-impulses using the primer vector. The method consists in using the gradient vector developed by Lion & Handelsman combined with a conjugate gradient iterator.

In 1971 Jezewski & Faust [Jezewski 1971] developed a theory that describes how a general differential cost function can be evaluated by using inequality constraints on the states and the control variables based on a penalty function approach, also known as cost well. Therefore, a completely general, two-body, N-impulsive, optimal trajectory can be generated for a set of constraints.

Considering the state vector $\mathbf{x}$, formed by the state variables position, velocity and control (define by the direction and magnitude of the thrust) as

$$\mathbf{x}(\mathrm{t}) = \begin{bmatrix} \mathbf{r}(\mathrm{t}) \\ \mathbf{v}(\mathrm{t}) \end{bmatrix} \Rightarrow \dot{\mathbf{x}}(\mathrm{t}) = \mathbf{f}(\mathrm{t}) = \begin{bmatrix} \dot{\mathbf{r}}(\mathrm{t}) \\ \dot{\mathbf{v}}(\mathrm{t}) \end{bmatrix} = \begin{bmatrix} \mathbf{v}(\mathrm{t}) \\ \mathbf{g}(\mathbf{r}) + \mathrm{a_T}(\mathrm{t})\mathbf{u}_\mathrm{T}(\mathrm{t}) \end{bmatrix} \tag{4.4}$$

where, the vectors $\mathbf{r}(\mathrm{t})$ and $\mathbf{v}(\mathrm{t})$ are respectively the spacecraft's position and the velocity, $\mathbf{g}(\mathbf{r}) = \frac{-\mu}{\mathrm{r}^3}\mathbf{r}(\mathrm{t})$ is the gravitational acceleration of the two-body with μ as the standard gravitational parameter, and the control variables are represented by the multiplication $\mathrm{a_T}(\mathrm{t})\mathbf{u}_\mathrm{T}(\mathrm{t})$ is the thrust acceleration and the unity vector in the thrust direction, respectively.

From the dynamic system described above, the Hamiltonian, H, and adjoint equations, ${}^{\mathrm{t}}\boldsymbol{\lambda}_\mathrm{r}$ and ${}^{\mathrm{t}}\boldsymbol{\lambda}_\mathrm{v}$, can be calculate and have the following form:

$$\mathrm{H}(\mathrm{t}) = \mathrm{a_T}(\mathrm{t}) + {}^{\mathrm{t}}\boldsymbol{\lambda}_\mathrm{r}(\mathrm{t})\mathbf{v}(\mathrm{t}) + {}^{\mathrm{t}}\boldsymbol{\lambda}_\mathrm{v}(\mathrm{t})\left(\mathbf{g}(\mathbf{r}) + \mathrm{a_T}(\mathrm{t})\mathbf{u}_\mathrm{T}(\mathrm{t})\right) \tag{4.5}$$

$${}^{\mathrm{t}}\dot{\boldsymbol{\lambda}}_\mathrm{r}(\mathrm{t}) = -\frac{\partial \mathrm{H}(\mathrm{t})}{\partial \mathrm{r}(\mathrm{t})} = -{}^{\mathrm{t}}\boldsymbol{\lambda}_\mathrm{v}(\mathrm{t})\frac{\partial \mathbf{g}(\mathbf{r})}{\partial \mathbf{r}} = -{}^{\mathrm{t}}\boldsymbol{\lambda}_\mathrm{v}(\mathrm{t})\mathbf{G}(\mathbf{r}) \tag{4.6}$$

$${}^{\mathrm{t}}\dot{\boldsymbol{\lambda}}_\mathrm{v}(\mathrm{t}) = -\frac{\partial \mathrm{H}(\mathrm{t})}{\partial \mathrm{v}(\mathrm{t})} = -{}^{\mathrm{t}}\boldsymbol{\lambda}_\mathrm{r}(\mathrm{t}) \tag{4.7}$$

For simplicity, the gravity gradient matrix, $\frac{\partial \mathbf{g}(\mathbf{r})}{\partial \mathbf{r}}$, is written as $\mathbf{G}(\mathbf{r})$. For the case of impulsive maneuvers, the thrust arc can be approximated as an impulse represent by the Dirac delta, δ, having unbounded magnitude and zero duration; additionally it's integration over time is defined as 1 and allows to consider $\int \mathrm{a_T}(\tau)\,\mathrm{d}\tau = \xi\delta(\mathrm{t})$, where ξ is a constant value of the thrust magnitude. Base on the fact that outside of the impulses $\mathrm{a_T}(\mathrm{t})\mathbf{u}_\mathrm{T}(\mathrm{t}) = 0$, the analytical Jacobian matrix of Eq. (4.4) can be written as

$$\frac{\partial \mathbf{f}}{\partial \mathbf{x}}(\mathrm{t}, \mathrm{t_o}) = \begin{bmatrix} \mathbf{O} & \mathbf{I} \\ \mathbf{G} & \mathbf{O} \end{bmatrix} \tag{4.8}$$

where, $\mathbf{I}$ is a 3×3 identity matrix and O is a 3×3 zero matrix. For the impulsive parts, the control variables, $\mathrm{a_T}(\mathrm{t})$ and $\mathbf{u}_\mathrm{T}(\mathrm{t})$, must be chosen to satisfy Pontryagin's minimum principle [Kirk 2004].

In Eq. (4.5), $\mathbf{u}_\mathrm{T}(\mathrm{t})$ is being multiplied by the adjoint vector of the spacecraft's equation of motion ${}^{\mathrm{t}}\boldsymbol{\lambda}_\mathrm{v}(\mathrm{t})$, therefore, in order to minimize H(t), the unit vector $\mathbf{u}_\mathrm{T}(\mathrm{t})$ and ${}^{\mathrm{t}}\boldsymbol{\lambda}_\mathrm{v}(\mathrm{t})$ are chosen parallel in opposite directions, generating the largest possible negative value, Eq. (4.9).

$$\mathbf{u}_\mathrm{T}(\mathrm{t}) = -\frac{\boldsymbol{\lambda}_\mathrm{v}(\mathrm{t})}{|\boldsymbol{\lambda}_\mathrm{v}(\mathrm{t})|} \tag{4.9}$$

Due to the importance of the vector $\boldsymbol{\lambda}_\mathrm{v}(\mathrm{t})$ Lawden named it primer vector.

Applying Eqs. (4.6), (4.7) and (4.9) on the Hamiltonian,

$$\mathrm{H}(\mathrm{t}) = \mathrm{a_T}(\mathrm{t})(1-\lambda_\mathrm{v}(\mathrm{t})) - {}^{\mathrm{t}}\dot{\boldsymbol{\lambda}}_\mathrm{v}(\mathrm{t})\mathbf{v}(\mathrm{t}) + {}^{\mathrm{t}}\boldsymbol{\lambda}_\mathrm{v}(\mathrm{t})\mathbf{g}(\mathbf{r}) \tag{4.10}$$

it is possible to notice that it is a linear function of $\mathrm{a_T}(\mathrm{t})$ and, therefore, the minimum value of Eq. (4.10) will depend on the sign of the of the coefficient $(1-\lambda_\mathrm{v}(\mathrm{t}))$. For values of $\lambda_\mathrm{v}(\mathrm{t}) \geq 1$, $\mathrm{a_T}(\mathrm{t}) = \mathrm{a_{Tmax}} = \xi$ and for values of $\lambda_\mathrm{v}(\mathrm{t}) < 1$, $\mathrm{a_T}(\mathrm{t}) = \mathrm{a_{Tmin}} = 0$. In conclusion, to minimize H the impulses will take place when the value of the primer vector reaches 1.

In order to obtain the primer vector's evolution, Eq. (4.7) can be differentiated once more and merged with Eq. (4.6), taking into account that the matrix $\mathbf{G}(\mathbf{r})$ is symmetric,

$$\ddot{\boldsymbol{\lambda}}_\mathrm{v}(\mathrm{t}) = {}^{\mathrm{t}}\boldsymbol{\lambda}_\mathrm{v}(\mathrm{t})\mathbf{G}(\mathbf{r}) = \mathbf{G}(\mathbf{r})\boldsymbol{\lambda}_\mathrm{v}(\mathrm{t}) \tag{4.11}$$

The resulting primer vector evolution in state space form, using Eq. (4.8), can be written in state space form as

$$\begin{bmatrix} \boldsymbol{\lambda}_\mathrm{v}(\mathrm{t}) \\ \dot{\boldsymbol{\lambda}}_\mathrm{v}(\mathrm{t}) \end{bmatrix} = \boldsymbol{\Phi}(\mathrm{t},\mathrm{t_o}) \begin{bmatrix} \boldsymbol{\lambda}_\mathrm{v}(\mathrm{t_o}) \\ \dot{\boldsymbol{\lambda}}_\mathrm{v}(\mathrm{t_o}) \end{bmatrix} \tag{4.12}$$

Moreover, the variation of perturbation on the states can also be evaluated with the same transition matrix in a similar way, resulting in

$$\begin{bmatrix} \boldsymbol{\delta}\dot{\mathbf{r}}(\mathrm{t}) \\ \boldsymbol{\delta}\dot{\mathbf{v}}(\mathrm{t}) \end{bmatrix} = \boldsymbol{\Phi}(\mathrm{t},\mathrm{t_o}) \begin{bmatrix} \boldsymbol{\delta}\mathbf{r}(\mathrm{t_o}) \\ \boldsymbol{\delta}\mathbf{v}(\mathrm{t_o}) \end{bmatrix} \tag{4.13}$$

using the second order form of Eqs. (4.12) and (4.13)

$$\begin{cases} \ddot{\boldsymbol{\lambda}}_\mathrm{v}(\mathrm{t}) = \mathbf{G}(\mathbf{r})\boldsymbol{\lambda}_\mathrm{v}(\mathrm{t}) \\ \boldsymbol{\delta}\ddot{\mathbf{r}}(\mathrm{t}) = \mathbf{G}(\mathbf{r})\boldsymbol{\delta}\mathbf{r}(\mathrm{t}) \end{cases} \tag{4.14}$$

multiplying the first equation by $\boldsymbol{\delta}\mathbf{r}^\mathrm{t}(\mathrm{t})$, the second by $\boldsymbol{\lambda}^\mathrm{t}{}_\mathrm{v}(\mathrm{t})$ and subtracting them the following relation is obtain

$$\boldsymbol{\delta}\mathbf{r}^\mathrm{t}(\mathrm{t})\ddot{\boldsymbol{\lambda}}_\mathrm{v}(\mathrm{t}) - \boldsymbol{\lambda}^\mathrm{t}{}_\mathrm{v}(\mathrm{t})\boldsymbol{\delta}\ddot{\mathbf{r}}(\mathrm{t}) = \boldsymbol{\delta}\mathbf{r}^\mathrm{t}(\mathrm{t})\mathbf{G}(\mathbf{r})\boldsymbol{\lambda}_\mathrm{v}(\mathrm{t}) - \boldsymbol{\lambda}^\mathrm{t}{}_\mathrm{v}(\mathrm{t})\mathbf{G}(\mathbf{r})\boldsymbol{\delta}\mathbf{r}_\mathrm{m} = 0 \tag{4.15}$$

by adding and subtracting $\dot{\boldsymbol{\lambda}}^\mathrm{t}{}_\mathrm{v}(\mathrm{t})\boldsymbol{\delta}\mathbf{v}(\mathrm{t})$ and knowing that $\boldsymbol{\delta}\ddot{\mathbf{r}}(\mathrm{t}) = \boldsymbol{\delta}\dot{\mathbf{v}}(\mathrm{t})$, the relation becomes

$$\boldsymbol{\delta}\mathbf{r}^\mathrm{t}(\mathrm{t})\ddot{\boldsymbol{\lambda}}_\mathrm{v}(\mathrm{t}) + \dot{\boldsymbol{\lambda}}^\mathrm{t}{}_\mathrm{v}(\mathrm{t})\boldsymbol{\delta}\mathbf{v}(\mathrm{t}) - \boldsymbol{\lambda}^\mathrm{t}{}_\mathrm{v}(\mathrm{t})\boldsymbol{\delta}\dot{\mathbf{v}}(\mathrm{t}) - \dot{\boldsymbol{\lambda}}^\mathrm{t}{}_\mathrm{v}(\mathrm{t})\boldsymbol{\delta}\mathbf{v}(\mathrm{t}) = 0 \tag{4.16}$$

which can be simplify as the total derivative over time of

$$\frac{\mathrm{d}}{\mathrm{dt}}(\boldsymbol{\lambda}^{\mathrm{t}}{}_{\mathrm{v}}(\mathrm{t})\boldsymbol{\delta}\mathbf{v}(\mathrm{t})-\dot{\boldsymbol{\lambda}}^{\mathrm{t}}{}_{\mathrm{v}}(\mathrm{t})\boldsymbol{\delta}\mathbf{r}(\mathrm{t}))=0 \tag{4.17}$$

by integrating the above equation one obtains

$$\boldsymbol{\lambda}_{\mathrm{v}}(\mathrm{t})\boldsymbol{\delta}\mathbf{v}(\mathrm{t})-\dot{\boldsymbol{\lambda}}_{\mathrm{v}}(\mathrm{t})\boldsymbol{\delta}\mathbf{r}(\mathrm{t})=\mathrm{const} \tag{4.18}$$

that is valid for any interval between to impulses.

4.3 Weighted Cost Function

The cost function used in this work takes into account the transfer terminal constraints, the sum of weighted Δv's along the trajectory

$$\mathrm{J}=\mathrm{K_o}\left|\Delta\mathbf{v}_{\mathrm{o}}\right|+\mathrm{K_m}\left|\Delta\mathbf{v}_{\mathrm{m}}\right|+\mathrm{K_f}\left|\Delta\mathbf{v}_{\mathrm{f}}\right| \tag{4.19}$$

At each point of the trajectory the velocity increments can be provided by different systems and at distinct dynamical environments. Therefore, the cost function is defined with each velocity increments associate with one constant, K. More details and the evaluations of the weights are address in section **V**.

As performed in the works [Lion 1968, Jezewski 1968, Jezewski 1971], the midcourse impulse, $\Delta\mathbf{v}_{\mathrm{m}}$, can be written as a function of the control parameters. For the optimality, the direction of the impulse needs to be parallel to the primer vector (Eq. (4.9)), which leaves the magnitude of the impulse, ξ, remaining to be calculated,

$$\Delta\mathbf{v}_{\mathrm{m}}=-\xi\frac{\boldsymbol{\lambda}_{\mathrm{v}}(\mathrm{t_m})}{|\boldsymbol{\lambda}_{\mathrm{v}}(\mathrm{t_m})|}=\xi\mathbf{u}_{\mathrm{T}}\left(\mathrm{t_m}\right) \tag{4.20}$$

with the control variable $\mathbf{u}_{\mathrm{T}}(\mathrm{t})$ bounded, the remaining control to be optimized is the impulse magnitude ξ, which is defined by the time of the impulse, $\mathrm{t_m}$ and its position, $\mathbf{r}_{\mathrm{m}}$.

Using Eqs. (4.19) and (4.20), the final form of the cost function becomes

$$\mathrm{J}=\mathrm{K_o}\left|\Delta\mathbf{v}_{\mathrm{o}}\right|+\mathrm{K_m}\xi+\mathrm{K_f}\left|\Delta\mathbf{v}_{\mathrm{f}}\right| \tag{4.21}$$

The cost's gradient around the optimal trajectory

$$\nabla\mathrm{J}=\begin{bmatrix}\frac{\partial\mathrm{J}}{\partial\mathrm{t_m}}\\ \frac{\partial\mathrm{J}}{\partial\mathbf{r}_{\mathrm{m}}}\end{bmatrix} \tag{4.22}$$

can be calculated by using the following relations: the first order relation between the non-linear and linear systems,

$$\mathrm{d}\mathbf{r}_{\mathrm{m}}=\boldsymbol{\delta}\mathbf{r}_{\mathrm{m}}+\dot{\mathbf{r}}_{\mathrm{m}}\mathrm{dt_m} \tag{4.23}$$

and the modular relation for the velocity vectors where

$$|\Delta\mathbf{v}-\boldsymbol{\delta}\mathbf{v}|-|\Delta\mathbf{v}|=\frac{\Delta^{\mathrm{t}}\mathbf{v}}{|\Delta\mathbf{v}|}\boldsymbol{\delta}\mathbf{v}=\frac{{}^{\mathrm{t}}\boldsymbol{\lambda}_{\mathrm{v}}}{|\boldsymbol{\lambda}_{\mathrm{v}}|}\boldsymbol{\delta}\mathbf{v} \tag{4.24}$$

having $\boldsymbol{\lambda}_{\mathrm{v}}$ in the direction of the impulse as the necessary condition for optimality and with maximum value equal to one at the time of impulse, $\frac{\Delta\mathbf{v}(\mathrm{t_i})}{|\Delta\mathbf{v}(\mathrm{t_i})|}=\boldsymbol{\lambda}_{\mathrm{v}}(\mathrm{t_i})$ (i = *o*, *m* and *f*), as derived before. Base on the above relations, it is assumed a comparison between a reference, $|\Delta\mathbf{v}_{\mathrm{m}}|=\left|\mathbf{v}_{\mathrm{m}}^{+}-\mathbf{v}_{\mathrm{m}}^{-}\right|$, and a perturbed orbit, $|\Delta\mathbf{v}_{\mathrm{m}}|=\left|\mathbf{v}_{\mathrm{m}}^{+}+\boldsymbol{\delta}\mathbf{v}_{\mathrm{m}}^{+}-(\mathbf{v}_{\mathrm{m}}^{-}+\boldsymbol{\delta}\mathbf{v}_{\mathrm{m}}^{-})\right|$, and the difference of both costs is

$$\begin{aligned}\mathrm{dJ}&=\mathrm{J_{pert}}-\mathrm{J_{ref}}\\&=\mathrm{K_o}\,|\Delta\mathbf{v}_{\mathrm{o}}+\boldsymbol{\delta}\mathbf{v}_{\mathrm{o}}|+\mathrm{K_m}\left|\mathbf{v}_{\mathrm{m}}^{+}+\boldsymbol{\delta}\mathbf{v}_{\mathrm{m}}^{+}-(\mathbf{v}_{\mathrm{m}}^{-}+\boldsymbol{\delta}\mathbf{v}_{\mathrm{m}}^{-})\right|+\mathrm{K_f}\,|\Delta\mathbf{v}_{\mathrm{f}}-\boldsymbol{\delta}\mathbf{v}_{\mathrm{f}}|\\&\quad-\mathrm{K_o}\,|\Delta\mathbf{v}_{\mathrm{o}}|-\mathrm{K_m}\left|\mathbf{v}_{\mathrm{m}}^{+}-\mathbf{v}_{\mathrm{m}}^{-}\right|-\mathrm{K_f}\,|\Delta\mathbf{v}_{\mathrm{f}}|\\&=\mathrm{K_o}\,(|\Delta\mathbf{v}_{\mathrm{o}}+\boldsymbol{\delta}\mathbf{v}_{\mathrm{o}}|-|\Delta\mathbf{v}_{\mathrm{o}}|)+\mathrm{K_m}(\left|\mathbf{v}_{\mathrm{m}}^{+}-\mathbf{v}_{\mathrm{m}}^{-}+(\boldsymbol{\delta}\mathbf{v}_{\mathrm{m}}^{+}-\boldsymbol{\delta}\mathbf{v}_{\mathrm{m}}^{-})\right|-\left|\mathbf{v}_{\mathrm{m}}^{+}-\mathbf{v}_{\mathrm{m}}^{-}\right|)\\&\quad+\mathrm{K_f}\,(|\Delta\mathbf{v}_{\mathrm{f}}-\boldsymbol{\delta}\mathbf{v}_{\mathrm{f}}|-|\Delta\mathbf{v}_{\mathrm{f}}|)\end{aligned} \tag{4.25}$$

where, the Δv represent the values in the reference trajectory. Using Eq. (4.24) in the above relation it becomes

$$\mathrm{dJ}=\mathrm{K_o}{}^{\mathrm{t}}\boldsymbol{\lambda}_{\mathrm{v}}(\mathrm{t_o})\,\boldsymbol{\delta}\mathbf{v}_{\mathrm{o}}+\mathrm{K_m}{}^{\mathrm{t}}\boldsymbol{\lambda}_{\mathrm{v}}(\mathrm{t_m})\left(\boldsymbol{\delta}\mathbf{v}_{\mathrm{m}}^{+}-\boldsymbol{\delta}\mathbf{v}_{\mathrm{m}}^{-}\right)-\mathrm{K_f}{}^{\mathrm{t}}\boldsymbol{\lambda}_{\mathrm{v}}(\mathrm{t_f})\,\boldsymbol{\delta}\mathbf{v}_{\mathrm{f}} \tag{4.26}$$

Meanwhile, using relation (4.18) at the trajectory's beginning or end until the point of the midcourse impulse we obtain

$$\begin{cases}{}^{\mathrm{t}}\boldsymbol{\lambda}_{\mathrm{v}}(\mathrm{t_o})\boldsymbol{\delta}\mathbf{v}_{\mathrm{o}}-{}^{\mathrm{t}}\dot{\boldsymbol{\lambda}}_{\mathrm{v}}(\mathrm{t_o})\boldsymbol{\delta}\mathbf{r}_{\mathrm{o}}={}^{\mathrm{t}}\boldsymbol{\lambda}_{\mathrm{v}}(\mathrm{t_m})\boldsymbol{\delta}\mathbf{v}_{\mathrm{m}}^{-}-{}^{\mathrm{t}}\dot{\boldsymbol{\lambda}}_{\mathrm{v}}^{-}(\mathrm{t_m})\boldsymbol{\delta}\mathbf{r}_{\mathrm{m}}^{-}\\{}^{\mathrm{t}}\boldsymbol{\lambda}_{\mathrm{v}}(\mathrm{t_f})\boldsymbol{\delta}\mathbf{v}_{\mathrm{f}}-{}^{\mathrm{t}}\dot{\boldsymbol{\lambda}}_{\mathrm{v}}(\mathrm{t_f})\boldsymbol{\delta}\mathbf{r}_{\mathrm{f}}={}^{\mathrm{t}}\boldsymbol{\lambda}_{\mathrm{v}}(\mathrm{t_m})\boldsymbol{\delta}\mathbf{v}_{\mathrm{m}}^{+}-{}^{\mathrm{t}}\dot{\boldsymbol{\lambda}}_{\mathrm{v}}^{+}(\mathrm{t_m})\boldsymbol{\delta}\mathbf{r}_{\mathrm{m}}^{+}\end{cases} \tag{4.27}$$

and applying on Eq. (4.26), remembering that the initial and final positions must remain the same, $\boldsymbol{\delta}\mathbf{r}_{\mathrm{o}}=\boldsymbol{\delta}\mathbf{r}_{\mathrm{f}}=0$,

$$\begin{aligned}\mathrm{dJ}=\mathrm{K_o}&\left({}^{\mathrm{t}}\boldsymbol{\lambda}_{\mathrm{v}}(\mathrm{t_m})\,\boldsymbol{\delta}\mathbf{v}_{\mathrm{m}}^{-}-{}^{\mathrm{t}}\dot{\boldsymbol{\lambda}}_{\mathrm{v}}^{-}(\mathrm{t_m})\,\boldsymbol{\delta}\mathbf{r}_{\mathrm{m}}^{-}\right)+\mathrm{K_m}{}^{\mathrm{t}}\boldsymbol{\lambda}_{\mathrm{v}}(\mathrm{t_m})\left(\boldsymbol{\delta}\mathbf{v}_{\mathrm{m}}^{+}-\boldsymbol{\delta}\mathbf{v}_{\mathrm{m}}^{-}\right)\\&+\mathrm{K_f}\left(-{}^{\mathrm{t}}\boldsymbol{\lambda}_{\mathrm{v}}(\mathrm{t_m})\,\boldsymbol{\delta}\mathbf{v}_{\mathrm{m}}^{+}+{}^{\mathrm{t}}\dot{\boldsymbol{\lambda}}_{\mathrm{v}}^{+}(\mathrm{t_m})\,\boldsymbol{\delta}\mathbf{r}_{\mathrm{m}}^{+}\right)\end{aligned} \tag{4.28}$$

$$\mathrm{dJ}={}^{\mathrm{t}}\boldsymbol{\lambda}_{\mathrm{v}}(\mathrm{t_m})\left[(\mathrm{K_o}-\mathrm{K_m})\,\boldsymbol{\delta}\mathbf{v}_{\mathrm{m}}^{-}+(\mathrm{K_m}-\mathrm{K_f})\,\boldsymbol{\delta}\mathbf{v}_{\mathrm{m}}^{+}\right]+\mathrm{K_f}{}^{\mathrm{t}}\dot{\boldsymbol{\lambda}}_{\mathrm{v}}^{+}(\mathrm{t_m})\,\boldsymbol{\delta}\mathbf{r}_{\mathrm{m}}^{+}-\mathrm{K_o}{}^{\mathrm{t}}\dot{\boldsymbol{\lambda}}_{\mathrm{v}}^{-}(\mathrm{t_m})\,\boldsymbol{\delta}\mathbf{r}_{\mathrm{m}}^{-} \tag{4.29}$$

Applying Eq. (4.23) to the perturbed trajectory we obtain

$$\begin{cases}\boldsymbol{\delta}\mathbf{r}_{\mathrm{m}}^{-}=\mathrm{d}\mathbf{r}_{\mathrm{m}}-\mathbf{v}_{\mathrm{m}}^{-}\mathrm{dt_m}\\\boldsymbol{\delta}\mathbf{r}_{\mathrm{m}}^{+}=\mathrm{d}\mathbf{r}_{\mathrm{m}}-\mathbf{v}_{\mathrm{m}}^{+}\mathrm{dt_m}\end{cases} \tag{4.30}$$

with this and Eq. (4.2) into Eq. (4.29) we obtain

$$\mathrm{dJ}=\left(\Lambda_1+\mathrm{K_f}{}^{\mathrm{t}}\dot{\boldsymbol{\lambda}}_{\mathrm{v}}^{+}(\mathrm{t_m})-\mathrm{K_o}{}^{\mathrm{t}}\dot{\boldsymbol{\lambda}}_{\mathrm{v}}^{-}(\mathrm{t_m})\right)\mathrm{d}\mathbf{r}_{\mathrm{m}}+\left(\Lambda_2+\mathrm{K_o}{}^{\mathrm{t}}\dot{\boldsymbol{\lambda}}_{\mathrm{v}}^{-}(\mathrm{t_m})\,\mathbf{v}_{\mathrm{m}}^{-}-\mathrm{K_3}{}^{\mathrm{t}}\dot{\boldsymbol{\lambda}}_{\mathrm{v}}^{+}(\mathrm{t_m})\,\mathbf{v}_{\mathrm{m}}^{+}\right)\mathrm{dt_m} \tag{4.31}$$

where,

$$\begin{cases}\Lambda_1={}^{\mathrm{t}}\boldsymbol{\lambda}_{\mathrm{v}}(\mathrm{t_m})\left[(\mathrm{K_o}-\mathrm{K_m})\,\mathbf{T}_{\mathrm{mo}}\mathbf{N}_{\mathrm{mo}}^{-1}+(\mathrm{K_f}-\mathrm{K_m})\,\mathbf{N}_{\mathrm{fm}}^{-1}\mathbf{M}_{\mathrm{fm}}\right]\\\Lambda_2={}^{\mathrm{t}}\boldsymbol{\lambda}_{\mathrm{v}}(\mathrm{t_m})\left[(\mathrm{K_m}-\mathrm{K_o})\,\mathbf{T}_{\mathrm{mo}}\mathbf{N}_{\mathrm{mo}}^{-1}\mathbf{v}_{\mathrm{m}}^{-}+(\mathrm{K_m}-\mathrm{K_f})\,\mathbf{N}_{\mathrm{fm}}^{-1}\mathbf{M}_{\mathrm{fm}}\mathbf{v}_{\mathrm{m}}^{+}\right]\end{cases} \tag{4.32}$$

Finally, the gradient of J around the optimal trajectory can be calculated as

$$\nabla \mathrm{J} = \begin{bmatrix} \frac{\partial \mathrm{J}}{\partial \mathrm{t_m}} \\ \frac{\partial \mathrm{J}}{\partial \mathbf{r}_\mathrm{m}} \end{bmatrix} = \begin{bmatrix} \Lambda_2 + \mathrm{K_o}{}^{\mathrm{t}}\dot{\boldsymbol{\lambda}}_\mathrm{v}^{-}(\mathrm{t_m})\,\mathbf{v}_\mathrm{m}^{-} - \mathrm{K_f}{}^{\mathrm{t}}\dot{\boldsymbol{\lambda}}_\mathrm{v}^{+}(\mathrm{t_m})\,\mathbf{v}_\mathrm{m}^{+} \\ \Lambda_1 + \mathrm{K_f}{}^{\mathrm{t}}\dot{\boldsymbol{\lambda}}_\mathrm{v}^{+}(\mathrm{t_m}) - \mathrm{K_o}{}^{\mathrm{t}}\dot{\boldsymbol{\lambda}}_\mathrm{v}^{-}(\mathrm{t_m}) \end{bmatrix} \tag{4.33}$$

Having defined the time and position of the impulse, the cost function can be obtained by solving two successive Lambert problems from $(\mathbf{r}_\mathrm{o}, \mathrm{t_o}) \rightarrow (\mathbf{r}_\mathrm{m} + \boldsymbol{\delta}\mathbf{r}_\mathrm{m}, \mathrm{t_m})$ and $(\mathbf{r}_\mathrm{m} + \boldsymbol{\delta}\mathbf{r}_\mathrm{m}, \mathrm{t_m}) \rightarrow (\mathbf{r}_\mathrm{f}, \mathrm{t_f})$, which will provide $\Delta\mathbf{v}_\mathrm{o}$, $\Delta\mathbf{v}_\mathrm{f}$ and $\Delta\mathbf{v}_\mathrm{m}$. Then, the magnitude of the impulse can be obtained by evaluating the solution generated by the combination of the $\mathrm{t_m}$ and $\mathbf{r}_\mathrm{m}$.

The optimal control problem is then set in the following way:

- Solve the Lambert problem (non-linear model);
- Linearize the solution in order to calculate ∇J using the result of the minimal principle;
- Use the gradient to evaluate the best direction to decrease the cost;
- Adjust $\mathrm{t_m}$ and $\mathbf{r}_\mathrm{m}$ accordingly; and
- Repeat the above steps until ∇J has all its values smaller than the desired tolerance.

Once the single midcourse impulsive solution is obtained the primer vector magnitude can be analyzed and if it reaches values higher than 1 (point to minimize H as derived in section 4.2.2), the trajectory's cost can be further decreased by the addition of another impulse. Then the above process can be repeated for each leg until the primer vector's magnitude is smaller than 1 during the whole trajectory.

The above gradient may generate a discontinuity on the primer vector's derivative and Hamiltonian depending on the choice of the weights. This discontinuities would violate the classic necessary conditions for optimality characterizing a non-optimal trajectory. However, the classic necessary conditions were derived using the non-weighted cost function, $\mathrm{K_o} = \mathrm{K_m} = \mathrm{K_f} = 1$, that has its gradient

$$\nabla \mathrm{J}_{\mathrm{classic}} = \begin{bmatrix} {}^{\mathrm{t}}\dot{\boldsymbol{\lambda}}_\mathrm{v}^{-}(\mathrm{t_m})\,\mathbf{v}_\mathrm{m}^{-} - {}^{\mathrm{t}}\dot{\boldsymbol{\lambda}}_\mathrm{v}^{+}(\mathrm{t_m})\,\mathbf{v}_\mathrm{m}^{+} \\ \dot{\boldsymbol{\lambda}}_\mathrm{v}^{+}(\mathrm{t_m}) - \dot{\boldsymbol{\lambda}}_\mathrm{v}^{-}(\mathrm{t_m}) \end{bmatrix} = \begin{bmatrix} \mathrm{H_m^-} - \mathrm{H_m^+} \\ \dot{\boldsymbol{\lambda}}_\mathrm{v}^{+}(\mathrm{t_m}) - \dot{\boldsymbol{\lambda}}_\mathrm{v}^{-}(\mathrm{t_m}) \end{bmatrix} \tag{4.34}$$

which in the optimal condition gives

$$\nabla \mathrm{J}_{\mathrm{classic}} = \begin{bmatrix} \mathrm{H_m^-} - \mathrm{H_m^+} \\ \dot{\boldsymbol{\lambda}}_\mathrm{v}^{+}(\mathrm{t_m}) - \dot{\boldsymbol{\lambda}}_\mathrm{v}^{-}(\mathrm{t_m}) \end{bmatrix} = \begin{bmatrix} 0 \\ 0 \end{bmatrix} \Rightarrow \begin{cases} \mathrm{H_m^-} = \mathrm{H_m^+} \\ \dot{\boldsymbol{\lambda}}_\mathrm{v}^{+}(\mathrm{t_m}) = \dot{\boldsymbol{\lambda}}_\mathrm{v}^{-}(\mathrm{t_m}) \end{cases} \tag{4.35}$$

Therefore, the classic necessary conditions are still valid for Eq. (4.33) if the weighting matrices are all equal to one, but other wise they do not provide the continuity on the Hamiltonian and primer vector's derivative. Nevertheless, it is important to point out that the gradient of the weighted cost function is still being converged to zero and, most important, Lawden's necessary condition for optimality for an impulsive trajectory [Lawden 1963], which provides the direction of the impulse, are still being complied.

4.4 Weighting Constants

In the first part of the trajectory where the spacecraft is escaping from Earth, $\Delta\mathrm{v_o}$ can be understood as the excess velocity, v_∞, at departure, which can be changed considerably by a small velocity increment at the perigee of the departing orbit. The $\Delta\mathrm{v_f}$ is the increment provided at the end of the transfer which for a flyby mission typically needs to be provided only if the flyby velocity is too high for the spacecraft's instruments to perform measurements. But for a rendezvous case it is required to match the spacecraft's velocity with the target's velocity. Therefore, $\Delta\mathrm{v_m}$ is the most critical element in the case of a flyby mission since it will decrease the cost and can only be controlled by a direct engine burn.

The constant $\mathrm{K_o}$ is directly related to $\Delta\mathrm{v_o}$, which, in the first arc of the transfer, is the planet's hyperbolic excess velocity calculated based on the perigee of the departing orbit. The fact that $\Delta\mathrm{v_o}$ can be altered with a relative small velocity increment at perigee makes it less critical for the cost. Note also that the $\Delta\mathrm{v_o}$ can be provided entirely by the launch vehicle. From classical celestial mechanics, the relation between the excess velocity and a circular planetary parking orbit is

$$\Delta\mathrm{v_{inj}} = |\mathbf{v}_\mathrm{p} - \mathbf{v}_\mathrm{LEO}| = \sqrt{\frac{2\mu}{\mathrm{r_p}} + \Delta\mathrm{v_o^2}} - \sqrt{\frac{\mu}{\mathrm{r_p}}} \tag{4.36}$$

where, $\mathbf{v}_\mathrm{p}$ is the velocity at the perigee of the escape orbit, $\mathbf{v}_\mathrm{LEO}$ is the velocity on the Earth's circular parking orbit, $\Delta\mathrm{v_{inj}}$ is the velocity increment at the orbit's perigee, $\mathrm{r_p}$ is the perigee's radius and μ is the Earth's gravitational parameter. Eq. (4.36) allows us to make the relation between the injection and excess velocities taking into account that an increase of $\Delta\mathrm{v_o}$ can be easily made at the perigee. The relation for $\mathrm{K_o}$ can be then evaluated as

$$\mathrm{K_o} = \frac{\Delta\mathrm{v_{inj}} - \Delta\mathrm{v_{inj0}}}{\Delta\mathrm{v_o}} \mathrm{K_m} \tag{4.37}$$

where $\Delta\mathrm{v_{inj0}}$ can be calculated by Eq. (4.36) with $\Delta\mathrm{v_o} = 0$. This makes $\mathrm{K_o}$ a function of the perigee's radius, the magnitude of the excess velocity and $\mathrm{K_m}$, $\mathrm{K_o} = \mathrm{K_o}(\mathrm{r_p}, \Delta\mathrm{v_o}, \mathrm{K_m})$. As the $\Delta\mathrm{v_o}$ is always larger than the injection velocity, $\mathrm{K_o}$ will always be smaller than $\mathrm{K_m}$. The reason for formulating the relationship as in Eq. (4.37) can be better understood by the fact that, hypothetically, the cost function considers the actual velocity increment provided at the perigee of the escape orbit since the $\Delta\mathrm{v_0}$ from $\mathrm{K_o}$ and from the cost function will cancel each other, as such:

$$\mathrm{J} = \frac{\Delta\mathrm{v_{inj}} - \Delta\mathrm{v_{inj0}}}{\Delta\mathrm{v_o}} \mathrm{K_m} |\Delta\mathbf{v}_\mathrm{o}| + \mathrm{K_m} |\Delta\mathbf{v}_\mathrm{m}| + \mathrm{K_f} |\Delta\mathbf{v}_\mathrm{f}| \tag{4.38}$$

$$\mathrm{J} = \mathrm{K_m}(\Delta\mathrm{v_{inj}} - \Delta\mathrm{v_{inj0}}) + \mathrm{K_m} |\Delta\mathbf{v}_\mathrm{m}| + \mathrm{K_f} |\Delta\mathbf{v}_\mathrm{f}| \tag{4.39}$$

The constant $\mathrm{K_m}$ multiplies the midcourse impulse can be seen as the most important element, for it relates with the factor that will decrease the cost; $\Delta\mathrm{v_m}$ is the main reason why the new trajectory represents an advantage over the two-impulse one, therefore, it is necessary to make sure that a second impulse will, in fact, improve the transfer. Due to its degree of importance, $\mathrm{K_m}$ can be assigned the highest value and the other two will follow based on this value.

The constant $\mathrm{K_f}$ relates to the final part of the transfer. Typically, single flyby missions do not require any Δv allowing $\mathrm{K_f} = 0$ and simplifying the problem by making it sensitive only to the initial and midcourse impulses. For rendezvous missions, however, $\mathrm{K_f}$ is critical, adjusting the importance of the arrival velocity compared to the others; in dealing with asteroid rendezvous the final speed correction is typically a deep space maneuver, much like $\mathrm{K_m}$, conferring it $\mathrm{K_f} = \mathrm{K_m}$. For the case of planetary orbit injection, the variable $\mathrm{K_f}$ is no longer associated with a deep space maneuver. Rather, it is link to an hyperbolic arrival, which could be evaluated similar to $\mathrm{K_o}$. Due to the focus of this work, planetary orbit injection cases will not be address here. Finally, it is important to point out that the reduction of the total transfer $\Delta\mathrm{v} = \Delta\mathrm{v_o} + \Delta\mathrm{v_m} + \Delta\mathrm{v_f}$ is not necessarily assured by this procedure. It may yield a large sum of Δvs if the relation between the Ks provide a lower cost.

4.5 Test Cases

This section is dedicated to present test cases that compare the weighted method in three different mission scenarios: the flyby of the asteroid Phaethon, possible parent body of the Geminid meteor shower and candidate target for the OSIRIS-Rex and Deep Impact missions, an example of asteroid selection for the PROCYON mission, and rendezvous with asteroid Itokawa, target of the first successful asteroid sample return mission. In these application examples, the Earth and asteroids' positions were obtained using NASA's Horizon system. The results of the weighted method are compare with a gradient-based direct method the interior point algorithm [Byrd 2000, Byrd 1999] with the gradient calculated by central finite differences. The interior point algorithm is suited for small dense problems satisfying the bounds at every iteration. Since both algorithms are local optimizers, the initial guess is the same for both the indirect and direct methods. It is important, however, to point out that the direct method provides no clues as to whether the trajectory's cost can be decreased by the addition of a midcourse impulse nor if the resulting trajectory is optimal. The designer could keep adding impulses to the transfer legs and evaluate to see if it improves the result. However, as the direct method provides only the local optimal, the results do not guarantee a global optimum; this means that even if the addition of a midcourse impulse generates a more expensive result this solution is local and another trajectory with the same number of impulses in different positions could result in a smaller cost. As oppose to the extensive search process required by the direct method, the PVT will, for every trajectory, point out if the cost can be improved independently from the initial guess or the resulting optimization. This is possible by analyzing if the evolution of the primer vector magnitude reaches values higher than one, as detailed in section 4.3.

For the Phaethon test case, the reference orbit is chosen as a simple ballistic transfer from Earth to Phaethon (section 3.4.1, Fig. 3.3a), obtained by solving the Lambert problem [Battin 1999, Vallado 2007, Wagner 2011, Shen 2003, Arora 2010] departing on September 2024 and flying by Phaethon on July 2025, Fig. 4.2 (see chapter 3 for details on the ballistic trajectory design). The baseline transfer chosen for this example results in a Lambert solution with an excess velocity of nearly 6 km/s. This is a relatively large $\Delta\mathrm{v_o}$ and this date could be considered non feasible for some missions.

The PVT can be applied to the Earth-Phaethon transfer using the classical $\mathrm{K_o} = \mathrm{K_m} = \mathrm{K_f} = 1$

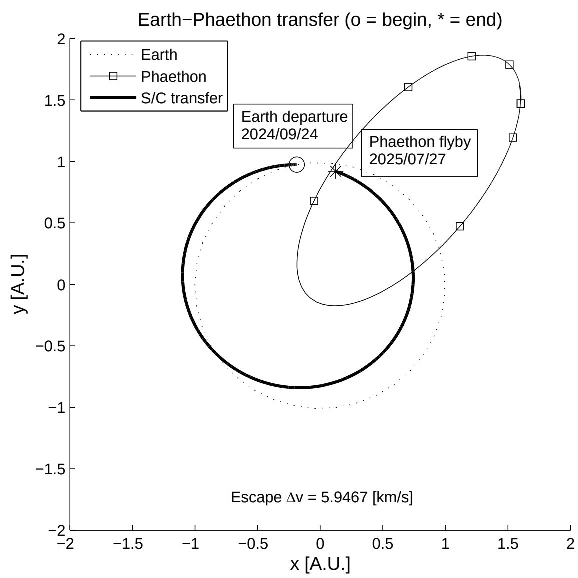

Figure 4.2: Earth-Phaethon flyby transfer sequence

formulation which generates the solution depicted on Fig. 4.3, where the excess velocity is increased to more than 14 km/s. The optimization also results in a large midcourse impulse, this is due to the fact that the cost function is also considering the final $\Delta \mathrm{v_f}$ in the minimization process which is not delivered in this case. The arrival conditions at Phaethon can be taken into account and the classical PVT formulation can be modified by setting $\mathrm{K_f} = 0$, since the $\Delta \mathrm{v_f}$ is out of interest in this case. The resulting transfer, Fig. 4.4, presents a considerable decrease in the excess velocity with the addition of a midcourse impulse, $\Delta \mathrm{v_o} = 1.4043$ and $\Delta \mathrm{v_m} = 0.54855$ km/s. The initial excess velocity is typically achieved by accelerating the spacecraft from a low Earth orbit (LEO), which gives less priority to the reduction of the excess velocity since $\mathrm{K_o}$ is smaller than $\mathrm{K_m}$. Following, $\mathrm{K_o}$ can also be considered as calculated by Eq. (4.37), where the perigee altitude is assumed to be at 300 km. Figure 4.5a presents the resulting transfer with $\Delta \mathrm{v_{inj}} = 4.009$ ($\Delta \mathrm{v_o} = 4.2813$) and $\Delta \mathrm{v_m} = 0.34245$ km/s. Note that the magnitude of the primer vector (Fig. 4.5b) is not smaller than 1 during the first leg, which means that the trajectory's cost can be further reduced by adding another midcourse impulse to it. The optimization process is then continued checking the primer vector evolution and adding midcourse impulses in the legs where the magnitude is still above 1. The resulting optimized trajectory is shown in Fig. 4.6a where the total cost is 4.2926 [km/s], $\Delta \mathrm{v_{inj}} = 3.9785$ ($\Delta \mathrm{v_o} = 4.1971$) and sum of $\Delta \mathrm{v_m} = 0.3134$ km/s ($\Delta \mathrm{v_{m1}} = 0.004352$, $\Delta \mathrm{v_{m2}} = 0.003026$, $\Delta \mathrm{v_{m3}} = 1.98852\mathrm{e}-06$, $\Delta \mathrm{v_{m4}} = 0.01669$, $\Delta \mathrm{v_{m5}} = 5.5831856\mathrm{e}-06$, $\Delta \mathrm{v_{m6}} = 0.1325$, $\Delta \mathrm{v_{m7}} = 0.15749$). Figure 4.6b shows that the second and the final legs can still have their costs reduced by adding midcourse impulses, however the magnitude of impulses are getting lower which means that the benefit in adding more is marginal.

The direct method can be also applied to reduce the total cost using one midcourse impulse us-

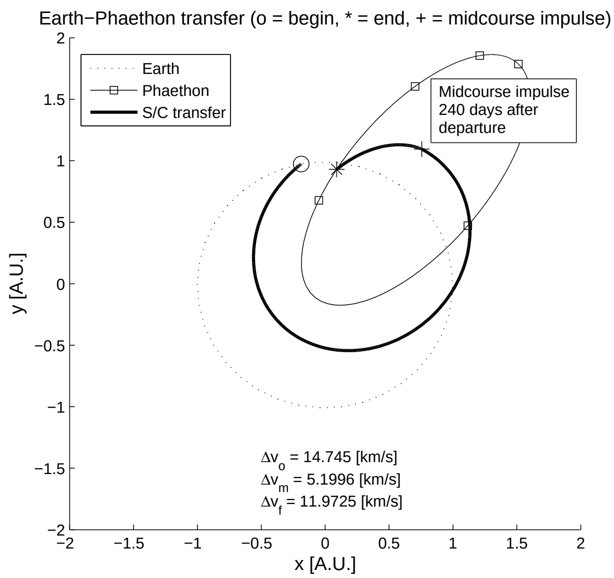

Figure 4.3: Classical solution for the Earth-Phaethon transfer

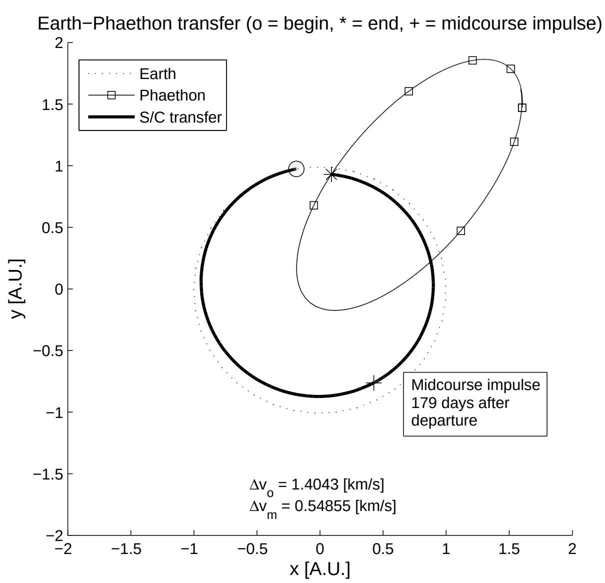

Figure 4.4: Weighted K_3 for the Earth-Phaethon transfer

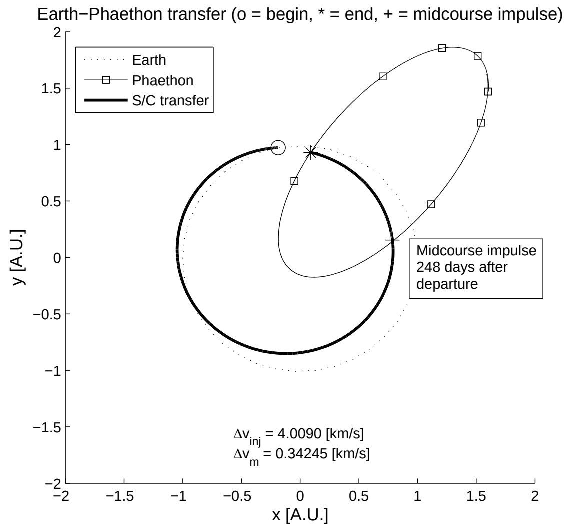

(a)

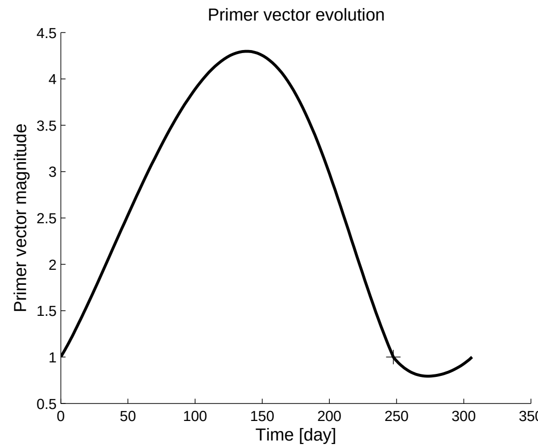

(b)

Figure 4.5: Weighted K_1, K_3 for the Earth-Phaethon transfer

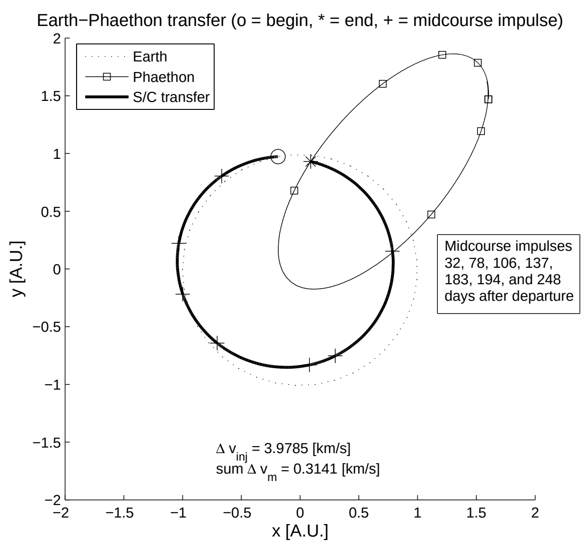

(a)

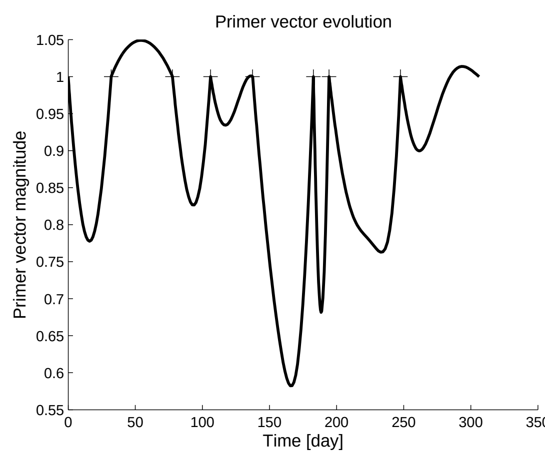

(b)

Figure 4.6: Weighted K_1, K_3 for the Earth-Phaethon transfer with multiple impulses

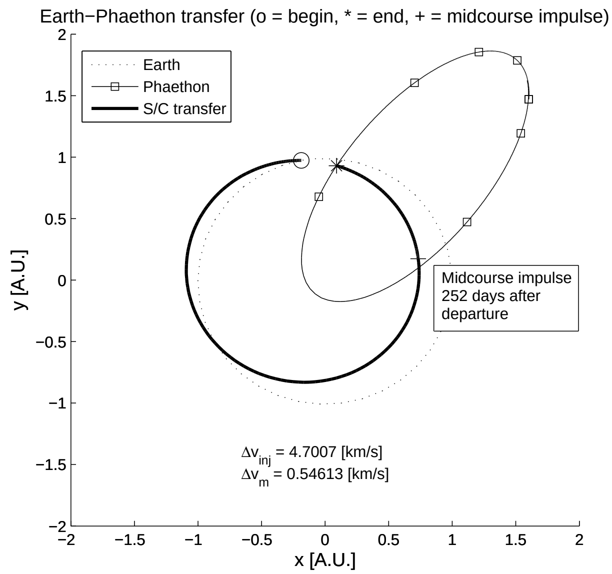

Figure 4.7: Direct method solution for the Earth-Phaethon transfer

ing the same cost function as the last weighted method, $\mathrm{K_o}$ calculated by Eq. (4.37) and $\mathrm{K_f} = 0$. The resulting trajectory (Fig. 4.7) with a single midcourse impulse presents a higher cost than the single impulse weighted method, $\Delta\mathrm{v_{inj}} = 4.7007$ and $\Delta\mathrm{v_m} = 0.54613$ km/s, which, among others, indicate the accuracy gained in using an analytical gradient in these types of problems. As this method provides no information about the trajectory's optimality and for the sake of the comparison being made here, a simulation that includes 7 midcourse impulses is performed (as in the weighted method) and the resulting trajectory (Fig. 4.8) presents a $\Delta\mathrm{v_{inj}} = 4.7136$ and sum of $\Delta\mathrm{v_m} = 0.062326$ km/s. The resulting 8-impulse (1 injection + 7 midcourses) direct method transfer requires 0.4840 km/s more $\Delta\mathrm{v}$ then the weighted method. Another important detail is that the simulation using the direct method took about 13 times more than the indirect method using the same 8 cores 1.80 GHz machine with the same coding language.

The asteroid selection for the PROCYON mission takes into account the full IAU minor planet center (MPC) database with over 600,000 minor bodies. For the backup mission scenario where the spacecraft doesn't perform the Earth gravity assist maneuver and goes directly to the flyby target, the asteroid candidates are selected by evaluating the Lambert solution to reach the asteroid 30 days after launching from Earth. The selected asteroid has to be reachable with less than 200 m/s [Ozaki 2014]. In reality, the mission uses low-thrust but the ballistic solutions are needed to search through the large MPC database and identify potential candidates, greatly reducing the search space for the low-thrust trajectory to only a few flyby candidates. Although the Lambert solutions provide a fast way to perform the search, some asteroids can be left out if the selection is made with a simple ballistic result instead of allowing at least one midcourse impulse. Since the calculated trajectory starts 30 days after Earth's departure and the final part is a flyby, the two maneuvers at the initial and

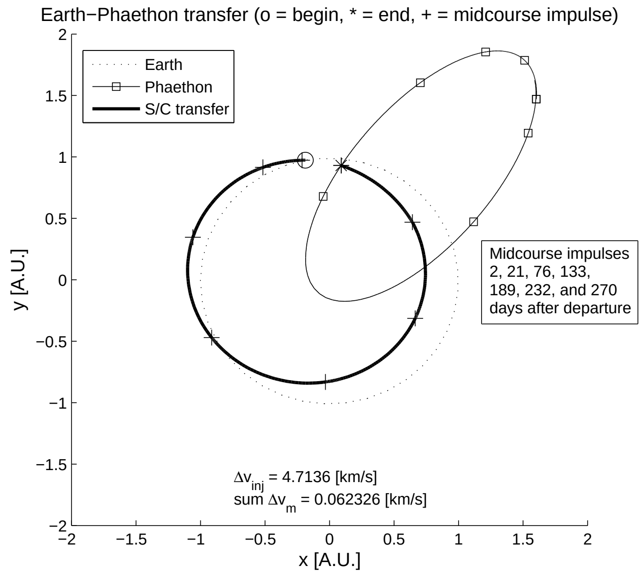

Figure 4.8: Direct method solution for the Earth-Phaethon transfer with 7 midcourse impulses

midcourse will be made essentially in deep space, $\mathrm{K_o} = \mathrm{K_m} = 1$ and $\mathrm{K_f} = 0$. Take, for example, asteroid 2003QZ89 (MPC ID# 152685). Its ballistic transfer (Fig. 4.9) results in 318.6 m/s, but by applying the weighted method with $\mathrm{K_o} = \mathrm{K_m} = 1$ and $\mathrm{K_f} = 0$, the resulting transfer, Fig. 4.10a, uses 145 m/s ($\Delta \mathrm{v_o} = 108.78$ and $\Delta \mathrm{v_m} = 36.21$ km/s), which would include this particular asteroid as one of the mission candidates. Due to the small velocities involved in this optimization only one midcourse impulse is used, even with the primer vector showing that the cost can be improved with more impulses (Fig. 4.10b). Once again, this result can be compared with the direct method that results in a transfer that requires $\Delta \mathrm{v_o} = 121.44$ and $\Delta \mathrm{v_m} = 77.458$ m/s (Fig. 4.11), 198.898 m/s in total. The direct method result also presents an improvement with respect to the two-impulse solution, but barely allowing this particular asteroid to be considered a candidate.

Finally, the Itokawa rendezvous case can be explored in order to show a second type of asteroid mission applicable to the weighted method. The baseline transfer is selected based on the Earth departure and asteroid arrival of the Hayabusa mission and the resulting two-impulse trajectory, Fig. 4.12, requires 2.73 km/s of excess velocity or $\Delta \mathrm{v_{inj}} = 3.5361$ km/s and 3.4443 km/s of rendezvous maneuver, totaling 6.9804 km/s. Applying the weighted method, Fig. 4.13a, results in a decrease in the midcourse impulse and the excess velocity and rendezvous impulse are increased, which generates a trajectory that requires 6.549 km/s in total ($\Delta \mathrm{v_{inj}} = 3.5961$, $\Delta \mathrm{v_m} = 0.66029$ and $\Delta \mathrm{v_f} = 2.2926$ km/s). For the sake of simplicity, only one impulse will be used in this example even though the evolution of the primer vector magnitude, Fig. 4.13b, reaches values higher than 1. Once more the weighted method result is compared with the direct method (Fig. 4.14), which requires more Δv, totaling 6.98243 km/s, $\Delta \mathrm{v_{inj}} = 3.5204$, $\Delta \mathrm{v_m} = 0.07643$ and $\Delta \mathrm{v_f} = 3.3856$ km/s.

The resulting values of the two flyby and the rendezvous transfer cases analyzed in this sec-

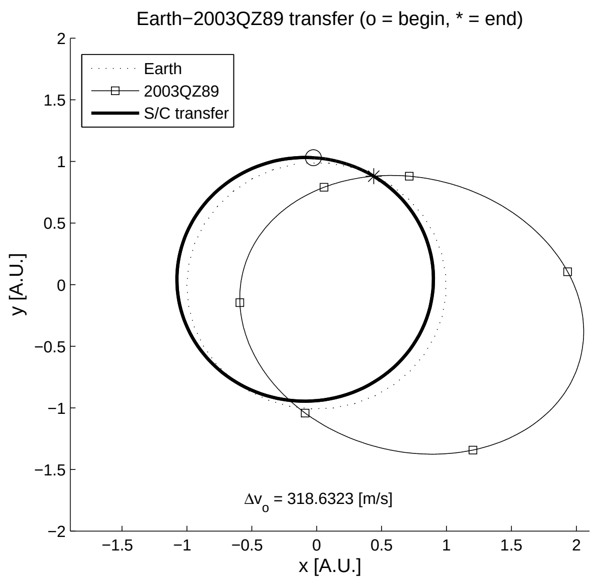

Figure 4.9: Ballistic solution for the 2003QZ89 transfer

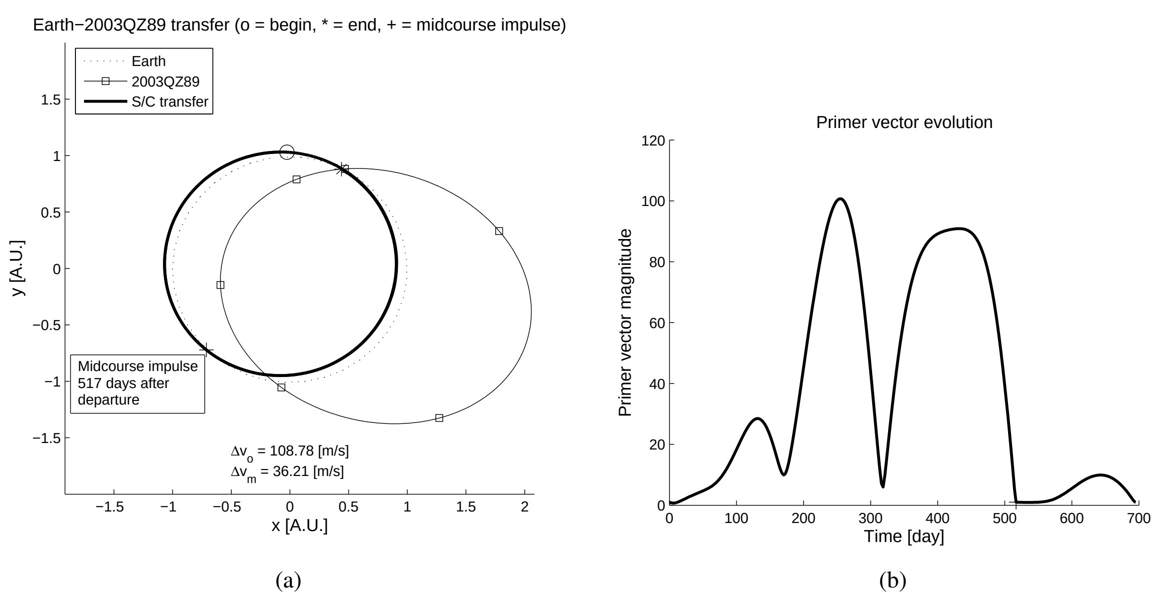

Figure 4.10: Weighted K_1, K_3 for the 2003QZ89 transfer

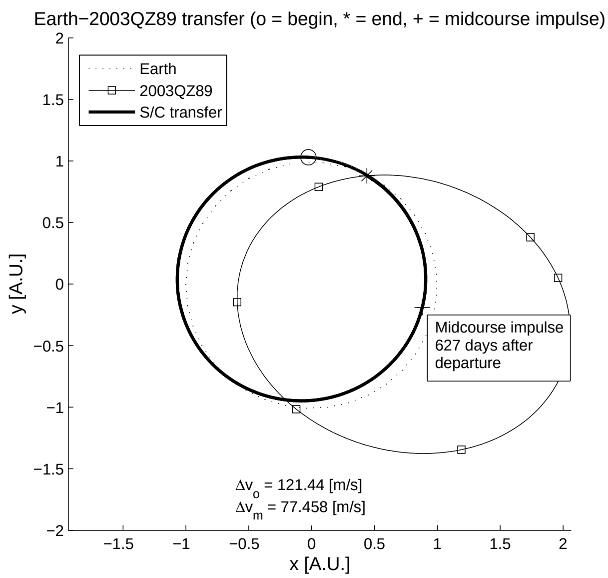

Figure 4.11: Direct method result for the 2003QZ89 transfer

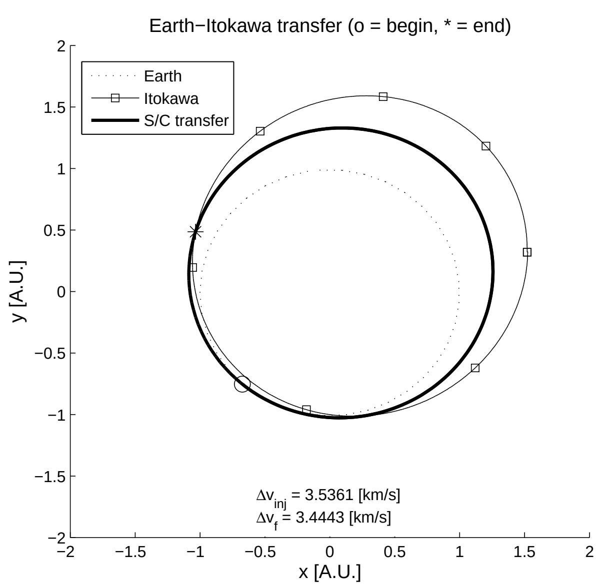

Figure 4.12: Two-impulse solution for the Earth-Itokawa transfer

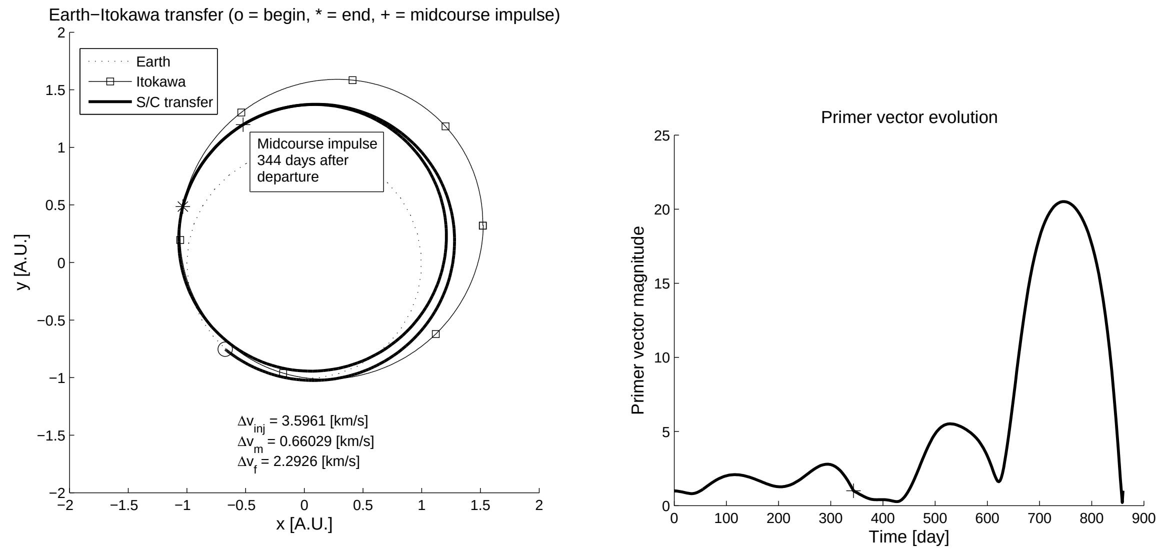

(a) (b)

Figure 4.13: Weighted K_1 for the Earth-Itokawa transfer

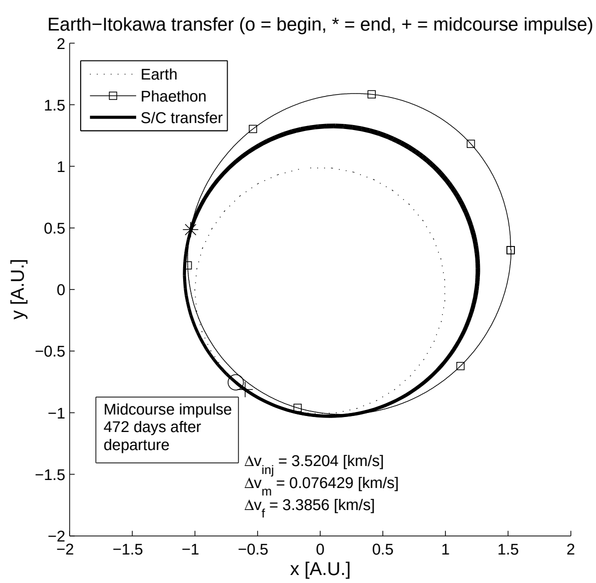

Figure 4.14: Direct method solution for the Earth-Itokawa transfer

Table 4.1: Comparison between the analyzed cases

Transfer Δv		Ballistic	Direct method	Weighted method
Earth-Phaethon flyby	Δv_{inj}[km/s]	4.7136	4.7136	3.9785
	sum Δv_m[km/s]	-	0.0623	0.3141
	Δv_{total} [km/s]	**4.7136**	**4.7759**	**4.2926**
Earth-2003QZ89 flyby	Δv_{inj} [m/s]	318.63	121.44	108.78
	Δv_m [m/s]	-	77.46	36.21
	Δv_{total} [m/s]	**318.63**	**198.90**	**144.99**
Earth-Itokawa rendezvous	Δv_{inj} [km/s]	3.5361	3.5204	3.5961
	Δv_m [km/s]	-	0.0764	0.6603
	Δv_f [km/s]	3.4443	3.3856	2.2926
	Δv_{total} [km/s]	**6.9804**	**6.9824**	**6.5490**

tion can be seen in Table 4.1 for the ballistic, direct method and weighted case. All the velocity increments are depicted int he table with the Δv_o and K_o use to calculate the Δv_{inj} for a LEO with 300 km of altitude, Eq. (4.36). The table shows that the weighted method reaches a better result in a shorter time than the direct method with the advantage that by analyzing the evolution of the primer vector's magnitude it is possible to determine if the result is optimal or if another impulse can further decrease the cost.

4.6 Conclusion

In this work an optimization method using the primer vector theory (PVT) to analyze a weighted cost function was presented. A detailed derivation of the cost function and its gradient was made and a comparison of the necessary conditions for optimality was performed against the direct method using an interior point algorithm. A discussion on the values of the weights was made taking into account the cases of single and multiple flybys, rendezvous and planetary insertion. Finally, three test cases were used to provide a better understanding of the advantages in optimizing a transfer using the weighted method. Comparing the weighted method against the direct method in the single flyby or rendezvous trajectory designs show an improvement in accuracy and speed by obtaining cheaper trajectories in terms of impulsive velocity increment (Δv) in less time. Problems such as the ones presented here are usually solved by non-linear programing utilizing direct methods; however, indirect methods present better accuracy and speed with the fundamental advantage that using the PVT it is possible to assess if the result is optimal or sub-optimal, i.e. could have the cost decreased by adding more impulses. The weighted method, being an indirect method, adds an useful tool for preliminary trajectory designs. This method can also be applied to a variety of other types of missions; for example, on planetary rendezvous missions or transfers with a high change in the inclination plane, it may present a significant improvement by taking into account the actual velocity increment used for Earth's hyperbolic escape and by providing a decrease in the Δv used for the rendezvous or velocity correction maneuvers by adding a deep space maneuver.

CHAPTER 5
Low-Thrust Trajectory Design

5.1 Introduction

Though there have been only a few asteroid dedicated missions, some past missions, e.g. Galileo and Rosetta, increased the mission's value by adding a secondary asteroid objective on the proximity of the main trajectory. With a small propellant addition, a flyby was obtained by performing a small change on the original trajectory. In such cases, asteroid selection and trajectory planning is a challenging task due to the large number of variables and unknowns present in the problem. This study presents a method for trajectory design, based on optimal control, and target selection for the case of a mission using low-thrust propulsion system. The objective is to perform the smallest possible change on the main trajectory to allow the flyby of a neighboring asteroid, while maintaining the initial and final conditions required for achieving the mission's main target.

Minimization of the fuel consumption for interplanetary trajectories is usually the main driver of a preliminary trajectory design. By saving fuel, it is possible to add payload, decrease the launch cost, and often increase the mission lifetime. Another important parameter when dealing with a midcourse asteroid flyby missions is the selection of the target and its flyby time. Currently the minor bodies database includes more than 700,000 elements, this allied with a phase-fix requirement for the flyby generate millions of possibilities for the midcourse.

With the rapid increase in computational performance, trajectory design of low-thrust missions have relied mainly on solutions provided by non-linear gradient based method solvers [Sims 2006, McConaghy 2003] performing extensive searches. Indirect methods, however, have also been proved useful for mission design of low-thrust trajectories [Russell 2007, Ranieri 2005] by solving a system of non-linear equations given by the two-point boundary value problem [Press 1997]. Among the different solution methods, the Primer Vector theory, a derivation using optimal control, is of special interest for space trajectories dealing with minimum mass optimization. The Primer Vector defines an analytical relation between the control variables that can be easily implemented into the spacecraft equations of motion. In this work, it is applied to provide a comprehensive method to define the direction and magnitude of the thrust that minimizes the propellant consumption. Particularly for space trajectory design, solutions of indirect methods are very sensitive to the initial estimation and a good convergence is sometimes difficult to obtain. In this particular situation, however, this difficulty is overcome by the fact that the modified trajectory lies close to the original reference trajectory, which is a good initial estimation. Indirect methods are, in general, faster than direct methods especially if analytical derivatives are provided, this is an important characteristic for problem settings such as this where many cases need to be analyzed.

The asteroid selection for a midcourse flyby is challenging: high number of possible targets, no predefined specific asteroid or group of asteroids, and flyby time has to be taken into account (not a phase-free problem). The target needs to be close to the main reference trajectory at a specific time and require little propellant to modify the trajectory. The fundamental assumption in this part is that, in order to use a small quantity of fuel, the flyby target or point has to be close to the trajectory. This implies that the point lies inside the linear region of the reference trajectory. Therefore, at some level first order evaluations are adequate to prune the asteroid candidates

In section 5.2, the equations of motion of a low-thrust propelled spacecraft in the two-body problem are derived. In section 5.3, the optimal control is defined using calculus of variations and Pontryagin maximum principle. Section 5.4 details the asteroid selection process based on reachability, reference orbit, and linear theory. In section 5.5, the solution method for the entire problem is described from selection to optimization. Section 5.6 presents a test case used for demonstrating the methodology described in this work, followed by section 5.7 that presents the conclusion of this work.

5.2 Equations of Motion

For the trajectory design performed in this work, the main forces acting on the spacecraft are considered to be the gravitational forces of the main bodies and the on-board thrust provided by the propulsion system. The equations of motion used for the test case presented here are inertial, Sun-centered for a spacecraft with a low-thrust propulsion system. Therefore, only the gravity of the primary body is considered to be acting on the spacecraft. Nevertheless, the procedure can be used also in the rotating frame with multiple bodies, the changes will come in the derivation of the equations of motion and on the optimal control law. The problem is then subject to a dynamical system described by 7 state variables as:

$$\mathbf{x} = {}^{\mathrm{t}}[\mathbf{r}, \mathbf{v}, \mathrm{m}]; \quad \mathbf{p} = {}^{\mathrm{t}}[\mathbf{u}, \mathrm{T}]; \tag{5.1}$$

$$\dot{\mathbf{x}} = \mathrm{f}(\mathbf{x}, \mathbf{p}, \mathrm{t}) = \begin{bmatrix} \dot{\mathbf{r}} \\ \dot{\mathbf{v}} \\ \dot{\mathrm{m}} \end{bmatrix} = \begin{bmatrix} \mathbf{v} \\ -\mu \frac{\mathbf{r}}{|\mathbf{r}|^3} + \frac{\mathbf{u}\mathrm{T}}{\mathrm{m}} \\ -\frac{\mathrm{T}}{\mathrm{c}} \end{bmatrix} \tag{5.2}$$

where $\mathbf{x}$ is a 7×1 state vector, $\mathbf{p}$ is a 4×1 control vector, $\mathbf{r}$ is a 3×1 position vector, $\mathbf{v}$ is a 3×1 velocity vector, m is the mass, $\mathbf{u}$ is a 3×1 unit vector that defines the thrust direction, μ is the central body gravitational parameter, T is the thrust magnitude and $\mathrm{c} = \mathrm{g}_0 \mathrm{I}_{\mathrm{SP}}$ is the propulsion exhaust velocity with g_0 the gravity acceleration at sea level and I_{SP} the engine specific impulse.

The control variables are the thrust direction, $\mathbf{u}$, and magnitude, T, which are constrained by the following relations:

$$\mathbf{u} = {}^{\mathrm{t}}\mathbf{u}\mathbf{u} \quad \text{and} \quad 0 \leq \mathrm{T} \leq \mathrm{T}_{\max} \tag{5.3}$$

Note that the notation of the thrust direction and magnitude in this chapter are different from the previous chapter to emphasize the distinction between the impulsive and low-thrust formulations.

5.3 Optimal Control

In this section, the control profile is defined for a minimum mass problem with the control variables T and u as presented on section 4.2. The objective or cost function used for the minimum mass problem is

$$\mathrm{J} = -\mathrm{m_f} \tag{5.4}$$

Therefore, the performance index J is being minimized and as a result of the negative sign, the final mass $\mathrm{m_f}$ is maximized. Considering the minimum mass cost function and the dynamics, the system's Hamiltonian can be derived as

$$\boldsymbol{\lambda} = {}^{\mathrm{t}}[\boldsymbol{\lambda}_{\mathrm{r}}, \boldsymbol{\lambda}_{\mathrm{v}}, \lambda_{\mathrm{m}}] \tag{5.5}$$

$$\begin{aligned} \mathrm{H} = 0 + {}^{\mathrm{t}}\boldsymbol{\lambda}\mathrm{f} &= {}^{\mathrm{t}}\boldsymbol{\lambda}_{\mathrm{r}}\mathbf{v} - {}^{\mathrm{t}}\boldsymbol{\lambda}_{\mathrm{v}}\mu\frac{\mathbf{r}}{|\mathbf{r}|^3} + {}^{\mathrm{t}}\boldsymbol{\lambda}_{\mathrm{v}}\mathbf{u}\frac{\mathrm{T}}{\mathrm{m}} - \lambda_{\mathrm{m}}\frac{\mathrm{T}}{\mathrm{c}} \\ &= {}^{\mathrm{t}}\boldsymbol{\lambda}_{\mathrm{r}}\mathbf{v} - {}^{\mathrm{t}}\boldsymbol{\lambda}_{\mathrm{v}}\mu\frac{\mathbf{r}}{|\mathbf{r}|^3} - \frac{\mathrm{T}}{\mathrm{m}}\left(-{}^{\mathrm{t}}\boldsymbol{\lambda}_{\mathrm{v}}\mathbf{u} + \lambda_{\mathrm{m}}\frac{\mathrm{m}}{\mathrm{c}}\right) \end{aligned} \tag{5.6}$$

where 0 represents the integral part of the cost function, in this case zero, $\boldsymbol{\lambda}$ is the costates vector for each of its associated states **r**, **v** and m.

The optimal control theory uses calculus of variation to identify the control relation with the problem states that minimizes a particular cost function for an unconstrained system. The theory also defines the conditions to be met by the states in order to achieve a particular initial, final or midcourse condition. During the derivation of these relations linear assumptions are made which as a result are valid only in neighboring conditions of the states. This in turn guarantees only a local optimum as opposed to a global optimum. The final form of the optimal relation between the control variables and the states derived by the optimal control theory is [Kirk 2004]

$$\frac{\partial \mathrm{H}}{\partial \boldsymbol{\lambda}} = -{}^{\mathrm{t}}\dot{\boldsymbol{\lambda}} \tag{5.7}$$

$$\frac{\partial \mathrm{H}}{\partial \mathbf{p}} = 0 \tag{5.8}$$

Using the Hamiltonian associated with the minimum mass cost function, the optimal control conditions are

$$\frac{\partial \mathrm{H}}{\partial \mathbf{u}} = {}^{\mathrm{t}}\boldsymbol{\lambda}_{\mathrm{v}}\frac{\mathrm{T}}{\mathrm{m}} = 0 \tag{5.9}$$

$$\frac{\partial \mathrm{H}}{\partial \mathrm{T}} = {}^{\mathrm{t}}\boldsymbol{\lambda}_{\mathrm{v}}\frac{\mathbf{u}}{\mathrm{m}} - \lambda_{\mathrm{m}}\mathrm{c} = 0 \tag{5.10}$$

The above conditions are not straightforward. Moreover, they are only valid for unconstrained states and controls which is not the case here, since the thrust magnitude is bounded between zero and $\mathrm{T_{max}}$.

The Pontryagin's Maximum Principle [Pontryagin 1987] comes primarily from a geometric interpretation of the system phase space and its relation with the control variables. The principle provides more stringent conditions for the control, allowing a better definition of the control profile. It is especially useful when the problem raises constraints on the states and/or on the controls. As in the optimal control theory, the Pontryagin's Maximum Principle also makes use of linear assumptions during its derivation; therefore, the optimal conditions are also valid only locally. A derivation of Pontryagin's Maximum Principle can be found in appendix B. The final form of the Pontryagin's Maximum Principle defining the optimal control profile is

$$\mathrm{H}\left[\mathbf{x}^*, \mathbf{p}^* + \delta\mathbf{p}, \boldsymbol{\lambda}^*, \mathrm{t}\right] \geq \mathrm{H}\left[\mathbf{x}^*, \mathbf{p}^*, \boldsymbol{\lambda}^*, \mathrm{t}\right] \tag{5.11}$$

where the asterisk represents the optimal condition and λ is the co-states vector.

Once again the Hamiltonian calculated for the minimum mass cost can be applied to the above relation, which results in the minimum value for the Hamiltonian generated by the controls. From Eq. 5.6, it is clear that the Hamiltonian will decrease by taking **u** parallel and in opposite direction of $\boldsymbol{\lambda}_{\mathrm{v}}$,

$$\mathrm{u} = -\frac{\boldsymbol{\lambda}_{\mathrm{v}}}{|\boldsymbol{\lambda}_{\mathrm{v}}|} \tag{5.12}$$

As **u** is a unit vector, it has to be divided by the magnitude of $\boldsymbol{\lambda}_{\mathrm{v}}$. The second relation for the control T comes from Eq. 5.6, by substituting Eq. 5.12 on it one gets

$$\mathrm{H} = {}^{\mathrm{t}}\boldsymbol{\lambda}_{\mathrm{r}}\mathbf{v} - {}^{\mathrm{t}}\boldsymbol{\lambda}_{\mathrm{v}}\mu\frac{\mathbf{r}}{|\mathbf{r}|^3} - \frac{\mathrm{T}}{\mathrm{m}}\left(\lambda_{\mathrm{v}} + \lambda_{\mathrm{m}}\frac{\mathrm{m}}{\mathrm{c}}\right) \tag{5.13}$$

Note that now the $\boldsymbol{\lambda}_{\mathrm{v}}$ in parenthesis is the norm and the value of T that minimizes H depend on the value of the expression multiplying it,

$$\mathrm{T} = \begin{cases} 0 & \text{if} \quad \mathrm{S} < 0 \\ 0 < \mathrm{T} < \mathrm{T}_{\mathrm{max}} & \text{if} \quad \mathrm{S} = 0 \\ \mathrm{T}_{\mathrm{max}} & \text{if} \quad \mathrm{S} > 0 \end{cases} \tag{5.14}$$

where $\mathrm{S} = (\lambda_{\mathrm{v}} + \lambda_{\mathrm{m}}\mathrm{m}/\mathrm{c})$ is generally called switching function. As described in Russell [Russell 2007], $\mathrm{S} = 0$ characterizes a "singular arc" that, even though it does exist for finite durations, is rare for practical applications. Therefore, in this work a bang-bang solution will be used defined by: $\mathrm{S} \leq 0$ and $\mathrm{S} > 0$.

5.3.1 Primer Vector Control Law

As mentioned before, In 1963, Lawden [Lawden 1963] derived the necessary conditions for an optimal impulsive trajectory utilizing the optimal control theory by examining the limiting conditions on an optimal finite thrust solution. Such conditions are known as Lawden's necessary conditions for an optimal impulsive trajectory. In impulsive trajectories, T is not limited, therefore, Eq. 5.14 is not applicable. However, Eq. 5.12 concerning the direction is still valid, as used on chapter 4.

So important is the co-state associated with the velocity, $\boldsymbol{\lambda}_{\mathrm{v}}$, that Lawden named the relation $-\boldsymbol{\lambda}_{\mathrm{v}}$ primer vector in allusion to the burning cord of a primer charge for a cannon. His results where complemented over the years by other researchers, some important steps already mentioned on chapter 4 were taken by Lion & Handelsman, 1968 [Lion 1968], Jezewski & Rozendaal, 1968

[Jezewski 1968], and Jezewski & Faust, 1971 [Jezewski 1971]. Since then, the primer vector control law has been applied to different types of space problems using constant specific impulse [Ranieri 2005], variable specific impulse [Senent 2005] in both inertial frame [Russell 2007] and rotational frame [Petropoulos 2008].

5.3.2 Minimum Mass Control Profile

Using the Primer Vector control law, Eqs. 5.12 and 5.14, in the dynamical system of Eq. 5.2, we obtain the equations of motion for a spacecraft whose thrust direction and magnitude are already locally optimized for a minimum mass usage of propellant,

$$\dot{\mathbf{y}} = \mathrm{f}(\mathbf{y}) = \begin{bmatrix} \dot{\mathbf{r}} \\ \dot{\mathbf{v}} \\ \dot{\mathrm{m}} \\ \dot{\boldsymbol{\lambda}}_{\mathrm{r}} \\ \dot{\boldsymbol{\lambda}}_{\mathrm{v}} \\ \dot{\lambda}_{\mathrm{m}} \end{bmatrix} = \begin{bmatrix} \mathbf{v} \\ -\mu \frac{\mathbf{r}}{|\mathbf{r}|^3} - \frac{\boldsymbol{\lambda}_{\mathrm{v}}}{|\boldsymbol{\lambda}_{\mathrm{v}}|}\frac{\mathrm{T}}{\mathrm{m}} \\ -\frac{\mathrm{T}}{\mathrm{c}} \\ -{}^{\mathrm{t}}\mathbf{G}\boldsymbol{\lambda}_{\mathrm{v}} \\ -\boldsymbol{\lambda}_{\mathrm{r}} \\ -\frac{\lambda_{\mathrm{v}}\mathrm{T}}{\mathrm{m}^2} \end{bmatrix} \tag{5.15}$$

$$\mathrm{T} = \begin{cases} 0 & \text{if} \quad (\lambda_{\mathrm{v}} + \lambda_{\mathrm{m}}\mathrm{m}/\mathrm{c}) \leq 0 \\ \mathrm{T}_{\max} & \text{if} \quad (\lambda_{\mathrm{v}} + \lambda_{\mathrm{m}}\mathrm{m}/\mathrm{c}) > 0 \end{cases} \tag{5.16}$$

Finally, the optimized minimum mass trajectory can be propagated by integrating Eq. 5.15 with the thrust magnitude provided by the relation at Eq. 5.16. In order to integrate the above system, the initial conditions are necessary. The initial states come naturally from the mission's starting time and departure planet, yet the initial costates are not clear and sometimes difficult to estimate.

5.3.3 Analytical Derivatives

As seen on chapter 4, the cost function gradient's is necessary for the solution of indirect and direct optimal control problems (gradient based methods). Analytical derivatives improve the quality and speed of the solutions as opposed to numerically estimated derivatives. In particular for indirect methods, analytical derivatives provide a good option for the high sensibility found in this method. As pointed out in [Russell 2007], the use of analytical derivatives in multiple-revolution solutions is particularly important due to the high sensitivity to small initial perturbations. The derivatives have to take into account the low-thrust arcs, the coast arcs and the switch between them.

We start this derivation by the general form of the state transition matrix, $\boldsymbol{\Phi}$ [Russell 2007]. It is important to point out that since the low-thrust is considered in $\boldsymbol{\Phi}$, it is no longer calculated for an elliptical orbit.

$$\boldsymbol{\Phi}(\mathrm{t}, \mathrm{t}_0) = \frac{\partial \mathbf{y}(\mathrm{t})}{\partial \mathbf{y}(\mathrm{t}_0)} \tag{5.17}$$

$$\dot{\boldsymbol{\Phi}}(\mathrm{t}, \mathrm{t}_0) = \left.\frac{\partial \mathrm{f}}{\partial \mathbf{y}}\right|_{\mathrm{t}} \boldsymbol{\Phi}(\mathrm{t}, \mathrm{t}_0) \tag{5.18}$$

where,

$$\mathbf{\Phi}(\mathrm{t}_0, \mathrm{t}_0) = \mathbf{I} \tag{5.19}$$

$$\frac{\partial \mathrm{f}}{\partial \mathbf{y}} = \begin{bmatrix} \mathbf{O} & \mathbf{I} & \mathbf{O} & \mathbf{O} & \mathbf{O} & \mathbf{O} \\ \mathbf{G} & \mathbf{O} & \frac{\boldsymbol{\lambda}_\mathrm{v}}{|\boldsymbol{\lambda}_\mathrm{v}|}\frac{\mathrm{T}}{\mathrm{m}^2} & \mathbf{O} & -\frac{\mathrm{T}}{\mathrm{m}}\left(\frac{\mathbf{I}}{|\boldsymbol{\lambda}_\mathrm{v}|} - \frac{{}^\mathrm{t}\boldsymbol{\lambda}_\mathrm{v}\boldsymbol{\lambda}_\mathrm{v}}{|\boldsymbol{\lambda}_\mathrm{v}|^3}\right) & \mathbf{O} \\ \mathbf{O} & \mathbf{O} & 0 & \mathbf{O} & \mathbf{O} & 0 \\ -\frac{\partial^\mathrm{t}\mathbf{G}\boldsymbol{\lambda}_\mathrm{v}}{\partial \mathbf{r}} & \mathbf{O} & \mathbf{O} & \mathbf{O} & -{}^\mathrm{t}\mathbf{G} & \mathbf{O} \\ \mathbf{O} & \mathbf{O} & \mathbf{O} & -\mathbf{I} & \mathbf{O} & \mathbf{O} \\ \mathbf{O} & \mathbf{O} & \frac{2|\boldsymbol{\lambda}_\mathrm{v}|\mathrm{T}}{\mathrm{m}^3} & \mathbf{O} & \frac{-{}^\mathrm{t}\boldsymbol{\lambda}_\mathrm{v}\mathrm{T}}{\boldsymbol{\lambda}_\mathrm{v}\mathrm{m}^2} & 0 \end{bmatrix} \tag{5.20}$$

Based on the above, the state transition matrix can be obtained for coast or thrust arcs at any time interval by integrating Eq. 5.18. Next, it is necessary to connect the different coast and low-thrust arcs in order to calculate $\mathbf{\Phi}$ from beginning to end. The switch points between the propelled and coast legs constitute discontinuities on $\mathbf{\Phi}$, a simple solution is to calculate $\mathbf{\Phi}$ in between the discontinuities (each leg) and connect then by a new matrix, $\mathbf{\Psi}$, that handles the discontinuities at the switching point. Therefore, for N discontinuities,

$$\frac{\partial \mathbf{y}(\mathrm{t})}{\partial \mathbf{y}(\mathrm{t}_0)} = \mathbf{\Phi}(\mathrm{t_f}, \mathrm{t}_{\mathrm{N}+})\mathbf{\Psi}_\mathrm{N}\mathbf{\Phi}(\mathrm{t}_{\mathrm{N}-}, \mathrm{t}_{(\mathrm{N}-1)+})\mathbf{\Psi}_{\mathrm{N}-1}\cdots\mathbf{\Psi}_2\mathbf{\Phi}(\mathrm{t}_{2-}, \mathrm{t}_{1+})\mathbf{\Psi}_1\mathbf{\Phi}(\mathrm{t}_{1-}, \mathrm{t}_0) \tag{5.21}$$

where, the discontinuity and the switching points are calculated as the partial derivative of the states after, $\mathrm{t}_{\mathrm{n}+}$, and before, $\mathrm{t}_{\mathrm{n}-}$, the switch,

$$\mathbf{\Psi}_\mathrm{n} = \frac{\partial \mathbf{y}(\mathrm{t}_{\mathrm{n}+})}{\partial \mathbf{y}(\mathrm{t}_{\mathrm{n}-})} = \mathrm{I} + \left(\dot{\mathbf{y}}|_{\mathrm{n}+} - \dot{\mathbf{y}}|_{\mathrm{n}-}\right)\left(\frac{\frac{\partial \mathrm{S}}{\partial \mathbf{y}}}{\dot{\mathrm{S}}}\right)\Bigg|_{\mathrm{n}-} \tag{5.22}$$

Finally, the gradient of the cost function can be obtained by calculating the state transition matrix (integrating Eq. 5.17) and extracting its relevant terms. Section 5.5.1 details the calculation of the coast function's gradient.

5.4 Asteroid Target Selection

Potentially, millions of midcourse flyby points need to be considered in the target selection because of the large number of possible candidates ($> 700,000$) combined with different flyby times. The large number of candidates makes the computational time to optimize all these points prohibitive; therefore, a strategy needs to be considered to decrease the optimization candidates' number. It is important to point out that a simple distance evaluation does not provide a good result because it does not consider: the plane change, different points on the reference orbit for the transfer maneuver, and it fails to provide a good initial estimation for the optimization on both the states and costates.

The fundamental assumption here is based on the fact that the auxiliary trajectory will not deviate much from the reference trajectory due to a limit on the propellant use and the constraints related to the initial and final conditions. Therefore, the flyby point will not be far from the reference trajectory and, due to this, the selected flyby point will lie inside the reference trajectory's linear region. This assumption allows the use of the linear theory in the selection process.

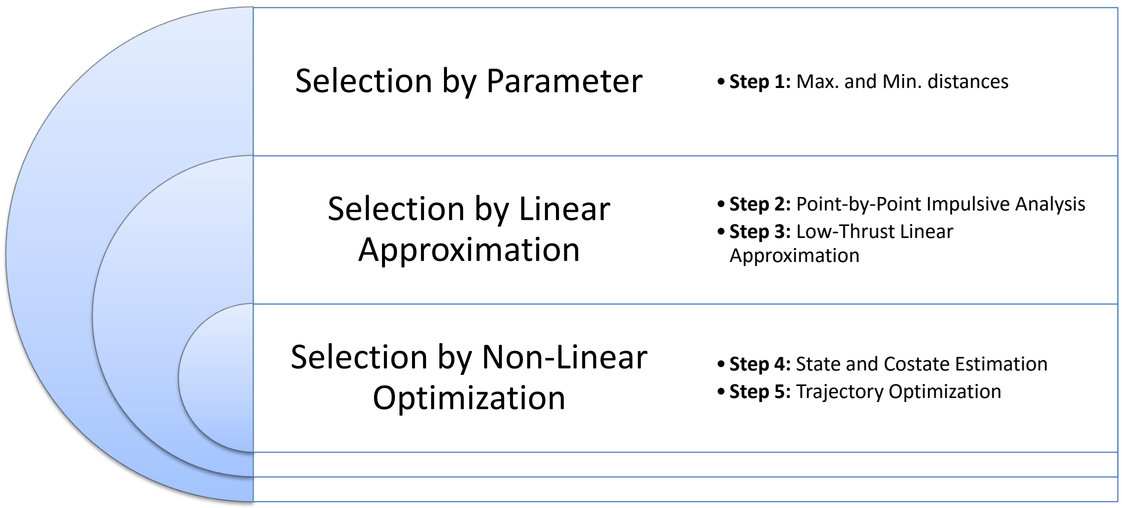

Figure 5.1: Asteroid selection flowchart

The asteroid selection for the midcourse flyby point is divided into 5 steps, with the fifth being the optimization itself, pertaining to 3 large areas: selection by parameter, selection by linear approximation and selection by non-linear optimization. The asteroid database considered in this study was provided by the Minor Planet Center [MPC 2013]. The flowchart of the step sequence can be seen on Fig 5.1 and the following sections describe in detail each step.

5.4.1 Selection by Parameter - Step 1: Maximum and Minimum Distances

In the first step the reference orbit is taken into account. Considering its initial conditions and engine characteristics, it is propagated with a constant tangential thrust in the direction of the velocity vector for the duration of the trajectory's time of flight. The maximum distance achieved from the orbit's center defines the farthest point that the spacecraft can reach from the reference orbit. It is important to point out that it has been proved on [Campagnola 2014b] that the tangential acceleration does not maximize the semi-major axis, but it constitutes a good approximation. This approximation is considered enough for this work since this limit is an over estimation; in the midcourse flyby case, it is not enough for the spacecraft to reach the point it is also necessary to return and reach the orbit's final conditions, i.e. main trajectory objective. The asteroids with the perihelion larger than the maximum reachable point, defined by the tangential thrust propagation, are excluded. Next, the asteroids orbits are precomputed for the duration of the mission; as the arrival time is a constraint, the time of flight is fixed. The time step can be selected by the user considering that a small time step will generate more points to be analyzed, which makes the analysis more robust but slower. However, since the linear theory is considered, in order to guarantee that no solution in between the points is better, irrespective of the time step selected, the time step size needs to be below the time defined by the following derivation, see Fig. 5.2.

With the step size defined by $\Delta t = t_n - t_{n-1}$ and considering the problem linear between the

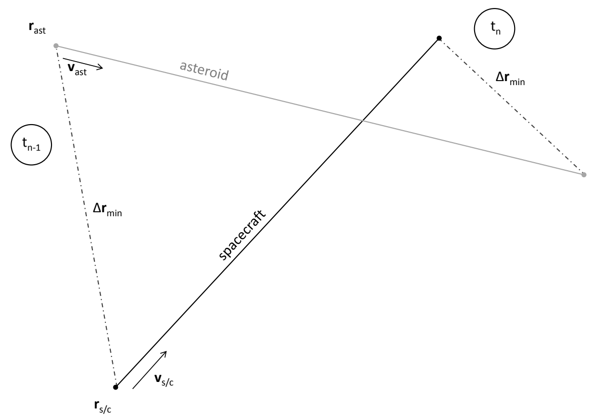

Figure 5.2: Step size limit

points (n) and $(n-1)$, we have

$$\begin{cases} \ddot{r}_{ast} = 0 \\ \ddot{r}_{s/c} = 0 \end{cases} \tag{5.23}$$

$$\begin{cases} \Delta\ddot{r} = \ddot{r}_{ast} - \ddot{r}_{s/c} = 0 \\ \Delta\dot{r} = \dot{r}_{ast} - \dot{r}_{s/c} = \dot{r}_{s/c} + v_{s/c0} - \dot{r}_{ast} - v_{ast0} \\ \Delta r = r_{s/c} + v_{s/c} t_{lin} + r_{s/c0} - r_{ast} - v_{ast} t_{lin} - r_{ast0} \end{cases} \tag{5.24}$$

Therefore, by computing the minimal distance between the asteroid orbits and the reference trajectory, Δr_{min}, it is possible to obtain the minimal allowed time step by

$$t_{lin} = \frac{\Delta r_{min} - r_{s/c} - r_{s/c0} + r_{ast} + r_{ast0}}{v_{s/c} - v_{ast}} \tag{5.25}$$

$$\Delta t < t_{lin} \tag{5.26}$$

where, the subscript s/c and ast refer to the spacecraft and asteroid, respectively, and t_{lin} is the time calculated assuming a linear assumption (no acceleration present, Eq. 5.23)

With the precomputed asteroid trajectory, the points on the asteroid orbit can be compared once again with the maximum reachable distance and, also, with the minimal reachable distance, which can be calculated in the same way as the maximum distance but with the tangential thrust in opposite direction to the velocity vector. The maximum and minimum reachable distances define a two-dimensional corridor in which the points have to lie within. After, all the remaining points are changed coordinates from the Keplerian to the Cartesian system for the next steps.

As a final selection on this step, the general reachability for each individual point of the trajectory is considered. The reachable limit can be defined in two ways, by a fixed value which is estimated to be more than the linear region, to include all the feasible points, or by calculating the linear reachability as derived in [Campagnola 2015].

Given a set of reachable positions $\mathrm{r}_{n+1} = \mathrm{r}(\mathrm{t}_{n+1})$ starting from a given position in the reference trajectory, $\mathrm{r}_n = \mathrm{r}(\mathrm{t}_n)$, for all possible controls (bounded by $|\mathrm{uT}| \leq \mathrm{Tmax}$), the reachability can be computed for each state, $\sigma_{(i)}$, based on the linearized dynamics. The set is approximated by a supporting polyhedron, with $2\mathrm{M}$ polygons, which is expressed as a set of inequalities for r_{n+1}

$$-\mathrm{T}_{max}\sigma_{(i)} \leq {}^{t}\upsilon_{(i)}\mathrm{r}_{n+1} \leq \mathrm{T}_{max}\sigma_{(i)}, \quad i = 1, \cdots, \mathrm{M} \tag{5.27}$$

Here, $\upsilon_{(i)}$ are the normal to the supporting planes tangent to the reachable set and $\sigma_{(i)}$ are the distances from the origin to the planes. They can be computed as,

$$\sigma_{(i)} = \int_{t_n}^{t_{n+1}} \left| {}^{t}\mathbf{\Phi}_{rv}(\tau, t_{n+1})\upsilon_{(i)} \right| d\tau \tag{5.28}$$

where, $\mathbf{\Phi}_{rv}$ is the 3×3 sub-matrix of the state transition matrix.

To check whether a point belongs to the set, one only needs to verify if the inequalities are satisfied. Note that in the linearized dynamics, the reachable set is compact, convex, and symmetric about the origin. In this work the support planes are chosen in the direction of each state, thus defining a cube region for the position and velocity,

$$\begin{cases} \upsilon_{(1)} = {}^{t}\begin{bmatrix} 1 & 0 & 0 \end{bmatrix} \\ \upsilon_{(2)} = {}^{t}\begin{bmatrix} 0 & 1 & 0 \end{bmatrix} \\ \upsilon_{(3)} = {}^{t}\begin{bmatrix} 0 & 0 & 1 \end{bmatrix} \\ \upsilon_{(4)} = {}^{t}\begin{bmatrix} 1 & 0 & 0 \end{bmatrix} \\ \upsilon_{(5)} = {}^{t}\begin{bmatrix} 0 & 1 & 0 \end{bmatrix} \\ \upsilon_{(6)} = {}^{t}\begin{bmatrix} 0 & 0 & 1 \end{bmatrix} \end{cases} \tag{5.29}$$

The calculation is performed forward and backward, since after the flyby the spacecraft still needs to reach the final point. With this, both solutions are intersected to generate the final reachable range.

5.4.2 Selection by linear Approximation - Step 2: Point-by-Point Impulsive Analysis

With the reference orbit state transition matrix (section 5.3.3) it is possible to calculate for each point an impulsive approximation to reach the target. The calculation with $\mathbf{\Phi}$ is faster than a Lambert solution, thus it allows the calculation of several points in a short time. The impulses will not be compared with a maximum Δv, but instead will be evaluated with respect to their associated Δt to check if the time available is enough to provide the necessary velocity change.

The Tsiolkovsky rocket equation (Eq. 5.30) will be used to estimate the Δt combined with the mass variation (third line of Eq. 5.15) and the mass dynamics (Eq. 5.31) as,

$$\Delta v = c \ln \left[\frac{m_n}{m_{n+1}} \right] \tag{5.30}$$

$$m_n = m_{n-1} - \dot{m}\Delta t \tag{5.31}$$

$$\Delta t = \frac{c}{\mathrm{T}_{max}} m_n \left(1 - e^{-\Delta v/c} \right) \tag{5.32}$$

It is important to point out that Eq. 5.32 uses $\mathrm{T_{max}}$ that makes the time variation smaller, which overestimates the points selected; it includes more points that would not be selected if the optimized T was known. Also, it uses the rocket equation that is a chemical evaluation of propulsion instead the of low-thrust, which once again provides a smaller value of the time variation than the low-thrust propulsion system would be able to achieve; once again, an overestimation on the points selected.

For this evaluation three impulses are considered: the first at the initial point, second somewhere in the trajectory in between beginning and end, and third at the final point, see Fig 4.1. The calculation considers a time free point, therefore, the distance between reference orbit and target is considered not necessarily in the correct time. In this way, all the points of the orbit can be used in the calculation of the second impulse without having to re-calculate $\boldsymbol{\Phi}$. This allows for the calculation of the lowest possible $\Delta\mathrm{t}$, which improves solutions with plane changes. It is noted that this 3 impulse approach is not necessarily optimal for a plane changing trajectory, but it is a reasonable approximation since the calculation is performed in the linear regime, which means that the variation between optimal and sub-optimal solutions will be small. As the trajectory in the midcourse is a flyby, only the impulses at o and f will be considered for the time check. This of course means that the correction maneuver at the midcourse point is not taken into account in the evaluation. This will result in possible infeasible points to be considered, but, on the other hand, it ensures that the feasible points are included.

In order to calculate the necessary velocity changes, we recall Eq. 4.1 for 2 arbitrary points $(\mathrm{n}+1)$ and n,

$$\begin{bmatrix} \delta\mathbf{r}_{\mathrm{n}+1} \\ \delta\mathbf{v}_{\mathrm{n}+1} \end{bmatrix} = \boldsymbol{\Phi}_{(\mathrm{n}+1)\mathrm{n}} \begin{bmatrix} \delta\mathbf{r}_{\mathrm{n}} \\ \delta\mathbf{v}_{\mathrm{n}} \end{bmatrix} \tag{5.33}$$

$$\begin{bmatrix} \delta\mathbf{v}_{\mathrm{n}} \\ \delta\mathbf{v}_{\mathrm{n}+1} \end{bmatrix} = \begin{bmatrix} -\boldsymbol{\Phi}_{\mathrm{rv}}^{-1}\boldsymbol{\Phi}_{\mathrm{rr}} & \boldsymbol{\Phi}_{\mathrm{rv}}^{-1} \\ \boldsymbol{\Phi}_{\mathrm{vr}}-\boldsymbol{\Phi}_{\mathrm{vv}}\boldsymbol{\Phi}_{\mathrm{rv}}^{-1}\boldsymbol{\Phi}_{\mathrm{rr}} & \boldsymbol{\Phi}_{\mathrm{vv}}\boldsymbol{\Phi}_{\mathrm{rv}}^{-1} \end{bmatrix}\Bigg|_{(\mathrm{n}+1)\mathrm{n}} \begin{bmatrix} \delta\mathbf{r}_{\mathrm{n}} \\ \delta\mathbf{r}_{\mathrm{n}+1} \end{bmatrix} \tag{5.34}$$

With Eq.5.34 it is possible to calculate the $\Delta\mathrm{v}$ at the points (n) and $(\mathrm{n}+1)$.

$$\begin{bmatrix} \Delta\mathbf{v}_{\mathrm{n}} \\ \Delta\mathbf{v}_{\mathrm{n}+1} \end{bmatrix} = \begin{bmatrix} \boldsymbol{\Phi}_{\mathrm{rv}}^{-1}\boldsymbol{\Phi}_{\mathrm{rr}} & \mathbf{I} \\ \boldsymbol{\Phi}_{\mathrm{vr}}-\boldsymbol{\Phi}_{\mathrm{vv}}\boldsymbol{\Phi}_{\mathrm{rv}}^{-1}\boldsymbol{\Phi}_{\mathrm{rr}} & \mathbf{O} \end{bmatrix}\Bigg|_{(\mathrm{n}+1)\mathrm{n}} \begin{bmatrix} \delta\mathbf{r}_{\mathrm{n}} \\ \delta\mathbf{v}_{\mathrm{n}} \end{bmatrix} + \begin{bmatrix} \boldsymbol{\Phi}_{\mathrm{rv}}^{-1} & \mathbf{O} \\ -\boldsymbol{\Phi}_{\mathrm{vv}}\boldsymbol{\Phi}_{\mathrm{rv}}^{-1} & \mathbf{I} \end{bmatrix}\Bigg|_{(\mathrm{n}+1)\mathrm{n}} \begin{bmatrix} \delta\mathbf{r}_{\mathrm{n}+1} \\ \delta\mathbf{v}_{\mathrm{n}+1} \end{bmatrix} \tag{5.35}$$

where, for the flyby case considered here,

$$\begin{bmatrix} \delta\mathbf{r}_{\mathrm{o}} \\ \delta\mathbf{v}_{\mathrm{o}} \end{bmatrix} = \begin{bmatrix} 0 \\ 0 \end{bmatrix}; \quad \begin{bmatrix} \delta\mathbf{r}_{\mathrm{o}} \\ \delta\mathbf{v}_{\mathrm{o}} \end{bmatrix} = \begin{bmatrix} \delta\mathrm{r} \\ 0 \end{bmatrix} = \begin{bmatrix} \mathrm{r_{ast}}-\mathrm{r_{S/C}} \\ 0 \end{bmatrix}; \quad \begin{bmatrix} \delta\mathbf{r}_{\mathrm{f}} \\ \delta\mathbf{v}_{\mathrm{f}} \end{bmatrix} = \begin{bmatrix} 0 \\ 0 \end{bmatrix} \tag{5.36}$$

which results in $\Delta\mathrm{v_o}$ for the trajectory's beginning and $\Delta\mathrm{v_f}$ for the last point. These are calculated for all possible combinations of m and the selected point is the one that results on $\min(\Delta\mathrm{v_o}+\Delta\mathrm{v_f})$. To account for approximation errors a margin is added to the time, $\mathrm{t_{margin}}$.

The point is then selected if,

$$\begin{cases} \Delta\mathrm{t_{mo}} < \mathrm{t_m}-\mathrm{t_o} \\ \Delta\mathrm{t_{fm}} < \mathrm{t_m}-\mathrm{t_o} \\ \Delta\mathrm{t_{mo}}+\Delta\mathrm{t_{fm}} < \mathrm{t_f}-\mathrm{t_o} \end{cases} \tag{5.37}$$

where, t_m and t_o are the actual times of the trajectory's beginning and Δt_{mo}, and Δt_{fm} are the time variation calculated using Eq. 5.32

5.4.3 Selection by linear Approximation - Step 3: Low-Thrust Linear Approximation

This step uses a linear approximation to the low-thrust problem to check if the low-thrust propulsion system can perform the flyby from both extremities, two legs originating from o and f. This approach does not match the velocity from the two legs at the flyby point, just the position. The velocity cannot be be computed at the midcourse because, since it is a flyby, δv_m is not available. This approach includes solutions that cannot be fully optimized due to the velocity mismatch at the flyby point; therefore, it results is a small overestimation of the points, however, once again, it ensures that the feasible points remain in the selection.

The low-thrust linear calculation works in a similar way as in step 2, but instead of a single impulse in each leg the trajectory contains several small impulses across the leg that results in an approximation for the low-thrust solution [Sims 2006]. Based on the work of [Campagnola 2014a], the low-thrust approximation is here modified for the flyby case. The cost function to be minimized is

$$\sum|\Delta v| = \int_{t_o}^{t_m} \left|u'(t)\right| dt + \int_{t_m}^{t_f} \left|u'(t)\right| dt \tag{5.38}$$

with, $|u'(t)| = |u(t)T(t)| < T_{max} \in [t_o \quad t_f]$.

As in [Campagnola 2014a] the trajectory is discretized, as already done previously on step 1, and the impulses are given in the middle of two consecutive nodes: t_i for the time, $x_i = x(t_i)$ for the position and velocity states, and $u'_i = u'_i(t_i)$ for the control that defines the thrust law as

$$u'(t) = \sum_{i=1}^{N_{mo}} u'_i \text{rect}\left(\frac{t_i}{\Delta t}\right) + \sum_{i=1}^{N_{fm}} u'_i \text{rect}\left(\frac{t_i}{\Delta t}\right) \tag{5.39}$$

where, N is the number of discretized points in each arc and $\text{rect}(t)$ is the rectangular function. The velocity variation in each node is

$$\Delta v_i = \int_{t_i-\delta t/2}^{t_i+\delta t/2} u'(t)\, dt = u'_i \Delta t \tag{5.40}$$

where, Δt is the time variation from each node. Since the control is constant for each interval Eq. 5.38 can be rewritten as

$$\sum|\Delta v| = \sum_{i=1}^{N_{mo}} u'_i \Delta t + \sum_{i=1}^{N_{fm}} u'_i \Delta t = \sum_{i=1}^{N_{mo}} |v_i| + \sum_{i=1}^{N_{fm}} |v_i| \tag{5.41}$$

The Δv in each node is calculated by Eq. 5.35 and the control can be computed as

$$u'_i = \alpha_i \frac{\Delta v_i}{\Delta t} \tag{5.42}$$

where, α is a scaling factor that reinforces the constraint $|u'(t)| < T_{max}$,

$$\alpha_i = \min\left(1, \frac{u_{max}\Delta t}{|\Delta v_i|}\right) \tag{5.43}$$

Since the final velocity change is not considered the calculation is aways performed from the node, i, to the flyby point, m. This implies in a forward evaluation from o to m and a backward evaluation from f to m. Every consecutive state can be calculated as

$$\begin{cases} x_{i+1} = x_i + \begin{bmatrix} 0 \\ \alpha_i \Delta v_i \end{bmatrix} & \text{if propagating from } o \text{ to } m \\ x_{i+1} = x_i - \begin{bmatrix} 0 \\ \alpha_i \Delta v_i \end{bmatrix} & \text{if propagating from } f \text{ to } m \end{cases} \tag{5.44}$$

The propagation continues until an $\alpha = 1$ is found, which means that from that point all the necessary Δv can be provided to reach the final point. On the other hand, if $\alpha = 1$ is not found it means that no feasible solution exists.

It is important to point out that, even though the optimal conditions are not applied here, the impulse direction is always provided in the optimal direction, primer vector, as derived on chapter 4.3 Eq. 4.20.

5.4.4 Selection by non-linear Optimization - Step 4: State and Costate Estimation

Step 4 provides a good estimation for the position, velocity, and control to be applied to the mid-course optimization on the next step. Recalling section 5.3, the optimized solution or the initial guess for the optimization requires the full **y** which also includes the mass and costates. The $\boldsymbol{\lambda}_r$ and $\boldsymbol{\lambda}_v$ can be estimated by recalling Eq. 4.14, and the original form of Eq. 4.12,

$$\begin{bmatrix} \dot{\boldsymbol{\lambda}}_r(t) \\ \dot{\boldsymbol{\lambda}}_v(t) \end{bmatrix} = -\begin{bmatrix} \mathbf{O} & {}^t\mathbf{G} \\ \mathbf{O} & \mathbf{I} \end{bmatrix} \begin{bmatrix} \boldsymbol{\lambda}_r(t) \\ \boldsymbol{\lambda}_v(t) \end{bmatrix} \tag{5.45}$$

Combining both equations and performing some mathematical manipulation, it results in

$$\delta\dot{r}(t) = -\dot{\boldsymbol{\lambda}}_v(t); \quad \delta\dot{v}(t) = \dot{\boldsymbol{\lambda}}_r(t) \tag{5.46}$$

If the initial conditions of states and associated costates are the same, $\delta r_0 = -\boldsymbol{\lambda}_{v0}$ and $\delta v_0 = \boldsymbol{\lambda}_{r0}$, then

$$\delta r(t) = -\boldsymbol{\lambda}_v(t); \quad \delta v(t) = \boldsymbol{\lambda}_r(t) \tag{5.47}$$

The two remaining variables to be found are m and λ_m. The mass can be easily estimated by the resulting control profile, $u'(t)$, of step 3,

$$m(t) = m(t_0) - \frac{u'(t)}{c}\Delta t(t); \qquad \text{where} \quad \Delta t(t) = \sum_{i=1}^{N=t} \Delta t_i \tag{5.48}$$

and, finally, λ_{m} is a simple quadrature that results from Eq. 5.47 applied in the last line of Eq. 5.15

$$\dot{\lambda}_{\mathrm{m}}(\mathrm{t}) = -\frac{\mathrm{u}'(\mathrm{t})}{\mathrm{m}(\mathrm{t})^2} |\boldsymbol{\delta}\mathbf{r}(\mathrm{t})| \tag{5.49}$$

The problem is reduced to a reasonable number of points with a good initial estimation for all the states and costates. As a result of the accurate initial guess the optimization can be performed fast, converging in just a few iterations for the feasible points.

5.4.5 Selection by non-linear Optimization - Step 5: Trajectory Optimization

The trajectory optimization with a midcourse condition, asteroid flyby, is the final and conclusive step where the points selected in step 3 combined with the initial guess calculated at step 4 are evaluated in a non-linear indirect method optimization. The solution consists in finding the initial costates that when propagated result in the desired final and midcourse conditions, only the initial costates are needed since the initial states are known. The problem to be solved is then to find the solution of a set of non-linear equations refereed to as Two Point boundary Value Problem, here with the flyby represented as the additional midcourse constraints (section 5.5.1) The next section, 5.5, details the methods used in the solution of this optimization. The problem is solved using the "feasible point" mode with the sequential quadratic programming software SNOPT [Gill 2002].

5.5 Solution Method

This section presents details of the solution method used in step 5, the trajectory optimization with midcourse flyby. In order to improve the convergence two main strategies are used: multiple shooting and analytical gradient for the cost function. These two are incorporated in the solution of the set of non-linear equations, Two Point boundary Value Problem (TPBVP), that here include the extra equations needed to comply with the midcourse constraints, midcourse asteroid flyby.

5.5.1 Two Point Boundary Value Problem with Midcourse Constraint

As outlined before on section 5.3.2, with Eqs. 5.15 and 5.16 the optimal control problem is solved. What remains is to find the initial costates such that a propagation with them will result in the desired conditions, or problem's constraints. To find the missing initial costates the problem is reduced to a set of non-linear equations originated from the transversality conditions, presented at appendix A, and solved.

The equations for the TPBVP are derived as follows. First, recalling Eqs. A.24 and A.25 we have a fixed initial and final time problem, $\delta\mathrm{t} = 0$, with fixed final conditions, $\delta\mathrm{w} = 0$. Also, regarding the midcourse constraint (apppendix B), the flyby point is fixed on time and position, requiring that all the states are continuous at the midcourse point, which, in turn, provides the following conditions at the midcourse point,

$$\begin{cases} -\boldsymbol{\lambda}_{\mathrm{r}}(\mathrm{t}_{\mathrm{m}}^{-}) + \boldsymbol{\lambda}_{\mathrm{r}}(\mathrm{t}_{\mathrm{m}}^{+}) + \boldsymbol{\nu} = 0 & \Rightarrow \quad \boldsymbol{\lambda}_{\mathrm{r}}(\mathrm{t}_{\mathrm{m}}^{-}) = \boldsymbol{\lambda}_{\mathrm{r}}(\mathrm{t}_{\mathrm{m}}^{+}) + \boldsymbol{\nu} \\ -\boldsymbol{\lambda}_{\mathrm{v}}(\mathrm{t}_{\mathrm{m}}^{-}) + \boldsymbol{\lambda}_{\mathrm{v}}(\mathrm{t}_{\mathrm{m}}^{+}) = 0 & \Rightarrow \quad \boldsymbol{\lambda}_{\mathrm{v}}(\mathrm{t}_{\mathrm{m}}^{-}) = \boldsymbol{\lambda}_{\mathrm{v}}(\mathrm{t}_{\mathrm{m}}^{+}) \\ -\lambda_{\mathrm{m}}(\mathrm{t}_{\mathrm{m}}^{-}) + \lambda_{\mathrm{m}}(\mathrm{t}_{\mathrm{m}}^{+}) = 0 & \Rightarrow \quad \lambda_{\mathrm{m}}(\mathrm{t}_{\mathrm{m}}^{-}) = \lambda_{\mathrm{m}}(\mathrm{t}_{\mathrm{m}}^{+}) \end{cases} \tag{5.50}$$

based on Eq. D.9. Note that the constant ν becomes a problem unknown to relate $\boldsymbol{\lambda}_{\mathrm{r}}(\mathrm{t}_{\mathrm{m}})$ before and after the midcourse; however, in this case this unknown can be replaced by $\boldsymbol{\lambda}_{\mathrm{r}}(\mathrm{t}_{\mathrm{m}}^{+})$ itself without loss of generality.

Considering the above conditions and constraints, the TPBVP is defined as

$$\mathbf{U} = \begin{pmatrix} \boldsymbol{\lambda}_{\mathrm{ro}} \\ \boldsymbol{\lambda}_{\mathrm{vo}} \\ \boldsymbol{\lambda}_{\mathrm{rm}}^{+} \end{pmatrix}; \quad \mathbf{C} = \begin{pmatrix} \mathbf{r}_{\mathrm{m}} - \mathbf{R}_{\mathrm{m}} \\ \mathbf{r}_{\mathrm{f}} - \mathbf{R}_{\mathrm{f}} \\ \mathbf{v}_{\mathrm{f}} - \mathbf{V}_{\mathrm{f}} \end{pmatrix} \tag{5.51}$$

where, $\mathbf{U}$ 9×1 is a vector of the problem's unknowns, $\mathbf{C}$ 9×1 is a vector of the problem's constraints, $\mathbf{R}_{\mathrm{m}}$ is the desired midcourse position at t_{m}, $\mathbf{R}_{\mathrm{f}}$ is the desired final position, and $\mathbf{V}_{\mathrm{f}}$ is the desired final velocity. Note that $\lambda_{\mathrm{m0}} = -1$, as it monotonically decreases the final condition is known.

5.5.2 Multiple Shooting

The convergence of an optimal problem in the indirect method frame is very sensitive to the initial conditions and small control perturbations; therefore, a convergence for this type of problems is difficult. In order to improve the solution, a multiple shooting strategy is used, which attempts to limit the sensitivity issue by splitting the integration interval to reduce the propagation error. Moreover, the multiple shooting combined with the initial guess provided at step 4, allows the optimization to achieve convergence with a small number of iteration steps for feasible solutions.

In essence the multiple shooting strategy breaks the problem into Q segments (Q number defined by the user) that have to be patched in the optimized solution. This, in turn, adds constraints and unknowns to the TPBVP,

$$\mathbf{U} = \begin{pmatrix} \boldsymbol{\lambda}_{\mathrm{ro}} \\ \boldsymbol{\lambda}_{\mathrm{vo}} \\ \mathbf{y}_{\mathrm{i}} \end{pmatrix} \quad \text{for i=2:Q;} \quad \mathbf{C} = \begin{pmatrix} \mathbf{y}_1 - \int_{\mathrm{t}_0}^{\mathrm{t}_1} \mathbf{y}_{\mathrm{o}}\,\mathrm{dt} \\ \mathbf{y}_{\mathrm{i+1}} - \int_{\mathrm{t}_{\mathrm{i}}}^{\mathrm{t}_{\mathrm{i+1}}} \mathbf{y}_{\mathrm{i}}\,\mathrm{dt} \\ \int_{\mathrm{t}_{\mathrm{i}}}^{\mathrm{t}_{\mathrm{Q}}} \mathbf{y}_{\mathrm{Q}}\,\mathrm{dt} - \mathbf{y}_{\mathrm{f}} \\ \mathbf{r}_{\mathrm{f}} - \mathbf{R}_{\mathrm{f}} \\ \mathbf{v}_{\mathrm{f}} - \mathbf{V}_{\mathrm{f}} \end{pmatrix} \quad \text{for i=2:Q-1} \tag{5.52}$$

where, Q is the extra number of segments that the problem has been broken, being the midcourse point m somewhere in i. This process adds $\mathrm{Q} \times 14$ unknowns and constraints to the problem.

5.5.3 Analytical gradient

The analytical gradient improves the convergence accuracy and speed, it is calculated based on the state transition matrix, Eq. 5.17. The gradient, including the multiple shooting, is calculated as

$$\nabla \mathbf{C} = \frac{\partial \mathbf{C}}{\partial \mathbf{U}} = \begin{bmatrix} -\mathbf{\Phi}_0 & \mathbf{I} & & & & & & & \\ & -\mathbf{\Phi}_1 & \mathbf{I} & & & & & & \\ & & -\mathbf{\Phi}_2 & \mathbf{I} & & & & & \\ & & & \ddots & & & & & \\ & & & & \mathbf{A} & \mathbf{B} & & & \\ & & & & & \mathbf{C} & \mathbf{I} & & \\ & & & & & & \ddots & & \\ & & & & & & & -\mathbf{\Phi}_{\mathrm{Q}-1} & \mathbf{I} \\ & & & & & & & & -\mathbf{\Phi}_{\mathrm{Q}} \end{bmatrix} \tag{5.53}$$

where, the subscript in $\mathbf{\Phi}$ denotes the leg of the trajectory with m being the initial point of the midcourse leg, the blank space on the matrix represent zeros, and

$$\begin{aligned} \mathbf{A} &= -\left[\frac{\partial \begin{bmatrix} \mathbf{r}_{\mathrm{f}} & \mathbf{v}_{\mathrm{f}} & \mathrm{m}_{\mathrm{f}} & \boldsymbol{\lambda}_{\mathrm{vf}} & \lambda_{\mathrm{mf}} \end{bmatrix}}{\partial \mathbf{y}_{\mathrm{o}}}\right]_{\mathrm{Q_i=m-1}} \\ \mathbf{B} &= \begin{bmatrix} \mathbf{O}_{3\times 11} & \mathbf{I}_{4\times 11} \\ \mathbf{O}_{4\times 7} & \mathbf{I}_{4\times 4} \end{bmatrix} \\ \mathbf{C} &= -\left[\frac{\partial \mathbf{y}_{\mathrm{f}}}{\partial \begin{bmatrix} \mathbf{v}_{\mathrm{o}} & \mathbf{m}_{\mathrm{o}} & \boldsymbol{\lambda}_{\mathrm{ro}} & \lambda_{\mathrm{vo}} & \lambda_{\mathrm{mo}} \end{bmatrix}}\right]_{\mathrm{Q_i=m}} \end{aligned} \tag{5.54}$$

Note the discontinuity cause by the midcourse since the costates associated with the position, Eq. 5.50, do not need to be continuous and the position at the midcourse, $\mathbf{r}_{\mathrm{m}}$, is not an unknown.

5.6 Test Case

This section applies the selection and optimization method described in the previous sections to two test cases, the first case is the Phaethon flyby with a launch window that is significant for the DESTINY extended mission [Kawakatsu 2012], and the second case is a Itokawa rendezvous with the dates of the successful asteroid sample return Hayabusa mission [Project 2015]. These cases were selected due to their importance, for a future mission or historically from a past mission, and being one a flyby and the other a rendezvous.

The Phaethon flyby case has a launch date on 2023 and a ballistic trajectory with an Earth resonance close to 1:1. This particular solution is extracted from the catalog made on chapter 3, Figs. 3.3a and 3.8a. From all the possible trajectories in 2023, the selected ballistic trajectory has the lowest departure v_∞, Fig. 5.3a. To make the problem more interesting the ballistic trajectory's initial and final conditions are used to design a low-thrust trajectory, Fig. 5.3b, based on the theory

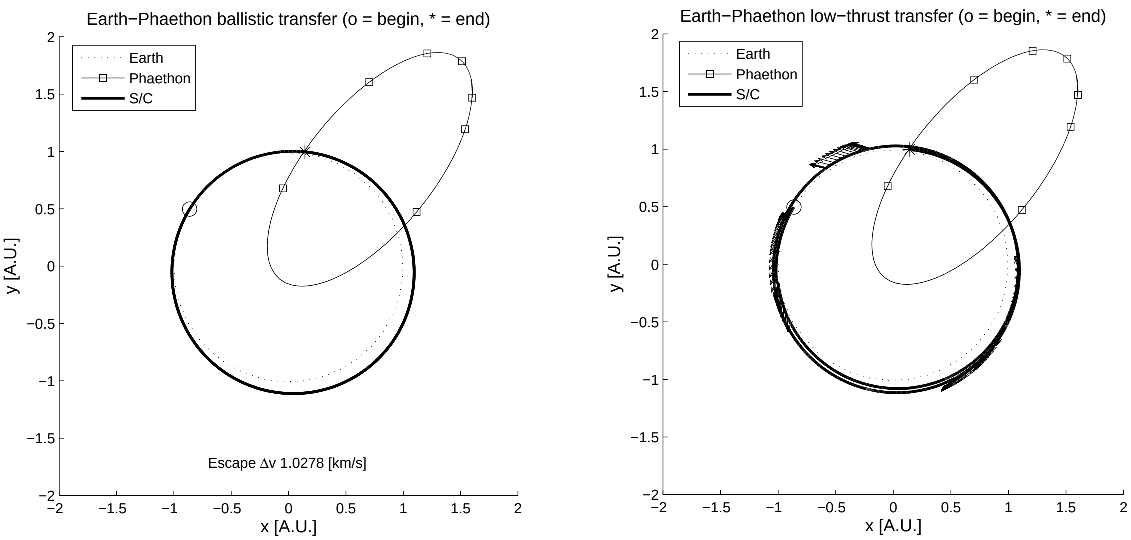

(a) Ballistic

(b) Low-thrust

Figure 5.3: Phaethon flyby ballistic and optimized low-thrust reference trajectories

Table 5.1: Spacecraft's Engine Characteristics

Total mass [kg]	400
Ion engine maximum thrust [N]	$40 \times 10^{-}3$
Ion engine specific impulse [s]	3800
Ion engine exhaust velocity [m/s]	37278
Amount of fuel available for the ion engine [kg]	30

presented in section 5.5, but without considering the midcourse. Table 5.1 presents the spacecraft's engine characteristics based on the DESTINY mission [Kawakatsu 2012] and the first column of Table 5.2 shows the low-thrust reference trajectory' initial and final constraints.

The Itokawa rendezvous case has a launch date on 9 May 2003 and rendezvous with the Itokawa asteroid on 15 September 2005. The ballistic trajectory is the same used on the test case of chapter 4, Fig. 5.4a. Once again to make the problem more interesting this trajectory's initial and final conditions are used to design a low-thrust trajectory (section 5.5), Fig. 5.4b, no midcourse present. The engine characteristics used in this problem are also from the DESTINY mission [Kawakatsu 2012], presented in Table 5.1. The second column of Table 5.2 shows the low-thrust reference trajectory' initial and final constraints.

Note that the low-thrust trajectories contain multiple thrusting arcs, inclination plan change, and have more than one revolution around the Sun; these characteristics make the selection process and optimization more challenging. Both low-thrust trajectories are taken as reference orbits for

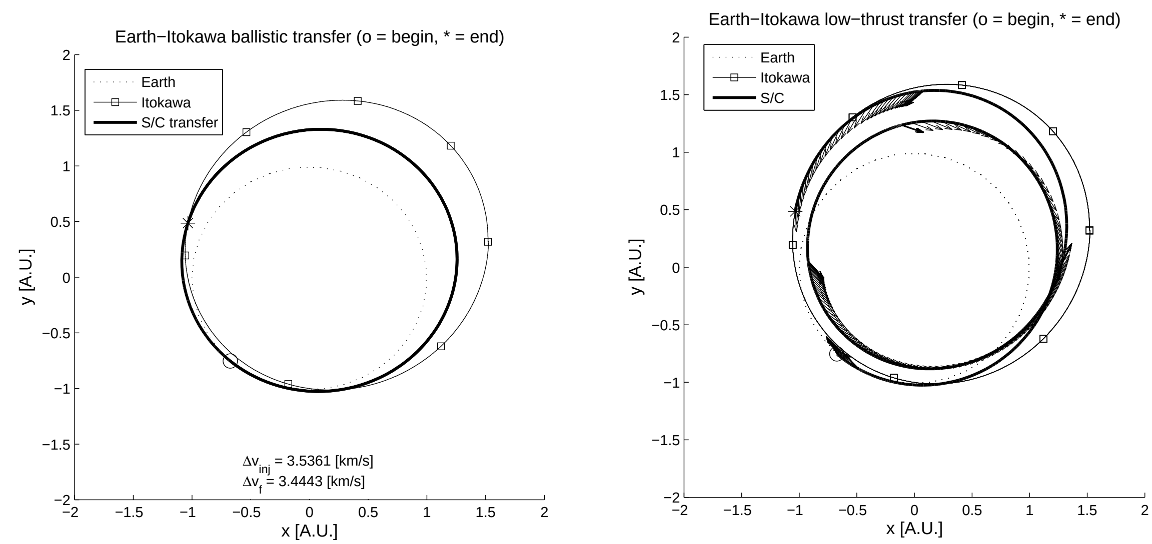

(a) Ballistic (b) Low-thrust

Figure 5.4: Itokawa rendezvous ballistic and optimized low-thrust reference trajectories

Table 5.2: Trajectories' Constraints

	Phaethon case	Itokawa case
Initial time [JD] [a]	2459994.50	2452768.50
Initial position [km] [b]	[-129069039.59, 68297033.40, 29641939.94]	[-100828403.28, -103436948.29, -44848186.14]
Initial velocity [km/s] [b]	[-15.50, -23.73, -10.29]	[24.18, -18.39, -8.99]
Final time [JD] [a]	2460722.50	2453628.50
Final position [km] [b]	[21369725.22, 135273745.92, 62827641.00]	[-154829289.66, 64733867.13, 33326886.71]
Final velocity [km/s] [b]	[-30.22, 2.94, 0.91]	[-8.23, -24.69, -11.09] [c]
Time step [point/day]	0.5	0.5

[a] Julian Date, JD.
[b] Values in the J2000 Ecliptic frame.
[c] v_∞ provided by the launcher.

the selection process described in section 5.4. Tables 5.3 and 5.4 show, respectively, the selection results for Phaethon and Itokawa cases highlighting the reference trajectory with each possible target point at each step represented by $\times$. Note that some asteroids can have more than one possible flyby point. A check was performed to confirm that no potential point is excluded in the selection process, the first 10 points excluded in steps 2, 3 and 4 are included in the optimization. As a result these excluded points did not converged, which means that no good point was excluded during the selection process. The points of the step 1 are not considered because the exclusion is based solely in the reachability defined by the engine characteristics.

Phaethon case presents 166 possible asteroid to fly by in 578 flyby points, while Itokawa case presents 256 different asteroids in 1362 flyby points. The simulation time for each step of the selection is presented in Table 5.5, where step 1 includes the precomputed database time. The simulations were performed in a MATLAB environment in a desktop machine with a dual processor, 16 cores, 2.40GHz and 16.0 GB of RAM memory. A considerable improvement on the simulation is expected if the process is made with native code. Finally, Fig. 5.5 presents the top 5 optimization results for the Phaethon case and Fig. 5.6 presents the top 5 optimization results for the Itokawa case. A list with the 166 asteroid targets for Phaethon and 256 for Itokawa is presented at the appendix F in Table F.1.

5.7 Conclusion

In this work a method for selecting and optimizing a midcourse flyby asteroid based on a reference trajectory was presented. Using optimal control, linear theory, and reachability a process was derived which allows the asteroid selection in a short time. The selection also provides a good initial guess for the posterior low-thrust trajectory optimization that, as a result of a good initial guess, converges in only a few iterations for feasible results. Finally, two test cases were used to provide a better understanding of the advantages of the selection and optimization methods.

The results show a fast selection and optimization for several midcourse asteroid flyby in both cases: a final Phaethon flyby and a Itokawa rendezvous. These test cases are of special interest because, not only they take into account realistic scenarios and engine characteristics, but also the reference trajectories have multiple revolutions, with multiple thrust and coast arcs, and a plane change. All these posed challenges for the trajectory selection and optimization methods, which were successfully completed for both test cases.

Table 5.3: Selected points at each step for the Phaethon case

Fist step	230235 points	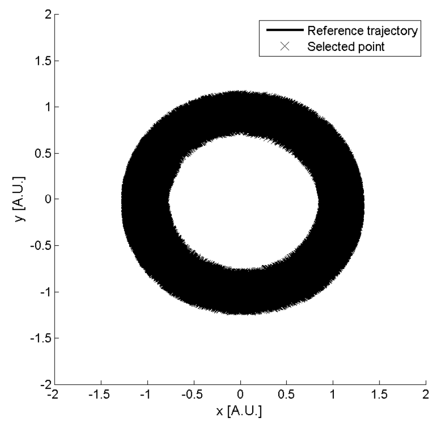
Second step	53614 points	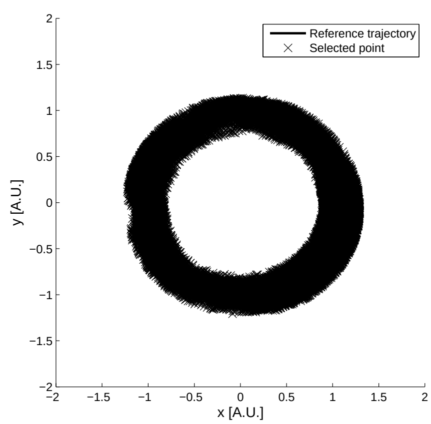
Third step	1045 points	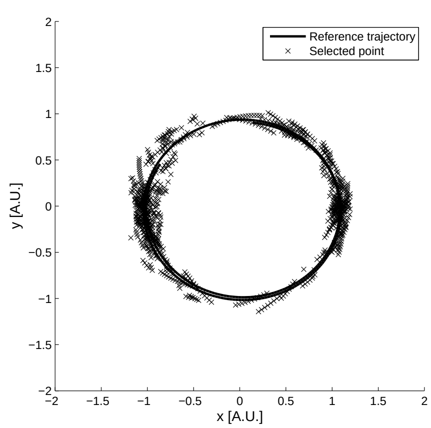
Fourth step	1045 points	Same points as the previous case, no exclusion.
Fifth step	578 points	Optimized orbits shown on Fig. 5.5

Table 5.4: Selected points at each step for the Itokawa case

Fist step	338425 points	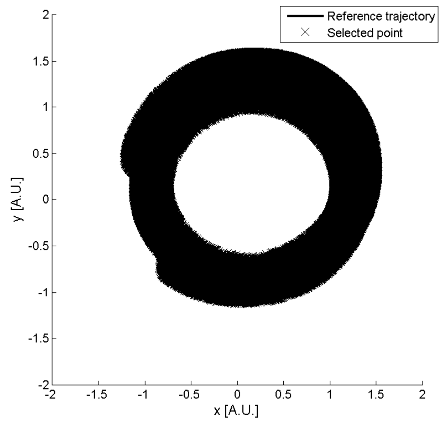
Second step	53706 points	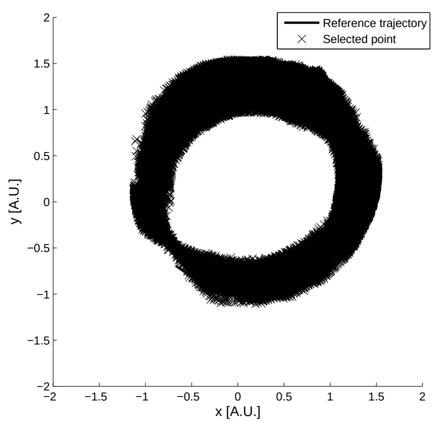
Third step	2253 points	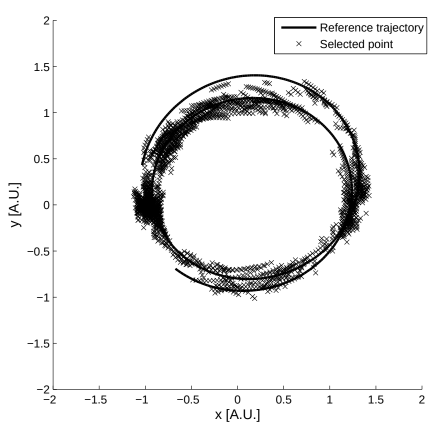
Fourth step	2253 points	Same points as the previous case, no exclusion.
Fifth step	1362 points	Optimized orbits shown on Fig. 5.6

Table 5.5: Simulation time

	Phaethon case	Itokawa case
Fist step	11.15 min	5.87 hours
Second step	32.31 min	57.24 min
Third step	31.51 min	41.85 min
Fourth step	1.53 sec	3.37 sec
Fifth step	5.42 hours	11.67 hours
Total	**7.20 hours**	**19.19 hours**

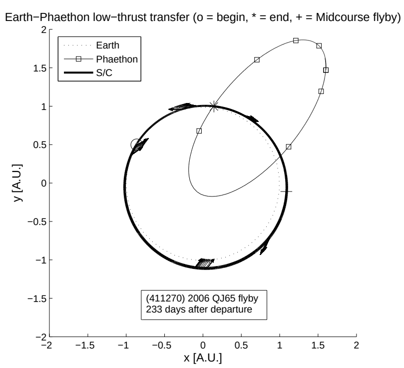

(a) Earth-(411270) 2006 QJ65-Phaethon

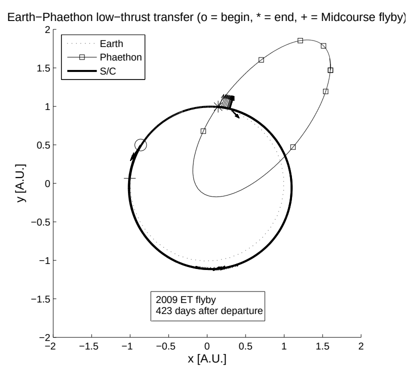

(b) Earth-2009 ET-Phaethon

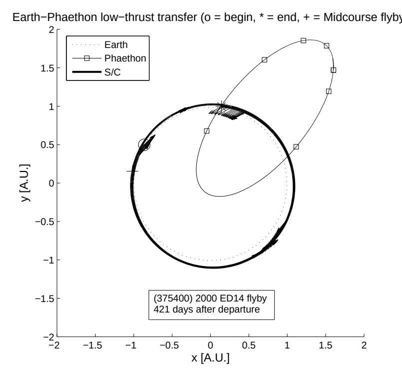

(c) Earth-(375400) 2000 ED14-Phaethon

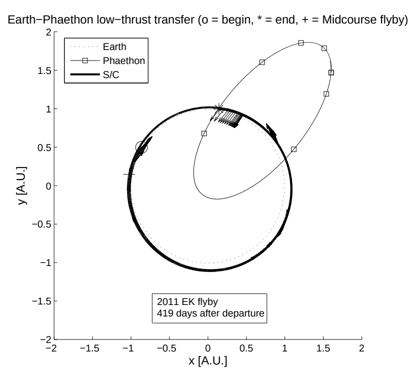

(d) Earth-2011 EK-Phaethon

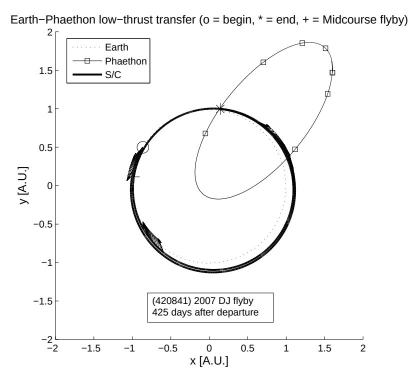

(e) Earth-(420841) 2007 DJ-Phaethon

Figure 5.5: Optimized low-thrust Phaethon flyby with midcourse asteroid flyby

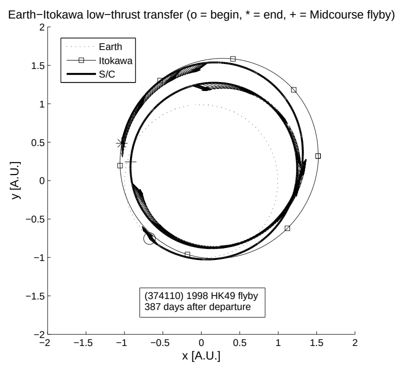

(a) Earth-(374110) 1998 HK49-Itokawa

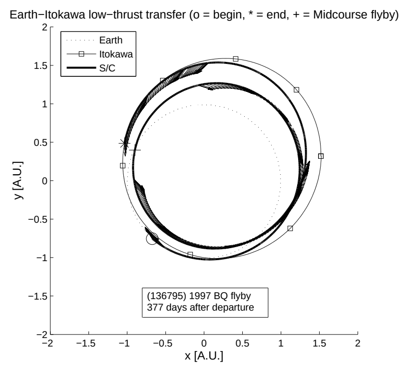

(b) Earth-(136795) 1997 BQ-Itokawa

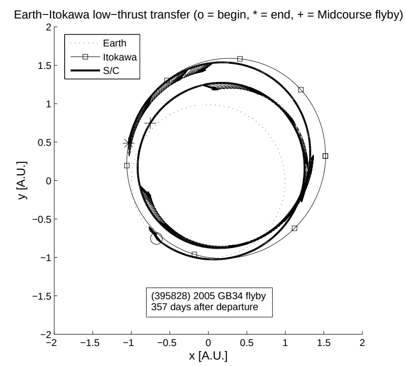

(c) Earth-(395828) 2005 GB34-Itokawa

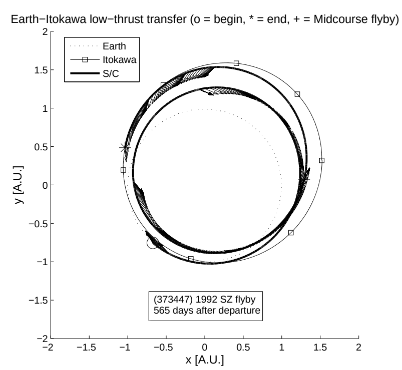

(d) Earth-(373447) 1992 SZ-Itokawa

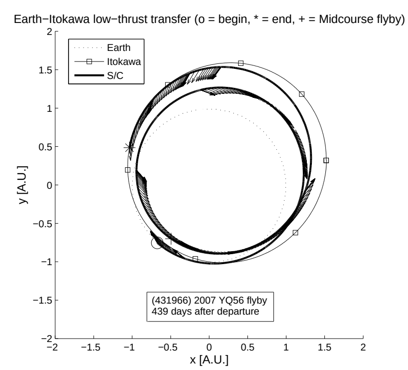

(e) Earth-(431966) 2007 YQ56-Itokawa

Figure 5.6: Optimized low-thrust Itokawa rendezvous with midcourse asteroid flyby

Chapter 6

Multiple Asteroid Flyby Mission Design

In this chapter a multiple asteroid flyby mission is designed using all concepts presented in the previous chapters. The design takes into account the ballistic search to find areas of interest, as presented in chapter 3. With an initially selected trajectory, it proceeds to make a low-thust trajectory with a midcourse asteroid flyby including the midcourse asteroid selection process (chapter 5). The spacecraft then is re-targeted back to Earth using a midcourse impulse for searching the arrival date (chapter 4). The GAM performed at the Earth arrival changes the trajectory to flyby another asteroid (chapter 3). As it will be seen, this mission, which was previously not possible, can be realized by using all the concepts and theories devised in this work.

As an example, the bodies of the Phaethon-Geminid complex are once again used as mission main targets. The design starts with a simple Phaethon asteroid flyby launching from Earth on 2023. The year 2023 is selected as a date of interest for the DESTINY extended mission [Kawakatsu 2012], as this work is also considered to be a preliminary assessment of one of the mission's extension proposal. Utilizing Fig. 3.3a (chapter 3) it is possible to select the cheapest ballistic flyby transfer to Phaethon on that year, Fig. 6.1. The selected trajectory coincides with the Phaethon case in chapter 5.

As presented on chapter 5, this Phaethon flyby is re-designed as a low-thrust trajectory (Fig. 6.2) and midcourse asteroid flyby trajectories are obtained using it as a reference. Note that the optimal solution is different from chapter 5 as the final velocity is free and not matching the ballistic result. For the propose of this example, the first rank result is selected: Earth departure, 1999 FR19 midcourse flyby, and (3200) Phaethon flyby, Fig. 6.3.

Although the final conditions at Phaethon flyby are a problem constraint, any asteroid selected on step 5 could be used since these are always the same in all solutions. A full list of all selected asteroids is presented in the appendix F in Table F.2.

Suppose that at the Phaethon flyby point the mission is not finalized and the objective of exploring (155140) 2005 UD is selected as an extension of the original mission. As seen on section 3.4.2 of chapter 3, there is no ballistic connection to 2005 UD for a launch window on 2023. However, new and improved solutions can be found if the a midcourse maneuver can be allowed; leveraging the required v_∞ at Phaethon. By using two impulses a good connection back to the Earth can be found if midcourse impulses are added. After the Phaethon flyby, an extensive search is performed using midcourse impulse method, as made in chapter 4, from the Phaethon flyby point back to Earth where the first impulse is considered at the Phaethon flyby point, Fig. 6.4.

An important consideration in analyzing the results from Fig. 6.4 is that the Earth arrival date needs to be such that an Earth departure date for 2005 UD with the maximum 3 km/s constraint

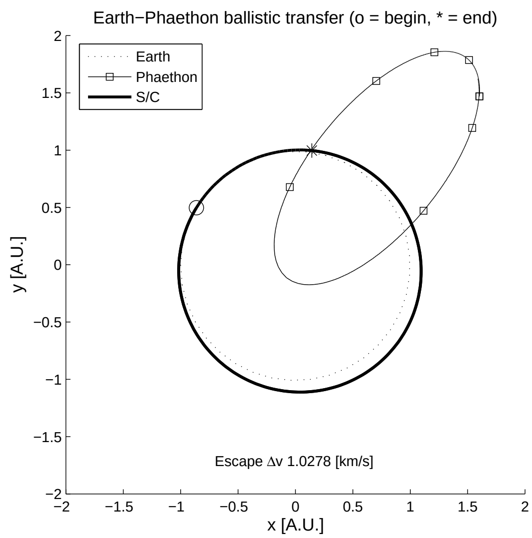

Figure 6.1: Cheapest ballistic Phaethon flyby on the year 2023

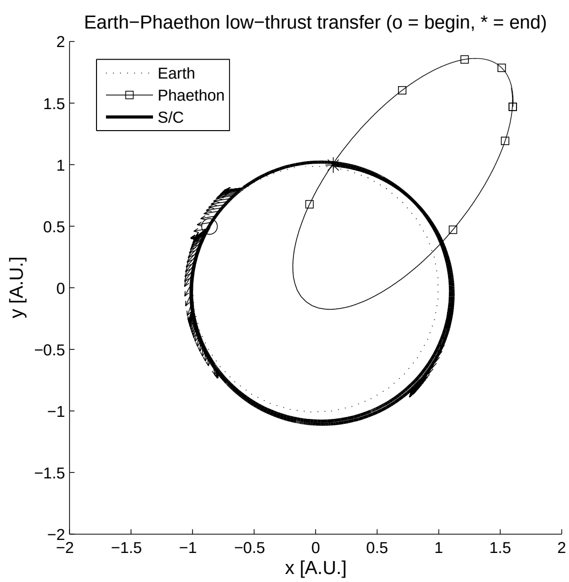

Figure 6.2: Phaethon flyby low-thrust reference trajectories

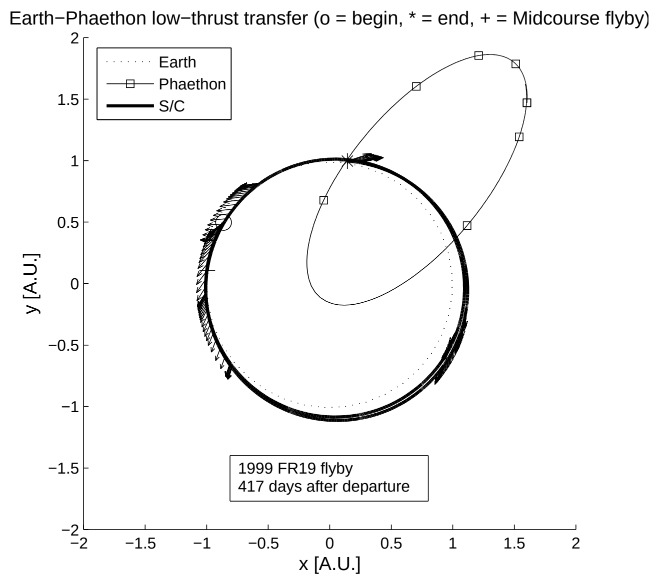

Figure 6.3: Optimized low-thrust Earth-1999 FR19-Phaethon trajectory

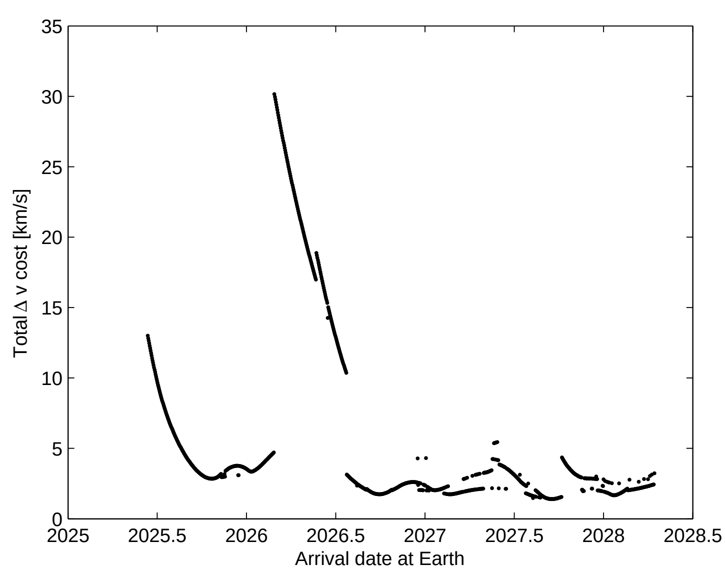

Figure 6.4: Midcourse impulse search Phaethon-to-Earth trajectory

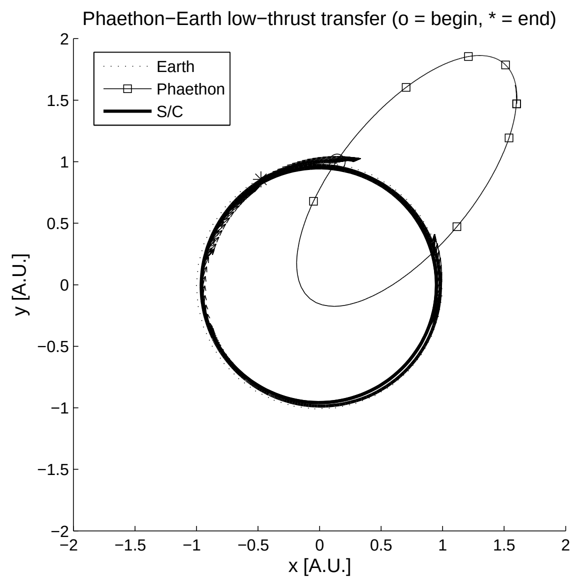

Figure 6.5: Phaethon-to-Earth Low-thrust transfer 19 January 2028 solution

exists. Utilizing Fig. 3.3b from chapter 3, an attractive Earth departure window to 2005 UD can be found in the beginning of 2028.

With the selected date a new low-thrust trajectory can be design from immediately after the Phaethon flyby back to Earth where the desired final condition is only in position (Earth flyby problem), Fig. 6.5.

Once again the theory presented on chapter 5 can be used to find another asteroid flyby between Phaethon and Earth while maintaining the Earth arrival conditions. The first rank result is selected: Phaethon flyby, 2011 SO189 midcourse flyby, and Earth return, Fig. 6.6. A full list of the 689 selected asteroids is presented at the appendix F in Table F.2.

The combined Earth-1999 FR19-Phaethon-2011 SO189-Earth trajectory has, at its final Earth encounter, the same low v_∞ as the required Earth departure v_∞ to flyby 2005 UD, which allows a ballistic transfer to 2005 UD if an appropriate Earth GAM is performed. It is interesting to point out that if the search is performed by a simple ballistic solution, this result would require almost 7 km/s. A final check needs to be performed to make sure that this Earth GAM can be made respecting the minimum altitude of 1000 km imposed on chapter 3. Utilizing, Eq. 3.1 an altitude of 46190 km above the Earth's surface is found.

The final multiple asteroid flyby trajectory it presented in Fig. 6.7, where the spacecraft departures from Earth on 19 February 2023 and utilizing its low-thrust propulsion system flies by 1999 FR19 on 9 April 2024 and (3200) Phaethon on 16 February 2025. After the Phaethon flyby, the spacecraft continues to use the low-thrust propulsion flying by the asteroid 2011 SO189 on 10 November 2025 and returning to Earth on 19 January 2028, performing an GAM at an altitude of 46190 km, which re-targets the vehicle to (155140) 2005 UD that is flown by on 23 October 2028.

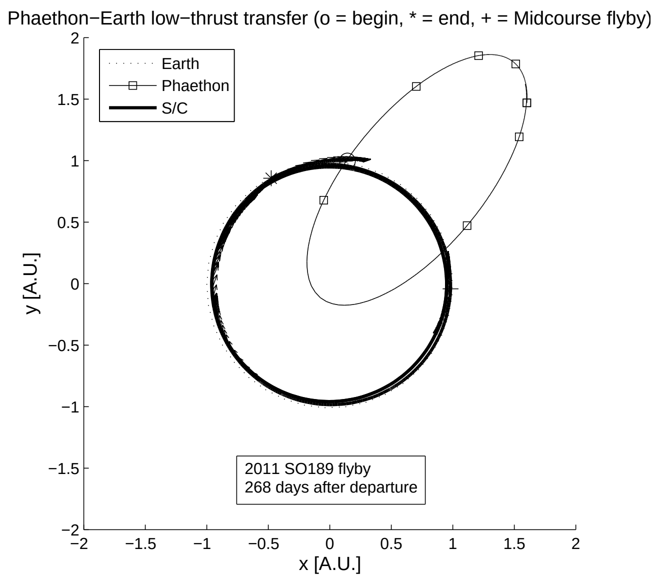

Figure 6.6: Optimized low-thrust Phaethon-2011 SO189-Earth trajectory

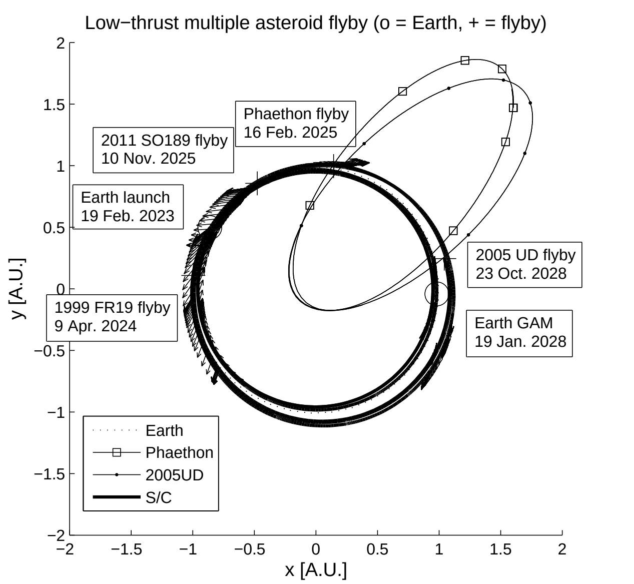

Figure 6.7: Multiple asteroid flyby trajectory Earth-1999 FR19-Phaethon-2011 SO189-Earth-2005 UD

CHAPTER 7

Conclusions

This work addresses the 2013 Global Exploration Roadmap that foresees deep space exploratory missions that are more frequent, cheaper, and with an increased scientific return. One of the possible answers to this demand is to flyby asteroids on the way to the main target by making a small change in the main trajectory. Particularly, asteroids have been chosen due to their great scientific relevance, e.g. they may posses answers to the solar system formation and the origins of life, and abundance, i.e. more than 700,000 cataloged. By modifying the main trajectory and adding an auxiliary flyby mission to a an asteroid, the mission's value is enhance with the addition of a small cost another body can be studied providing a bigger scientific return and making the mission as a whole more valuable as it is no longer dedicated to a single target; although it is still the mission's main target. Throughout this work, method and theories were developed for constructing and analyzing the main trajectory, as well as the auxiliary trajectory. The main types of trajectories used in trajectory design were studied: ballistic, impulsive and low-thrust. The latter also includes the asteroid selection process, which also provides the initial estimation for the low-thrust trajectory optimization.

The first area analyzed provides a global understanding of the problem allowing to identify the problem's most relevant trajectories and regions with lowest energy transfers. The design included ballistic trajectories which were path using gravity assist maneuvers allowing for different targets in a single mission. The second area takes into account the trajectory arcs developed in the previous step and by adding midcourse impulses it decreases the total propellant cost. The method to add the impulses looks for optimal solutions to decrease the cost taking into account the physical characteristics and conditions of where the impulse is provided, as well as if this impulse is indeed necessary. Finally, the third area takes the main trajectory, designed on the previous two areas, and uses as a reference for the auxiliary trajectory design that, while it maintains the mission's original target, adds a midcourse asteroid flyby by making a small modification to the original trajectory. The asteroid selection process, also included in the third area, is made to be progressive and fast, providing a good initial estimation for the posterior optimization.

The entire study developed here allows a global analysis of the complex problem of multiple asteroid flyby mission design. For all the areas comparisons were made against usual solution methods, the results showed a clear advantage in using the derivation presented here as it provides a better understanding of the problem with faster and, sometimes, more accurate solutions. As a final goal, the multiple asteroid flyby mission design study was successfully achieved including all the necessary considerations and presenting clear benefits. Future works can include transcribing the programs in native language to add speed, perform the final optimization with multiple midcourse targets, explore the problem in different dynamical systems such as the three-body problem, and perform a final optimization in the high-fidelity full-body dynamic system.

Bibliography

[Arora 2010] Nitin Arora and Ryan P. Russell. *A GPU Accelerated Multiple Revolution Lambert Solver for Fast Mission Design*. In 20th AAS/AIAA Space Flight Mechanics Meeting, volume AAS 10-198, San Diego, California, February 2010. American Astronautical Society. (Cited on pages 13 and 34.)

[Battin 1999] Richard H. Battin. An introduction to the mathematics and methods of astrodynamics. AIAA Education Series, Reston, Virginia, 1999. (Cited on pages 7, 13 and 34.)

[Blume 2005] William Blume. *Deep Impact Mission Design*. Space Science Reviews, vol. 117, no. 1-2, pages 23–42, March 2005. doi: 10.1007/s11214-005-3386-4. (Cited on pages 11 and 26.)

[Byrd 1999] Richard H. Byrd, Mary E. Hribar and Jorge Nocedal. *An Interior Point Algorithm for Large-Scale Nonlinear Programming*. SIAM Journal on Optimization, vol. 9, no. 4, pages 877–900, 1999. doi: 10.1137/S1052623497325107. (Cited on page 34.)

[Byrd 2000] Richard H. Byrd, Jean C. Gilbert and Jorge Nocedal. *A Trust Region Method Based on Interior Point Techniques for Nonlinear Programming*. Mathematical Programming, vol. 89, no. 1, pages 149–185, November 2000. doi: 10.1007/PL00011391. (Cited on page 34.)

[Campagnola 2014a] Stefano Campagnola. *Simple Fast Algorithm for Low-Thrust Guidance Problems*. In ISAS/JAXA Internal Note, Sagamihara, Japan, December 2014. Institute of Space and Astronautical Science. (Cited on page 55.)

[Campagnola 2014b] Stefano Campagnola and Ryan P. Russell. *Optimal Control on Gauss' Equations*. In 2nd IAA Conference on Dynamics and Control of Space Systems, volume IAA-AAS-DyCoSS2-14-14-01, Rome, Italy, March 2014. IAA Academie Internationale d'Astronautique. (Cited on page 51.)

[Campagnola 2015] Stefano Campagnola. *Linear Reachability Theory*. In ISAS/JAXA Internal Note, Sagamihara, Japan, May 2015. Institute of Space and Astronautical Science. (Cited on page 52.)

[Cochran 2006] A. Cochran and et al. *The Comet Nucleus Tour (Contour); A NASA Discovery Mission*. Earth, Moon, and Planets, vol. 89, no. 1-4, pages 289–300, July 2006. doi: 10.1023/A:1021567007750. (Cited on page 11.)

[Conway 2010] Bruce A. Conway. Spacecraft trajectory optimization. Cambridge University Press, Cambridge, 2010. (Cited on page 7.)

[de León 2010] J. de León, H. Campins, K. Tsiganis, A. Morbidelli and J. Licandro. *Origin of the near-Earth asteroid Phaethon and the Geminids meteor shower*. Astronomy and Astrophysics, vol. 513, no. A26, pages 1–7, April 2010. doi: 10.1051/0004-6361/200913609. (Cited on page 11.)

[Funase 2014] R. Funase, H. Koizumi, S. Nakasuka, Y. Kawakatsu, Y. Fukushima, A. Tomiki, Y. Kobayashi, J. Nakatsuka, M. Mita, D. Kobayashi and T. Nonomura. *50kg-class Deep Space Exploration Technology Demonstration Micro-spacecraft PROCYON*. In 28th Annual AIAA/USU Conference on Small Satellites, volume SSC14-VI-3, Logan, Utah, August 2014. The American Institute of Aeronautics and Astronautics. (Cited on page 26.)

[Gill 2002] Philip E. Gill, Walter Murray and Michael A. Saunders. *SNOPT: An SQP Algorithm for Large-Scale Constrained Optimization*. SIAM Journal of Optimization, vol. 12, no. 4, pages 979–1006, 2002. doi: 10.1137/S1052623499350013. (Cited on page 57.)

[Glandorf 1969] D. R. Glandorf. *Lagrange Multipliers and the State Transition Matrix for Coasting Arcs*. AIAA Journal, vol. 7, no. 2, pages 363–365, February 1969. doi: 10.2514/3.5109. (Cited on page 26.)

[ISECG 2013] International Space Exploration Coordination Group ISECG. The global exploration roadmap. ISECG, August 2013. Online: accessed 10-February-2014. (Cited on page 1.)

[Jewitt 2010] David Jewitt and Jing Li. *Activity in Geminid Parent (3200) Phaethon*. The Astronomical Journal, vol. 140, no. 5, pages 1519–1527, November 2010. doi:10.1088/0004-6256/140/5/1519. (Cited on page 11.)

[Jewitt 2013] David Jewitt, Jing Li and Jessia Agarwal. *The Dust Tail of Asteroid (3200) Phaethon*. The Astrophysical Journal Letters, vol. 771, no. 2, page L36, July 2013. doi: 10.1088/2041-8205/771/2/L36. (Cited on page 11.)

[Jezewski 1968] D. J. Jezewski and H. L. Rozendaal. *An Efficient Method for Calculating Optimal Free-Space N-impulsive Trajectories*. AIAA Journal, vol. 6, no. 11, pages 2160–2165, November 1968. doi: 10.2514/3.4949. (Cited on pages 8, 25, 28, 30 and 49.)

[Jezewski 1971] D. J. Jezewski and N. L. Faust. *Inequality Constraints in Primer-Optimal, N-Impulse Solutions*. AIAA Journal, vol. 9, no. 4, pages 760–763, April 1971. doi: 10.2514/3.6272. (Cited on pages 8, 25, 28, 30 and 49.)

[Kasuga 2006] T. Kasuga, J. Watanabe and M. Sato. *Direct Impact Mission to (3200) Phaethon: Artificial meteor shower of the once-active comet*. In 36th COSPAR Scientific Assembly, Beijing, China, July 2006. Committee on Space Research. (Cited on page 11.)

[Kasuga 2009] Toshihiro Kasuga. *Thermal Evolution of the Phaethon-Geminid Stream Complex*. Earth, Moon, and Planets, vol. 105, no. 2-4, pages 321–326, September 2009. doi: 10.1007/s11038-009-9311-1. (Cited on page 11.)

[Kawakatsu 2012] Yasuhiro Kawakatsu and Takahiro Itawa. *DESTINY Mission Overview: A Small Satellite Mission for Deep Space Exploration Technology Demonstration*. In The 13th International Space Conference of Pacific-basin Societies, volume 146, Kyoto, Japan, May 2012. American Astronautical Society. (Cited on pages 12, 13, 59, 60 and 67.)

[Kirk 2004] Donald E. Kirk. Optimal control theory: An introduction. Dover Publications, New York, 2004. (Cited on pages 7 and 28.)

[Lauretta 2012] Dante Lauretta and The OSIRIS-REx Team. *An overview of the OSIRIS-REx asteroid sample return mission*. In 43rd Lunar and Planetary Science Conference, page Paper 2491, The Woodlands, Texas, March 2012. Lunar and Planetary Inst. (Cited on pages 11 and 26.)

[Lawden 1963] Derek F. Lawden. Optimal trajectories for space navigation. Butterworths, London, 1963. (Cited on pages 7, 8, 25, 27, 32 and 48.)

[Lion 1968] Paul M. Lion and Morris Handelsman. *Primer Vector on Fixed-Time Impulsive Trajectories*. AIAA Journal, vol. 6, no. 1, pages 127–132, January 1968. doi: 10.2514/3.4452. (Cited on pages 8, 25, 28, 30 and 48.)

[McConaghy 2003] T. Troy McConaghy, Theresa J. Debban, Anastassios E. Petropoulos and James M. Longuski. *Design and Optimization of Low-Thrust Trajectories with Gravity Assists*. Journal of Spacecraft and Rockets, vol. 40, no. 3, pages 380–387, May 2003. doi: 10.2514/2.3973. (Cited on page 45.)

[MPC 2013] The Minor Planet Center MPC. Minor planet center orbit database (mpcorb). The International Astronomical Union, October 2013. Online: accessed 12-October-2013. (Cited on page 51.)

[Ohtsuka 2006] K. Ohtsuka, T. Sekiguchi, D. Kinoshita, J. I. Watanabe, T. Ito, H. Arakida and T. Kasuga. *Apollo asteroid 2005 UD: split nucleus of (3200) Phaethon?* Astronomy and Astrophysics, vol. 450, no. 3, pages L25–L28, May 2006. doi: 10.1051/0004-6361:200600022. (Cited on page 11.)

[Ohtsuka 2008] K. Ohtsuka, H. Arakida, T. Ito, M. Yoshikawa and D. J. Asher. *Apollo Asteroid 1999 YC: Another Large Member of the PGC?* Meteoritics and Planetary Science Supplement, vol. 43, no. S7, page A121, July 2008. doi:10.1111/j.1945-5100.2008.tb00711.x. (Cited on page 11.)

[Ozaki 2014] N. Ozaki, R. Funase, S. Nakajima, C. H. Yam, S. Campagnola, B. Sarli, Y. Sugimoto, H. Chen, S. Ogura, Y. Kawakatsu and S. Nakasuka. *Preliminary Mission Design of PROCYON: A Micro Spacecraft to Asteroid*. In 24rd International Symposium on Space Flight Dynamics, volume S2-4, Laurel, Maryland, May 2014. (Cited on pages 26 and 38.)

[Padevet 1986] V. Padevet, P. Lala and V. Bumba. *Scientific mission to asteroid Phaethon*. In 37th International Astronautical Congress, page 8, Innsbruck, Austria, October 1986. International Astronautical Federation. (Cited on page 11.)

[Perozzi 2001] Ettore Perozzi, Alessandro Rossi and Giovanni B. Valsecchi. *Basic targeting strategies for rendezvous and flyby missions to the near-Earth asteroids*. Planetary and Space Science, vol. 48, no. 1, pages 3–22, January 2001. doi: 10.1016/S0032-0633(00)00124-0. (Cited on page 11.)

[Petropoulos 2008] Anastassios E. Petropoulos and Ryan P. Russell. *Low-Thrust Transfers using Primer Vector Theory and a Second-Order Penalty Method*. In AIAA/AAS Astrodynamics Specialist Conference and Exhibit, volume AIAA 2008-6955, Honolulu, Hawaii, August 2008. American Institute of Aeronautics and Astronautics. (Cited on pages 8 and 49.)

[Pontryagin 1987] Lev Semyonovich Pontryagin. Mathematical theory of optimal processes. CRC Press, London, 1987. (Cited on pages 8 and 47.)

[Press 1997] William H. Press, Saul Teukolsky, William T. Vetterling and Brian P. Flannery. Numerical recipies in c, the art of scientific computing. Cambridge University Press, Cambridge, 1997. (Cited on page 45.)

[Project 2015] HAYABUSA Project. Hayabusa project - science and data archive. Data Archives and Transmission System DARTS, September 2015. Online: accessed 30-September-2015. (Cited on page 59.)

[Ranieri 2005] Christopher L. Ranieri and Cesar A. Ocampo. *Optimization of Round-Trip, Time-Constrained, Finite-Burn Trajectories via and Indirect Method*. Journal of Guidance, Control, and Dynamics, vol. 28, no. 2, pages 306–314, March 2005. doi: 10.2514/1.5540. (Cited on pages 8, 45 and 49.)

[Russell 2007] Ryan P. Russell. *Primer Vector Theory Applied to Global Low-Thrust Trade Studies*. Journal of Guidance, Control, and Dynamics, vol. 30, no. 2, pages 460–472, March 2007. doi: 10.2514/1.22984. (Cited on pages 8, 45, 48 and 49.)

[Sarli 2013] Bruno V. Sarli and Yasuhiro Kawakatsu. *Orbit Transfer Optimization for Multiple Asteroid Flybys*. In SICE Annual Conference, volume TuBT7.4, Nagoya, Japan, September 2013. The Society of Instrument and Control Engineers. (Cited on page 25.)

[Senent 2005] Juan Senent, Cesar Ocampo and Antonio Capella. *Low-Thrust Variable Specific Impulse Transfers and Guidance to Unstable Periodic Orbits*. Journal of Guidance, Control, and Dynamics, vol. 28, no. 2, pages 280–290, March 2005. doi: 10.2514/1.6398. (Cited on pages 8 and 49.)

[Shen 2003] Haijun Shen and Panagiotis Tsiotras. *Using Battin's Method to Obtain Multiple-Revolution Lambert's Solutions*. In 2003 AAS/AIAA Space Flight Mechanics Meeting, volume AAS 03-568, Big Sky, Montana, August 2003. American Astronautical Society. (Cited on pages 13 and 34.)

[Sims 2006] Jon A. Sims, Paul A. Finlayson, Edward A. Rinderle, Matthew A. Vavrina and Theresa D. Kowalkowski. *Implementation of a Low-Thrust Trajectory Optimization Algorithm for Preliminary Design*. In AIAA/AAS Astrodynamics Specialist Conference and Exhibit, volume AIAA 2006-6746, Keystone, Colorado, August 2006. American Institute of Aeronautics and Astronautics. (Cited on pages 45 and 55.)

[Vallado 2007] David A. Vallado. Fundamental of astrodynamics and applications, 3rd edition. Microcosm Publishing, Portland, Oregon, 2007. (Cited on pages 7, 13 and 34.)

[Wagner 2011] Sam Wagner and Bong Wie. *GPU Accelerated Lambert Solution Methods for the Orbital Targeting Problem*. In 21th AAS/AIAA Space Flight Mechanics Meeting, volume AAS 11-263, New Orleans, Louisiana, February 2011. American Astronautical Society. (Cited on pages 13 and 34.)

APPENDIX A

Calculus of Variations Applied to Optimal Control

A.1 Fundamental Concepts

A Functional J is a correspondence rule that assigns to each function, of a certain class Ω (functional's domain), a single real number (Fig. A.1).

If q and $q+\Delta q$ are elements in which a function f is defined, them the increment of f is

$$\Delta f(q,\Delta q) = f(q+\Delta q) - f(q) \tag{A.1}$$

The increment of a function $f:\mathbb{R}^n \to \mathbb{R}$ can be written as $\Delta f(q,\Delta q) = df(q,\Delta q) + g(q,\Delta q)\|\Delta q\|$, if J is linear in Δq. If $\lim_{\Delta q \to \infty} g(q,\Delta q) = 0$, then f is differentiable in the point q and df is the differentiation at this point,

$$df = \frac{\partial f}{\partial q_1}\Delta q_1 + \frac{\partial f}{\partial q_2}\Delta q_2 + \cdots + \frac{\partial f}{\partial q_n}\Delta q_n \tag{A.2}$$

On the other hand, if x and $x+\delta x$ are two functions, in which the functional J is defined, the increment of J, ΔJ, is, Fig. A.2,

$$\Delta J(x,\delta x) = J(x+\delta x) - J(x) \tag{A.3}$$

In a similar way as the function, the increment of a functional $J:\Omega \to \mathbb{R}$ can be written as

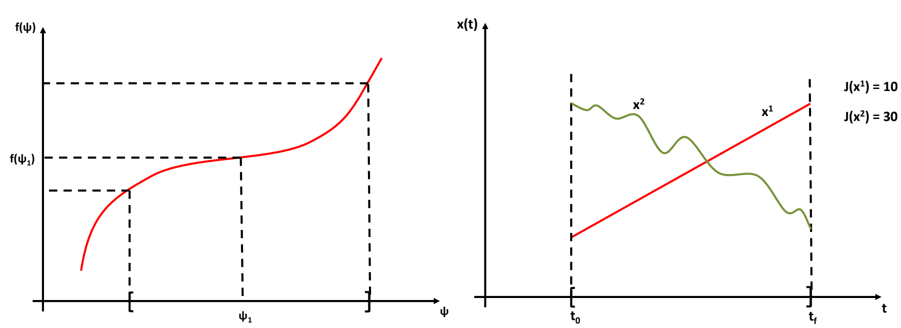

Figure A.1: Example of the function and functional domains

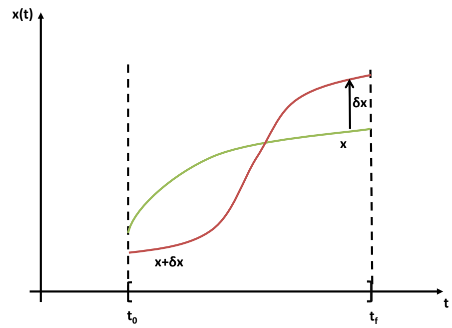

Figure A.2: Example of a functional increment

$\Delta J(x, \delta x) = \delta J(x, \delta x) + g(x, \delta x)\|\delta x\|$ with δJ linear in δx. If $\lim_{\delta x \to \infty} g(x, \Delta x) = 0$, then J is differentiable in x and δJ is the variation of J with respect to the function x.

As a function, the functional can also have maximum and minimum values, these points are called extremas. A functional $J : \Omega \to \mathbb{R}$ has a local extrema in x^* if an infinitesimal positive value exists, $\exists\ \varepsilon > 0$, in which the increment of J to every function $x \in \Omega$, $\|x - x^*\| < \varepsilon$, has the same signal (Eq. A.4).

$$\begin{cases} \Delta J = J(x) - J(x^*) \geqslant 0, J(x^*) \text{ is a local minimum} \\ \Delta J = J(x) - J(x^*) \leqslant 0, J(x^*) \text{ is a local maximum} \end{cases} \tag{A.4}$$

If the extrema conditions are satisfied for an arbitrary large ε, the maximum or minimum extrema is global and x^* is called extremal.

A.2 Fundamental Lemma of Calculus of Variations

Let $J : \Omega \to \mathbb{R}$ be a differentiable functional with its functions not constrained in value. If x^* is one of the extremal of this functional, then the variation of J in x^* is equal to zero (Eq. A.5).

$$\delta J(x^*, \delta x) = 0, \forall\ \delta x \text{ admissible} \tag{A.5}$$

A formal proof of the fundamental lemma of the calculus of variations can be found in appendix E.

A.3 Optimal Control Problem

Consider a cost function of the Bolza form given by a functional $J : \Omega \to \mathbb{R}$ of the form

$$J(x_f, u_f, t_f, x_0, u_0, t_0, x, u, t) = h(x_f, u_f, t_f, x_0, u_0, t_0) + \int_{t_0}^{t_f} g(x, u, t)\, dt \tag{A.6}$$

where, h is a function of the end and start point conditions (Mayer function) $h(x_f, u_f, t_f, x_0, u_0, t_0) \in \mathbb{C}^2$, g is a function of the path conditions (Lagrange function) $g(x, u, t) \in \mathbb{C}^2$, $x(t)$ is a vector containing the state variables $x(t) \in \mathbb{R}^n$, $u(t)$ is a vector containing the control variables $u(t) \in \mathbb{R}^m$ and t is the time.

The cost function is constrained in its path by the dynamics of the system, $\dot{x}(t) = f(x,u,t)$, and the control, $d(u,t) = 0 \in \mathbb{R}^q$; also, it is constrained at the start and end points by the boundary conditions $c(x_f,u_f,t_f,x_0,u_0,t_0) = 0 \in \mathbb{R}^p$. It is important to point out that c and d may introduce new variables that will have to be taken into account as extra state or control variables in the formulation.

It is possible to augment the cost function in order to include the constrains by using Lagrange multipliers.

$$\begin{aligned}\bar{J}(x,u,\boldsymbol{\lambda},\boldsymbol{\eta},t) &= h(x_f,u_f,t_f,x_0,u_0,t_0) + {}^t\boldsymbol{\nu} c(x_f,u_f,t_f,x_0,u_0,t_0) \\ &+ \int_{t_0}^{t_f} \left\{ g(x,u,t) + {}^t\boldsymbol{\lambda}(t)[f(x,u,t) - \dot{x}(t)] + {}^t\boldsymbol{\eta}(t)d(u,t) \right\} dt\end{aligned} \tag{A.7}$$

where, ν are constant Lagrange multipliers associated with the boundary constraints, $\boldsymbol{\lambda}(t)$ and $\boldsymbol{\eta}(t)$ are the Lagrange multipliers associated with the states and controls, respectively. The Lagrange multipliers outside the integral are constant while the ones inside the integral are a function of time. The augmented cost is then a function of all the new variables, note that ν is not a new state for it is a vector of constants.

For analysis, it is possible to transform $\bar{J}$ into a full Lagrange function combining Eqs. A.8 and A.9,

$$\frac{d\boldsymbol{\varphi}(x,t)}{dt} = {}^t\frac{\partial \boldsymbol{\varphi}(x,t)}{\partial x}\frac{dx}{dt} + \frac{\partial \boldsymbol{\varphi}(x,t)}{\partial t} \tag{A.8}$$

$$\int_{t_0}^{t_f} \frac{d\boldsymbol{\varphi}(x,t)}{dt} dt = \boldsymbol{\varphi}(x_f,t_f) - \boldsymbol{\varphi}(x_0,t_0) \tag{A.9}$$

which generates

$$\boldsymbol{\varphi}(x_f,t_f) - \boldsymbol{\varphi}(x_0,t_0) = \int_{t_0}^{t_f} \left\{ {}^t\frac{\partial \boldsymbol{\varphi}(x,t)}{\partial x}\dot{x} + \frac{\partial \boldsymbol{\varphi}(x,t)}{\partial t} \right\} dt \tag{A.10}$$

Important, note that in Eq. A.10 the constants at the beginning are with opposite sign of the convention used here. Therefore, the values of the integration at $\boldsymbol{\varphi}(x_0,t_0)$ will have opposite sign.

The augmented cost function in Lagrange format is

$$\begin{aligned}\bar{J}(x,u,\boldsymbol{\lambda},\boldsymbol{\eta},t) = \int_{t_0}^{t_f} \Bigg\{ & g(x,u,t) + {}^t\boldsymbol{\lambda}(t)[f(x,u,t) - \dot{x}(t)] + {}^t\boldsymbol{\eta}(t)d(u,t) + {}^t\frac{\partial h(x,u,t)}{\partial x}\dot{x}(t) \\ & + \frac{\partial h(x,u,t)}{\partial t} + {}^t\boldsymbol{\nu}^t\frac{\partial c(x,u,t)}{\partial x}\dot{x}(t) + {}^t\boldsymbol{\nu}\frac{\partial c(x,u,t)}{\partial t} \Bigg\} dt\end{aligned} \tag{A.11}$$

It is also possible to recall form the analytical mechanics the definition of Hamiltonian, $H(x,u,\boldsymbol{\lambda},t) \in \mathbb{C}^2$,

$$H(x,u,\boldsymbol{\lambda},t) = g(x,u,t) + {}^t\boldsymbol{\lambda}(t)f(x,u,t) \tag{A.12}$$

and apply it to Eq. A.11,

$$\begin{aligned}\bar{J}(x,u,\boldsymbol{\lambda},\boldsymbol{\eta},t) = \int_{t_0}^{t_f} \Bigg\{ & H(x,u,\boldsymbol{\lambda},t) - {}^t\boldsymbol{\lambda}(t)\dot{x}(t) + {}^t\boldsymbol{\eta}(t)d(u,t) + {}^t\frac{\partial h(x,u,t)}{\partial x}\dot{x}(t) \\ & + \frac{\partial h(x,u,t)}{\partial t} + {}^t\boldsymbol{\nu}^t\frac{\partial c(x,u,t)}{\partial x}\dot{x}(t) + {}^t\boldsymbol{\nu}\frac{\partial c(x,u,t)}{\partial t} \Bigg\} dt\end{aligned} \tag{A.13}$$

Defining $\bar{\mathrm{q}}$ to be equal to the integral contents, $\bar{\mathrm{J}}$ becomes

$$\bar{\mathrm{J}}(\mathrm{w},\dot{\mathrm{w}},\mathrm{t}) = \int_{\mathrm{t}_0}^{\mathrm{t}_\mathrm{f}} \bar{\mathrm{q}}(\mathrm{w},\dot{\mathrm{w}},\mathrm{t})\,\mathrm{dt} \tag{A.14}$$

where, ${}^{\mathrm{t}}\mathrm{w}(\mathrm{t}) = [\mathrm{x}(\mathrm{t}),\mathrm{u}(\mathrm{t}),\boldsymbol{\lambda}(\mathrm{t}),\boldsymbol{\eta}(\mathrm{t})]$.

Referring back to the theory presented at sections A.1 and A.2, $\bar{\mathrm{J}}$ will be stationary if its variation is zero in every variable.

$$\begin{aligned}\delta\bar{\mathrm{J}}(\mathrm{w},\dot{\mathrm{w}},\mathrm{t}) &= \frac{\partial\bar{\mathrm{J}}(\mathrm{w},\dot{\mathrm{w}},\mathrm{t})}{\partial\mathrm{w}}\delta\mathrm{w} + \frac{\partial\bar{\mathrm{J}}(\mathrm{w},\dot{\mathrm{w}},\mathrm{t})}{\partial\dot{\mathrm{w}}}\delta\dot{\mathrm{w}} + \frac{\partial\bar{\mathrm{J}}(\mathrm{w},\dot{\mathrm{w}},\mathrm{t})}{\partial\mathrm{t}}\delta\mathrm{t} \\ &= \int_{\mathrm{t}_0}^{\mathrm{t}_\mathrm{f}}\left\{\frac{\partial\bar{\mathrm{q}}(\mathrm{w},\dot{\mathrm{w}},\mathrm{t})}{\partial\mathrm{w}}\delta\mathrm{w} + \frac{\partial\bar{\mathrm{q}}(\mathrm{w},\dot{\mathrm{w}},\mathrm{t})}{\partial\dot{\mathrm{w}}}\delta\dot{\mathrm{w}} + \frac{\partial\bar{\mathrm{q}}(\mathrm{w},\dot{\mathrm{w}},\mathrm{t})}{\partial\mathrm{t}}\delta\mathrm{t}\right\}\mathrm{dt}\end{aligned} \tag{A.15}$$

Note in the above equation that the infinitesimal increments are given not only in the variables, w and t, but also in one of its derivatives, $\dot{\mathrm{w}}$. Therefore, in order to evaluate a stationary $\bar{\mathrm{J}}$ with the fundamental lemma of Calculus of Variations, $\delta\dot{\mathrm{w}}$ needs to be translated into the other two variables w and t. For simplicity, the partial derivatives will be represented by a subscript, $\frac{\partial \mathrm{f}}{\partial \mathrm{x}} = \mathrm{f}_\mathrm{x}$.

Using the chain rule,

$$\begin{aligned}\frac{\mathrm{d}(\mathrm{u}(\mathrm{t})\mathrm{v}(\mathrm{t}))}{\mathrm{dt}} &= \frac{\mathrm{du}(\mathrm{t})}{\mathrm{dt}}\mathrm{v}(\mathrm{t}) + \mathrm{u}(\mathrm{t})\frac{\mathrm{dv}(\mathrm{t})}{\mathrm{dt}} \\ \int\frac{\mathrm{d}(\mathrm{u}(\mathrm{t})\mathrm{v}(\mathrm{t}))}{\mathrm{dt}}\,\mathrm{dt} &= \int\left\{\frac{\mathrm{du}(\mathrm{t})}{\mathrm{dt}}\mathrm{v}(\mathrm{t}) + \mathrm{u}(\mathrm{t})\frac{\mathrm{dv}(\mathrm{t})}{\mathrm{dt}}\right\}\mathrm{dt} \\ \mathrm{u}(\mathrm{t})\mathrm{v}(\mathrm{t}) &= \int\frac{\mathrm{du}(\mathrm{t})}{\mathrm{dt}}\mathrm{v}(\mathrm{t})\,\mathrm{dt} + \int\mathrm{u}(\mathrm{t})\frac{\mathrm{dv}(\mathrm{t})}{\mathrm{dt}}\,\mathrm{dt} \\ \int\mathrm{u}(\mathrm{t})\frac{\mathrm{dv}(\mathrm{t})}{\mathrm{dt}}\,\mathrm{dt} &= \mathrm{u}(\mathrm{t})\mathrm{v}(\mathrm{t}) - \int\frac{\mathrm{du}(\mathrm{t})}{\mathrm{dt}}\mathrm{v}(\mathrm{t})\,\mathrm{dt}\end{aligned} \tag{A.16}$$

and defining $\mathrm{u} = \bar{\mathrm{q}}_{\dot{\mathrm{w}}}$ and $\mathrm{dv} = \delta\dot{\mathrm{w}}$, the integral

$$\int_{\mathrm{t}_0}^{\mathrm{t}_\mathrm{f}}\{\bar{\mathrm{q}}_{\dot{\mathrm{w}}}\delta\dot{\mathrm{w}}\}\,\mathrm{dt} = \{\bar{\mathrm{q}}_{\dot{\mathrm{w}}}\delta\mathrm{w}\}|_{\mathrm{t}_0}^{\mathrm{t}_\mathrm{f}} - \int_{\mathrm{t}_0}^{\mathrm{t}_\mathrm{f}}\left\{\frac{\mathrm{d}\bar{\mathrm{q}}_{\dot{\mathrm{w}}}}{\mathrm{dt}}\delta\mathrm{w}\right\}\mathrm{dt} \tag{A.17}$$

Also, with a first order approximation, Fig. A.3,

$$\delta\mathrm{w}(\mathrm{t}+\delta\mathrm{t}) \simeq \delta\mathrm{w}(\mathrm{t}) + \dot{\mathrm{w}}(\mathrm{t})\delta\mathrm{t} \longrightarrow \delta\mathrm{w}(\mathrm{t}) \simeq \delta\mathrm{w}(\mathrm{t}+\delta\mathrm{t}) - \dot{\mathrm{w}}(\mathrm{t})\delta\mathrm{t} \tag{A.18}$$

Using Eq. A.18 into Eq. A.17, the final form of $\delta\dot{\mathrm{w}}$ becomes

$$\{\bar{\mathrm{q}}_{\dot{\mathrm{w}}}\delta\mathrm{w}\}|_{\mathrm{t}_0}^{\mathrm{t}_\mathrm{f}} - \int_{\mathrm{t}_0}^{\mathrm{t}_\mathrm{f}}\left\{\frac{\mathrm{d}\bar{\mathrm{q}}_{\dot{\mathrm{w}}}}{\mathrm{dt}}\delta\mathrm{w}\right\}\mathrm{dt} = \{\bar{\mathrm{q}}_{\dot{\mathrm{w}}}(\delta\mathrm{w} - \dot{\mathrm{w}}\delta\mathrm{t})\}|_{\mathrm{t}_0}^{\mathrm{t}_\mathrm{f}} - \int_{\mathrm{t}_0}^{\mathrm{t}_\mathrm{f}}\left\{\frac{\mathrm{d}\bar{\mathrm{q}}_{\dot{\mathrm{w}}}}{\mathrm{dt}}\delta\mathrm{w}\right\}\mathrm{dt} \tag{A.19}$$

and

$$\int_{\mathrm{t}_0}^{\mathrm{t}_\mathrm{f}}\{\bar{\mathrm{q}}_\mathrm{t}\delta\mathrm{t}\}\,\mathrm{dt} = \int_{\mathrm{t}_0}^{\mathrm{t}_\mathrm{f}}\left\{\frac{\partial\bar{\mathrm{q}}}{\partial\mathrm{t}}\delta\mathrm{t}\right\}\mathrm{dt} \approx \left\{\int_{\mathrm{t}_0}^{\mathrm{t}_\mathrm{f}}\frac{\partial\bar{\mathrm{q}}}{\partial\mathrm{t}}\mathrm{dt}\right\}\delta\mathrm{t} \approx \{\bar{\mathrm{q}}\delta\mathrm{t}\}|_{\mathrm{t}_0}^{\mathrm{t}_\mathrm{f}} \tag{A.20}$$

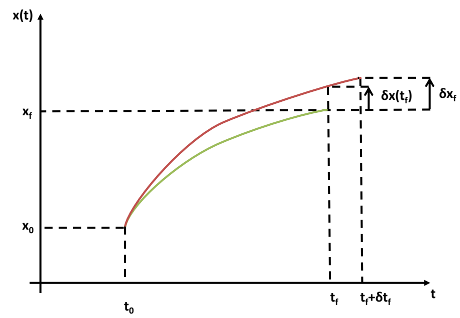

Figure A.3: First order approximation of the states variation

With Eq. A.20, the final form of the cost variation is,

$$\delta\bar{J} = \{(\bar{q} - \bar{q}_{\dot{w}}\dot{w})\,\delta t + \bar{q}_{\dot{w}}\delta w\}|_{t_0}^{t_f} + \int_{t_0}^{t_f}\left\{\bar{q}_w - \frac{d\bar{q}_{\dot{w}}}{dt}\right\}\delta w\, dt \tag{A.21}$$

For a stationary cost each term of the above integral has to be zero,

$$\delta\bar{J}[w(t), \dot{w}(t), t] = 0 \tag{A.22}$$

$$\{(\bar{q} - \bar{q}_{\dot{w}}\dot{w})\,\delta t\}|_{t_0}^{t_f} = 0 \tag{A.23}$$

$$\{\bar{q}_{\dot{w}}\delta w\}|_{t_0}^{t_f} = 0 \tag{A.24}$$

$$\bar{q}_w - \frac{d\bar{q}_{\dot{w}}}{dt} = 0 \tag{A.25}$$

expanding the partial derivatives for each variable

$$\bar{q}_w = \begin{bmatrix} \bar{q}_x \\ \bar{q}_u \\ \bar{q}_\lambda \\ \bar{q}_\eta \end{bmatrix} = \begin{bmatrix} H_x + {}^t h_{x^2}\dot{x} + h_{xt} + {}^t\boldsymbol{\nu}^t c_{x^2}\dot{x} + {}^t\boldsymbol{\nu} c_{xt} \\ H_u + {}^t\boldsymbol{\eta} d_u + {}^t h_{xu}\dot{x} + h_{ut} + {}^t\boldsymbol{\nu}^t c_{xu}\dot{x} + {}^t\boldsymbol{\nu} c_{ut} \\ H_\lambda - \dot{x} \\ d \end{bmatrix} \tag{A.26}$$

$$\bar{q}_{\dot{w}} = \begin{bmatrix} \bar{q}_{\dot{x}} \\ \bar{q}_{\dot{u}} \\ \bar{q}_{\dot{\lambda}} \\ \bar{q}_{\dot{\eta}} \end{bmatrix} = \begin{bmatrix} -{}^t\boldsymbol{\lambda} + {}^t h_x + {}^t\boldsymbol{\nu}^t c_x \\ 0 \\ 0 \\ 0 \end{bmatrix} \tag{A.27}$$

Starting with Eq. A.25, better know as the Euler-Lagrange equation, we obtain a set of equations for each line:

First line

$$H_x + {}^t h_{x^2}\dot{x} + h_{xt} + {}^t\boldsymbol{\nu}^t c_{x^2}\dot{x} + {}^t\boldsymbol{\nu} c_{xt} - \frac{d}{dt}\left(-{}^t\boldsymbol{\lambda} + {}^t h_x + {}^t\boldsymbol{\nu}^t c_x\right) \tag{A.28}$$

Observation,

$$\frac{dh_x}{dt} = h_{x^2}\dot{x} + h_{xt} \tag{A.29}$$

Developing Eq. A.28 and including Eq. A.29

$$H_x + h_{x^2}^T\dot{x} + h_{xt} + {}^t\boldsymbol{\nu}^t c_{x^2}\dot{x} + {}^t\boldsymbol{\nu} c_{xt} - (-\dot{\boldsymbol{\lambda}} + {}^t h_{x^2}\dot{x} + h_{xt} + {}^t\boldsymbol{\nu}^t c_{x^2}\dot{x} + {}^t\boldsymbol{\nu} c_{xt}) = 0 \tag{A.30}$$

$$\dot{\boldsymbol{\lambda}} = -H_x \tag{A.31}$$

In its full form,

$$\dot{\boldsymbol{\lambda}}(t) = -\frac{\partial H(x,u,\boldsymbol{\lambda},t)}{\partial x} \text{ (Costate equations)} \tag{A.32}$$

Second line

$$H_u + {}^t\boldsymbol{\eta} d_u + {}^t h_{xu}\dot{x} + h_{ut} + {}^t\boldsymbol{\nu}^t c_{xu}\dot{x} + {}^t\boldsymbol{\nu} c_{ut} = 0 \tag{A.33}$$

In its full form,

$$\begin{gathered}\frac{\partial H(x,u,\boldsymbol{\lambda},t)}{\partial u} + {}^t\boldsymbol{\eta}(t)\frac{\partial d(u,t)}{\partial u} + {}^t\frac{\partial^2 h(x,u,t)}{\partial x \partial u}\dot{x}(t) + \frac{\partial^2 h(x,u,t)}{\partial u \partial t} + \\ {}^t\boldsymbol{\nu}^t\frac{\partial^2 c(x,u,t)}{\partial x \partial u}\dot{x}(t) + {}^t\boldsymbol{\nu}\frac{\partial^2 c(x,u,t)}{\partial u \partial t} = 0 \text{ (Stationary condition)}\end{gathered} \tag{A.34}$$

In the above equation, it is assumed that none of the variables are constrained. For cases where the control u is constrained the Pontryagin Maximum Principle can be used (appendix B), which provides more stringent conditions.

Third line

$$H_{\boldsymbol{\lambda}} - \dot{x} = 0 \tag{A.35}$$

$$\dot{x} = H_{\boldsymbol{\lambda}} \tag{A.36}$$

In its full form,

$$\dot{x}(t) = \frac{\partial H(x,u,\boldsymbol{\lambda},t)}{\partial \boldsymbol{\lambda}} = f(x,u,t) \text{ (State equations)} \tag{A.37}$$

The fourth and final line provides $d[u,t] = 0$ that is an know solution.

Proceeding to analyze Eqs. A.23 and A.24, as it can be seen, both equations are dependent of an infinitesimal variation, δt and δw. As a result two possible cases need to be consider for the initial and final conditions:

- Infinitesimal variations are present on time and/or states (free), $\delta t \neq 0 \to \{(\bar{q} + \bar{q}_{\dot{w}}\dot{w})\}|_{t_0}^{t_f} = 0$ and/or $\delta w \neq 0 \to \{\bar{q}_{\dot{w}}\}|_{t_0}^{t_f} = 0$; or

- Infinitesimal variations are not present on time and/or states (fix), $\delta t = 0 \to \{(\bar{q} + \bar{q}_{\dot{w}}\dot{w})\}|_{t_0}^{t_f} \neq 0$ and/or $\delta w = 0 \to \{\bar{q}_{\dot{w}}\}|_{t_0}^{t_f} \neq 0$; or

- Combination of both, the time can be free or fix in combination with some states been free and some fix.

As a result, Eqs. A.23 and A.24 are use to calculate the initial and final conditions for free time and the states. The full form of Eq. A.23 is,

$$\left\{\mathrm{H}-{}^{t}\boldsymbol{\lambda}\dot{\mathrm{x}}+{}^{t}\boldsymbol{\eta}\mathrm{d}+{}^{t}\mathrm{h}_{\mathrm{x}}\dot{\mathrm{x}}+\mathrm{h}_{\mathrm{t}}+{}^{t}\boldsymbol{\nu}^{t}\mathrm{c}_{\mathrm{x}}\dot{\mathrm{x}}+{}^{t}\boldsymbol{\nu}\mathrm{c}_{\mathrm{t}}-\left(-{}^{t}\boldsymbol{\lambda}+{}^{t}\mathrm{h}_{\mathrm{x}}+{}^{t}\boldsymbol{\nu}^{t}\mathrm{c}_{\mathrm{x}}\right)\dot{\mathrm{x}}\right\}\Big|_{\mathrm{t}_0}^{\mathrm{t}_\mathrm{f}}=0 \tag{A.38}$$

$$\left\{\mathrm{H}+{}^{t}\boldsymbol{\eta}\mathrm{d}+\mathrm{h}_{\mathrm{t}}+{}^{t}\boldsymbol{\nu}\mathrm{c}_{\mathrm{t}}\right\}\Big|_{\mathrm{t}_0}^{\mathrm{t}_\mathrm{f}}=0 \tag{A.39}$$

$$\left\{\begin{array}{l}\mathrm{H}(\mathrm{x_f},\mathrm{u_f},\boldsymbol{\lambda}_\mathrm{f},\mathrm{t_f})+{}^{t}\boldsymbol{\eta}(\mathrm{t_f})\mathrm{d}(\mathrm{u_f},\mathrm{t_f})+{}^{t}\frac{\partial\mathrm{h}(\mathrm{x_f},\mathrm{u_f},\mathrm{t_f})}{\partial\mathrm{t_f}}+{}^{t}\boldsymbol{\nu}^{t}\frac{\partial\mathrm{c}(\mathrm{x_f},\mathrm{u_f},\mathrm{t_f})}{\partial\mathrm{t_f}}=0\\ -\mathrm{H}(\mathrm{x_0},\mathrm{u_0},\boldsymbol{\lambda}_0,\mathrm{t_0})-{}^{t}\boldsymbol{\eta}(\mathrm{t_0})\mathrm{d}(\mathrm{u_0},\mathrm{t_0})+{}^{t}\frac{\partial\mathrm{h}(\mathrm{x_0},\mathrm{u_0},\mathrm{t_0})}{\partial\mathrm{t_0}}+{}^{t}\boldsymbol{\nu}^{t}\frac{\partial\mathrm{c}(\mathrm{x_0},\mathrm{u_0},\mathrm{t_0})}{\partial\mathrm{t_0}}=0\end{array}\right. \tag{A.40}$$

And the full form of Eq. A.24 is,

$$\{-\boldsymbol{\lambda}+\mathrm{h_x}+\boldsymbol{\nu}\mathrm{c_x}\}\big|_{\mathrm{t}_0}^{\mathrm{t}_\mathrm{f}}=0 \tag{A.41}$$

$$\left\{\begin{array}{l}-\boldsymbol{\lambda}(\mathrm{t_f})+\frac{\partial\mathrm{h}(\mathrm{x_f},\mathrm{u_f},\mathrm{t_f})}{\partial\mathrm{x_f}}+\boldsymbol{\nu}\frac{\partial\mathrm{c}(\mathrm{x_f},\mathrm{u_f},\mathrm{t_f})}{\partial\mathrm{x_f}}=0\\ \boldsymbol{\lambda}(\mathrm{t_0})+\frac{\partial\mathrm{h}(\mathrm{x_0},\mathrm{u_0},\mathrm{t_0})}{\partial\mathrm{x_0}}+\boldsymbol{\nu}\frac{\partial\mathrm{c}(\mathrm{x_0},\mathrm{u_0},\mathrm{t_0})}{\partial\mathrm{x_0}}=0\end{array}\right. \tag{A.42}$$

Note that the sign for the variables that come from the integral at "0" have opposite sign in accordance to Eq. A.10.

The variables in which $\delta\mathrm{t}|_0^\mathrm{f}=0$ and $\delta\mathrm{w}|_{\mathrm{t}_0}^{\mathrm{t}_\mathrm{f}}=0$ are called boundary conditions and Eqs. A.40 and A.42 are called transversality conditions.

In conclusion, the problem comprehends $2\mathrm{n}$ variables, n states and n costates, with $2\mathrm{n}$ ordinary differential equations, n for the states (Eq. A.32) $+$ n for the costates (Eq. A.37). To solve this system of equations it is necessary $2\mathrm{n}+2$ boundary condition, $2\mathrm{n}$ for the states and costates $+$ 2 for t_0 and t_f, which are given by defining the boundary condition, $\delta\mathrm{t}|_0^\mathrm{f}=0$ and $\delta\mathrm{w}|_{\mathrm{t}_0}^{\mathrm{t}_\mathrm{f}}=0$, and using the transversality conditions for free initial and final conditions, Eqs. A.40 and A.42. The m control variables follow the m equations provided by the stationary condition (Eq. A.34), or Pontryagin minimum principle as we will se further.

APPENDIX B

Pontryagin's Maximum Principle

Previously the optimal control condition was derived assuming that the functional and its functions are continuous, while this is true most of the time for the states and costates, it is not true for the controls in most cases.

Formulated in 1956 by Lev Semenovich Pontryagin, a Russian mathematician, the maximum principle (sometimes referred as the minimum principle) allows to find the optimal control direction (substituting the stationary conditions Eq. A.34) in problems with constraints on the states or controls.

A point x^* is a local minimum of the function f, Fig. B.1, if

$$\Delta f(x^*, \Delta x) = f(x^* + \Delta x) - f(x^*) \geqslant 0 \tag{B.1}$$

for small and admissible values of Δx

$$x^* = \begin{cases} x_1 \Rightarrow \Delta x > 0 \\ x' \Rightarrow \Delta x > 0 \text{ or } \Delta x < 0 \\ x_2 \Rightarrow \Delta x < 0 \end{cases} \tag{B.2}$$

Then, the differential of the function is

$$df(x, \Delta x) = f'(x)\Delta x \tag{B.3}$$

that has to satisfy the fundamental lemma of the Calculus of Variations $df(x^*, \Delta x) \geqslant 0$ for all admissible Δx.

Applying the above to the optimal control problem with constraints in the controls, described by the functional in Eq. A.13, results in the same variation shown in Eq. A.21. According to the fundamental lemma of the Calculus of Variations, $\delta \bar{J}(x^*, \Delta x) \geqslant 0$ for all admissible Δx. Therefore,

$$\delta \bar{J} = \{(\bar{q} - \bar{q}_{\dot{w}} \dot{w})\, \delta t + \bar{q}_{\dot{w}} \delta w\}\big|_{t_0}^{t_f} + \int_{t_0}^{t_f} \left\{ \bar{q}_w - \frac{d\bar{q}_{\dot{w}}}{dt} w \right\} \delta w \, dt \geqslant 0 \; \forall \delta w \text{ admissible} \tag{B.4}$$

The contour conditions remain unchanged

$$\{(\bar{q} - \bar{q}_{\dot{w}} \dot{w})\, \delta t + \bar{q}_{\dot{w}} \delta w\}\big|_{t_0}^{t_f} = 0 \tag{B.5}$$

$$\bar{q}_w - \frac{d\bar{q}_{\dot{w}}}{dt} = \begin{bmatrix} H_x + \dot{\boldsymbol{\lambda}} \\ H_u + {}^t\boldsymbol{\eta} d_u + {}^t h_{xu} \dot{x} + h_{ut} + {}^t\boldsymbol{\nu}{}^t c_{xu} \dot{x} + {}^t\boldsymbol{\nu} c_{ut} \\ H_{\boldsymbol{\lambda}} - \dot{x} \end{bmatrix} \tag{B.6}$$

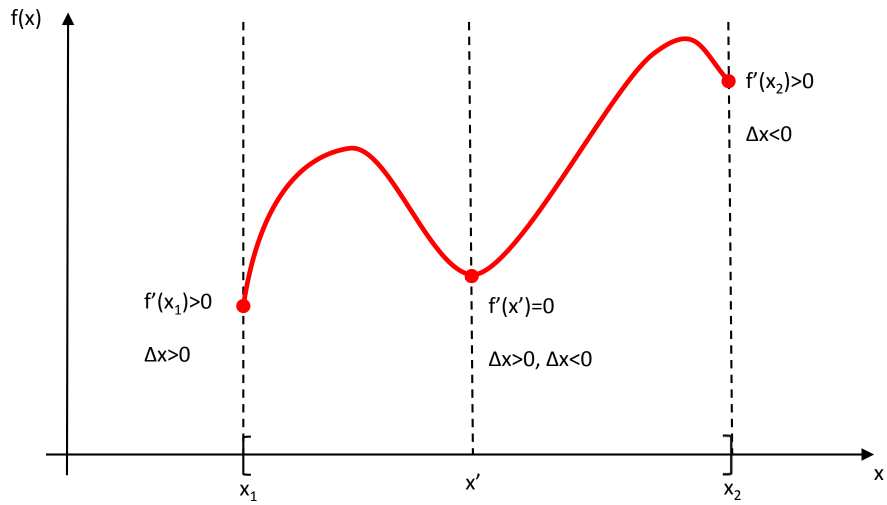

Figure B.1: Example of function minimization

Therefore,

$$\int_{t_0}^{t_f} \left\{ \left(-H_x + \dot{\lambda} \right) \delta x + \left(H_u + {}^t\eta d_u + {}^t h_{xu} \dot{x} + h_{ut} + {}^t \nu {}^t c_{xu} \dot{x} + {}^t \nu c_{ut} \right) \delta u \right. \\ \left. + \left(H_\lambda - \dot{x} \right) \delta \lambda \right\} dt \geqslant 0 \; \forall \delta x, \delta u \text{ and } \delta \lambda \text{ admissible} \tag{B.7}$$

for constraints on the controls, the previously derived equations for the states and costates remain the same,

$$\begin{cases} H_x + \dot{\lambda} = 0 \\ H_\lambda - \dot{x} = 0 \end{cases} \tag{B.8}$$

which results in

$$\int_{t_0}^{t_f} \left\{ \left(H_u + {}^t\eta d_u + {}^t h_{xu} \dot{x} + h_{ut} + {}^t \nu {}^t c_{xu} \dot{x} + {}^t \nu c_{ut} \right) \delta u \right\} dt \geqslant 0 \; \forall \; \delta u \text{ admissible} \tag{B.9}$$

since the value of the controls is constrained, it is sure to not be violated anywhere on the problem (boundary and path constraints, nor end and start point conditions). Therefore, it is possible to exclude these constraints from this derivation: $c(x_f, u_f, t_f, x_0, u_0, t_0) \to c(x_f, t_f, x_0, t_0)$, $d(u, t) = 0$ and $h(x_f, u_f, t_f, x_0, u_0, t_0) \to h(x_f, t_f, x_0, t_0)$; resulting in

$$\int_{t_0}^{t_f} \{ H_u \delta u \} \, dt \geqslant 0 \; \forall \; \delta u \text{ admissible} \tag{B.10}$$

for a first order approximation, similarly in what was done in Eq. A.18, the above integral is

$$\int_{t_0}^{t_f} \{ H_u \delta u \} \, dt \approx \int_{t_0}^{t_f} \{ H \} \Big|_{\delta u} dt \geqslant 0 \tag{B.11}$$

$$H|_{\delta u} = H[x^*, u^* + \delta u, \boldsymbol{\lambda}^*, t] - H[x^*, u^*, \boldsymbol{\lambda}^*, t] \geqslant 0 \tag{B.12}$$

Finally, the condition to be satisfied is

$$H[x^*, u^* + \delta u, \boldsymbol{\lambda}^*, t] \geqslant H[x^*, u^*, \boldsymbol{\lambda}^*, t] \tag{B.13}$$

for all $\delta u(t)$ admissible, $\forall\, t \in [t_0, t_f]$. Therefore, the maximum or in this case the minimum principle requires that the admissible controls are chosen in such a way to minimize the Hamiltonian at all points along its path.

APPENDIX C

Recipe for Setting the Optimal Control Problem

An optimal control problem can be set by using the equations derived in sections A.3 and B, as presented in the next steps.

1 Generate the desired cost function;

2 Add on the cost function the constraints related to path (states and controls) and the constrains related to the initial and final conditions (states and controls);

3 Obtain the problem's Hamiltonian utilizing Eq. A.12;

4 Obtain the equation of motion in state space representation utilizing the state equations, Eq. A.37;

5 Obtain the equation of the costates in state space representation utilizing the costate equations, Eq. A.32;

6 Obtain the optimal conditions on the use of the controls utilizing the stationary conditions, Eq. A.34, for unconstrained controls or the Pontryagin Maximum Principle, Eq. B.13, for constrained controls; and

7 Establish the contour conditions making use of Eqs. A.40 and A.42 for the non fix conditions.

The above steps will set and provide the optimal conditions for the control problem. With this, the problem is solve from the mathematical point of view. However, practical applications require the actual evolution of the states and control over time. This means the non-linear system of equations that provides the initial conditions of the problem needs to be solved and propagate over time. Such problems created by the set of non-linear equations are called Two Point boundary Value Problem and its solution is presented in chapter 5.5.1.

APPENDIX D

Addition of Midcourse Constraints

A midcourse constraint can be though as an extra set of variables on the problem that have to be taken into account in the optimal control solution. In this case, the extra set of conditions will be specific conditions for the state variables to be meet at a specific time.

Assuming for example the most demanding scenario where all the states and time have to meet certain conditions, $\mathrm{n}+1$ extra equations are needed, in addition to the $2\mathrm{n}+2$ equations defined at Appendix A, in order to solve the non-linear system of equations where the variables are the states and time at the initial, midcourse and final conditions. This generates a system with total of $3\mathrm{n}+3$ equations.

The optimal problem can be then describe by the optimal path from a set of possible initial conditions to a set of final conditions which meets the midcourse constraints during its path, Fig. D.1. The setting can be then simplify by separating the problem in two independent optimal problems, Fig. D.2. The cost of each problem can be described as,

$$\mathrm{J_{m^-0}(x,u,t) = h(x_m^-, u_m^-, t_m^-, x_0, u_0, t_0) + \int_{t_0}^{t_m^-} g(x,u,t)\,dt} \tag{D.1}$$

$$\mathrm{J_{fm^+}(x,u,t) = h(x_f, u_f, t_f, x_m^+, u_m^+, t_m^+) + \int_{t_m^+}^{t_f} g(x,u,t)\,dt} \tag{D.2}$$

In both cases the path conditions, $\mathrm{g(x,u,t)}$, remains the same. Nevertheless, it would be also possible to use two different path constraints with a similar derivation.

These to problems now have to be connected by its midcourse and the optimal condition that need to be solved for the entire path. This means that the cost function has to encompass both costs,

$$\begin{aligned}&\mathrm{J'(x,u,t) = J_{m^-0}(x,u,t) + J_{fm^+}(x,u,t)}\\&\mathrm{= h(x_m^-, u_m^-, t_m^-, x_0, u_0, t_0) + \int_{t_0}^{t_m^-} g(x,u,t)\,dt + h(x_f, u_f, t_f, x_m^+, u_m^+, t_m^+) + \int_{t_m^+}^{t_f} g(x,u,t)\,dt}\end{aligned} \tag{D.3}$$

as the states and the controls are required to be continuous the integral part can be rearranged to

$$\mathrm{\int_{t_0}^{t_m^-} g(x,u,t)\,dt + \int_{t_m^+}^{t_f} g(x,u,t)\,dt = \int_{t_0}^{t_f} g(x,u,t)\,dt} \tag{D.4}$$

also, as the two constants of the cost are simply vectors with the initial and end point conditions, they can be rewritten as

$$\mathrm{h(x_m^-, u_m^-, t_m^-, x_0, u_0, t_0) + h(x_f, u_f, t_f, x_m^+, u_m^+, t_m^+) = h'(x_f, u_f, t_f, x_m^+, u_m^+, t_m^+, x_m^-, u_m^-, t_m^-, x_0, u_0, t_0)} \tag{D.5}$$

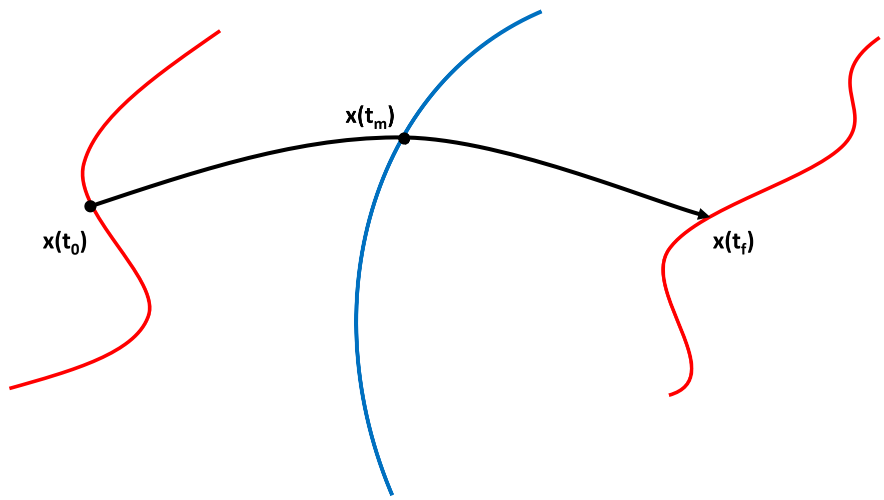

Figure D.1: Example of optimal control problem with midcourse constraints.

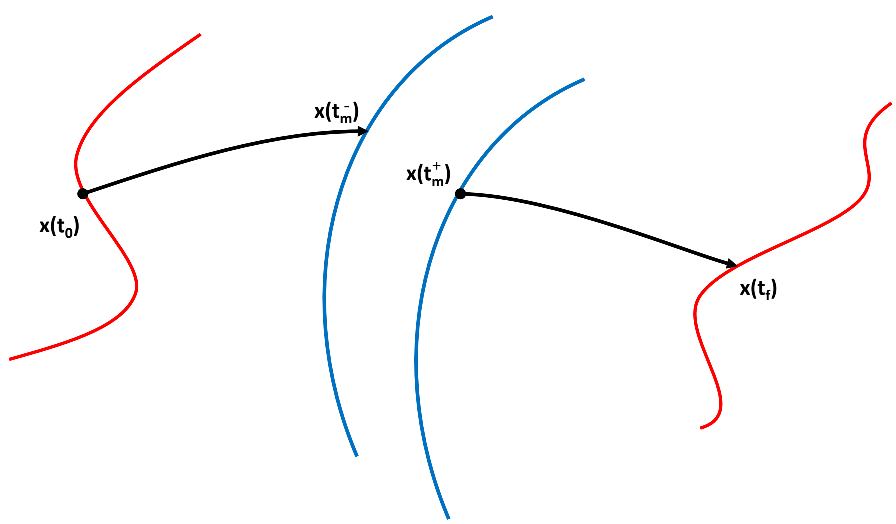

Figure D.2: Example on how to separate the optimal control problem with midcourse constraints.

Resulting in

$$J'(x,u,t) = h'(x_f,u_f,t_f,x_m^+,u_m^+,t_m^+,x_m^-,u_m^-,t_m^-,x_0,u_0,t_0) + \int_{t_0}^{t_f} g[x(t),u(t),t]\,dt \tag{D.6}$$

The above can be then derived as made in Appendix A. The extra variables will revert in extra $n+1$ transversality conditions coming from $\delta t_m \neq 0$ and $\delta x_m \neq 0$,

$$\begin{aligned} &\left\{-H - {}^t\eta d + h_t + {}^t\nu c_t\right\}\delta t_0 + \left\{H + {}^t\eta d + h_t + {}^t\nu c_t\right\}\delta t_m^- + \\ &\left\{-H - {}^t\eta d + h_t + {}^t\nu c_t\right\}\delta t_m^+ + \left\{H + {}^t\eta d + h_t + {}^t\nu c_t\right\}\delta t_f = 0 \end{aligned} \tag{D.7}$$

$$\begin{aligned} &\{\lambda + h_x + \nu c_x\}^t\delta x_0 + \{-\lambda + h_x + \nu c_x\}^t\delta x_m^- \\ &+ \{\lambda + h_x + \nu c_x\}^t\delta x_m^+ + \{-\lambda + h_x + \nu c_x\}^t\delta x_f = 0 \end{aligned} \tag{D.8}$$

Once more the sign of the variables that come from the integral at t_0 and t_m^+ are changed in accordance to Eq. A.10.

From previous results in Appendix A, the results associated with $\delta t_0 = 0$, $\delta t_f = 0$, $\delta x_0 = 0$ and $\delta x_f = 0$ are already known. Therefore, for a stationary cost the terms δt_m^- with δt_m^+, and δx_m^- with δx_m^+ have to cancel each other. Due to the continuity of the states and the controls, the values for h and d at t_m^- and t_m^+ have to be the same, $\left\{{}^t\eta d + h_t\right\}\big|_{t_m^-} + \left\{{}^t\eta d + h_t\right\}\big|_{t_m^+} = 0$ and $\{h_x\}|_{t_m^-} + \{h_x\}|_{t_m^+} = 0$. Moreover, the midcourse condition which is given by c is unique to both points, $c|_{t_m^-} = c|_{t_m^+} = c|_{t_m}$.

Therefore, Eqs. D.7 and D.8 become

$$\begin{cases} H|_{t_m^-} - H|_{t_m^+} + {}^t\nu c_t\big|_{t_m} = 0 \\ -\lambda|_{t_m^-} + \lambda|_{t_m^+} + \nu c_x|_{t_m} = 0 \end{cases} \tag{D.9}$$

The set of equations above define the $n+1$ extra equations required for solving the Two Point boundary Value Problem with midcourse conditions. Of course, it may be cases where not all the variables have to meet certain conditions; some variables can be let free to vary without fixing a particular condition. For such variables, the equations provided by the transversality conditions will not be used since they will be bound by the Euler-Lagrange equations. Generating, then, a problem with less unknowns which requires less equations to solve the non-linear system.

Appendix E

Proof of the Fundamental Lemma of the Calculus of Variations

There are different proofs of the fundamental lemma of the calculus of variations, perhaps one of the most simple is the proof by contradiction. Assume that x^* is an extremal and $\delta J(x^*, \delta x) \neq 0$. It can be shown that, under this hypothesis, the increment of $\Delta J(x, \delta x)$ can change its sign in a arbitrarily small vicinity of x^*.

By definition,

$$\Delta J(x^*, \delta x) = \delta J(x^*, \delta x) + \delta J(x^*) = \delta J(x^*, \delta x) + g(x^*, \delta x)\|\delta x\| \tag{E.1}$$

where, $g(x^*, \delta x) = 0$ with $\|\delta x\| \to 0$.

If $\|\delta x\| < \varepsilon$ with ε sufficient small, Eq. E.1 is dominated by $\delta J(x^*, \delta x)$. Consider now a variation $\delta x = \varsigma$ in such a way that $\|\varsigma\| < \varepsilon$ and $\delta J(x^*, \varsigma)$. As δJ is linear,

$$\delta J(x^*, -\varsigma) = -\delta J(x^*, \varsigma) > 0 \tag{E.2}$$

Once the signal of ΔJ follows the signal of δJ, in the vicinity considered here, it can be concluded that the increment of a functional can change its signal in a vicinity arbitrarily small of x^*, which contradicts the definition of an extremal.

Appendix F

Asteroid Selection Results

Table F.1: Asteroid selection IDs from chapter 5

Rank	Phaethon case	Itokawa case	Rank	Phaethon case	Itokawa case
1	2006 QJ65	1998 HK49	36	2012 BC62	2009 EW
2	2009 ET	(136795) 1997 BQ	37	2012 VK76	(154029) 2002 CY46
3	2000 ED14	2005 GB34	38	2007 BY48	2012 MR7
4	2011 EK	1992 SZ	39	2012 RJ15	2006 BA
5	2007 DJ	2007 YQ56	40	(276049) 2002 CE26	2004 BG86
6	1999 FR19	(4775) Hansen	41	1992 BC	2006 MY13
7	2013 SM24	2010 JH3	42	2012 YP6	2002 CU46
8	2010 EG21	2006 HU50	43	2007 BC8	2007 RQ133
9	2009 UD	2012 DS32	44	2010 NM	2000 WL63
10	2005 VY3	2008 GA4	45	2006 BJ55	2009 YF
11	2003 YO3	2005 VE	46	2006 WL3	2011 UJ169
12	2013 CZ87	2009 BC11	47	2003 QW30	(152931) 2000 EA107
13	(141593) 2002 HK12	(10165) 1995 BL2	48	2012 FC71	2009 HK73
14	2009 OW6	2008 GY21	49	(138359) 2000 GX127	2012 LA11
15	2011 EO11	2008 WY94	50	2008 EF32	(367943) 2012 DA14
16	2013 TG135	2007 FT3	51	2007 EZ	2000 SG344
17	2010 VM139	(172425) Taliajacobi	52	2009 FJ1	2009 SL2
18	2007 XA23	2006 AN	53	2012 WQ10	2002 MT3
19	2008 TD	2013 GE55	54	2011 TP6	2002 CT118
20	2011 UX275	1998 WB2	55	2004 FE4	2005 UH5
21	2007 EY25	2012 MN2	56	2010 FX9	2011 JN5
22	2006 UY64	2010 HX107	57	2009 VN1	2002 AC29
23	(310442) 2000 CH59	(288592) 2004 JW20	58	2010 TN167	2009 PA3
24	2004 ER21	(217430) 2005 SN25	59	2005 WZ55	(100004) 1983 VA
25	2012 AT22	2001 BB16	60	2010 CN	2012 AB11
26	2005 EU2	2011 QF23	61	2010 TD55	2009 UD2
27	2010 VQ98	2011 LL2	62	2010 FT9	(152770) 1999 RR28
28	2008 EJ85	2004 HQ1	63	2007 UT	2000 ED14
29	2005 NB56	1998 GC1	64	2009 QJ2	2001 RV17
30	2007 EF	2011 SC25	65	2010 TK55	2006 MD12
31	2013 FM9	2007 UH	66	2010 RQ64	(369984) 1998 QR52
32	2010 VB99	1997 YM9	67	2004 QG13	2001 WW1
33	2009 FX10	(25330) 1999 KV4	68	2006 FW	2007 EV
34	2004 FH29	2004 RY109	69	2005 EJ225	2003 GD42
35	2005 CK	2000 RE52	70	2011 GM44	2013 SG25

continued

Rank	Phaethon case	Itokawa case	Rank	Phaethon case	Itokawa case
71	2004 TD10	(152563) 1992 BF	114	(180186) 2003 QZ30	2008 XQ2
72	2006 OT9	(68216) 2001 CV26	115	(235756) 2004 VC	2012 LU
73	2013 AR72	2007 DG8	116	2011 PS	2007 EO88
74	2009 WS25	2008 EB8	117	2007 WE	2008 CS1
75	2003 WP7	(137078) 1998 XZ4	118	2007 TD	2013 PG10
76	2010 VR	2005 MO13	119	2012 FX13	2010 EF43
77	2004 JO20	2007 MF	120	2010 EB43	2008 AU28
78	2010 TE	2009 PQ1	121	2003 YO1	(307161) 2002 DY3
79	2007 XB23	2009 VZ51	122	2006 YF13	2009 HE60
80	2002 PR1	2009 KR4	123	2007 VZ137	2010 RM82
81	2008 SU1	2011 GC55	124	2007 BX48	2002 TA60
82	2010 SO16	2005 YR3	125	2008 AU28	2002 XT90
83	2008 SD85	2011 GJ44	126	2013 RH74	2009 UK20
84	2011 FS2	2010 VH1	127	2010 XF3	2013 TN127
85	2006 VQ13	(90403) 2003 YE45	128	2003 QK5	2011 SP68
86	2010 AO60	(216258) 2006 WH1	129	2004 QJ7	2006 AK8
87	2004 RX164	(325102) 2008 EY5	130	2008 CC175	2006 TU7
88	2003 YN1	2013 EN20	131	2006 CT9	2008 EQ
89	2011 SS25	(136818) Selqet	132	2002 VR14	(303450) 2005 BY2
90	(315098) 2007 EX	2000 WG10	133	2004 DK1	2008 LW16
91	2012 SZ2	2012 MF7	134	2011 SE25	2013 ON5
92	2009 WM6	2010 UJ	135	2001 TC45	2006 QQ56
93	(143649) 2003 QQ47	2007 UY1	136	2002 CR11	2013 KT1
94	2002 XB	2010 PQ10	137	(164121) 2003 YT1	2006 SP131
95	2010 JR34	2010 HW20	138	2011 YC29	2005 ET95
96	2006 SY5	2011 AB3	139	2012 VK6	2007 HW3
97	2011 ER74	2013 RX80	140	2013 TR4	2011 CF66
98	2012 LU	2006 OE10	141	2000 TU28	2004 MP7
99	2007 TH71	2004 TB10	142	2008 JW2	2007 EN26
100	2009 TQ	2006 FC35	143	2008 EY68	2010 FA81
101	1995 DW1	2010 VB	144	2011 SA25	2006 BB8
102	2011 WL2	(196625) 2003 RM10	145	2009 TB	2009 HX51
103	2013 BP15	2011 FS9	146	(152754) 1999 GS6	2011 UP20
104	(155110) 2005 TB	2003 OC3	147	(175921) 2000 DM1	2007 UU3
105	2012 FS35	(230111) 2001 BE10	148	2008 CJ	2008 AG33
106	1992 YD3	2008 HZ1	149	2011 YJ6	1994 UG
107	2006 WX3	2011 BP24	150	2006 SP131	2007 YO56
108	2007 VW7	2000 WH10	151	(163697) 2003 EF54	2005 QR173
109	2008 YF3	2011 US91	152	2007 GU4	2008 AF32
110	2011 GC3	(162162) 1999 DB7	153	2013 EO89	2001 VC2
111	1998 FN9	1999 VN6	154	2010 AL60	2003 FY6
112	2013 EQ	2007 CM26	155	2011 EB12	2006 QL33
113	2011 AA37	2009 TK8	156	2007 AA2	(162510) 2000 QW69

continued

Rank	Phaethon case	Itokawa case	Rank	Phaethon case	Itokawa case
157	2004 HQ1	2012 DZ	200		2004 RQ252
158	(363067) 2000 CO101	2010 WS	201		(361754) 2007 YV29
159	2008 CX118	2007 EG	202		2004 BE11
160	1996 RY3	2008 UB95	203		2010 KA8
161	2003 XB22	2008 RG1	204		2004 BB75
162	2009 CB3	(1620) Geographos	205		(68372) 2001 PM9
163	2012 GA12	2008 CL1	206		1991 GO
164	2011 EK47	2010 SJ15	207		2003 AS42
165	2005 YS165	2008 DH23	208		2012 HZ33
166	2005 YU128	2012 HL31	209		2006 QB31
167		(369986) 1998 SO	210		2004 RY164
168		2012 HS15	211		2008 DF5
169		2008 UC7	212		2013 ER89
170		2011 OL5	213		2008 FX6
171		2010 DH	214		2013 HU14
172		2013 ET	215		2000 WM63
173		2005 GO59	216		2008 FL7
174		2009 FK	217		2006 DQ14
175		2013 BP15	218		2003 UF22
176		2002 BG	219		2005 GZ128
177		2010 EN44	220		2010 FT
178		2009 SB15	221		2010 JW34
179		2003 KM11	222		2001 EC16
180		2010 TB54	223		2011 HN24
181		(162687) 2000 UH1	224		2008 QV11
182		2010 VB1	225		2008 SS
183		2002 MN	226		2004 FH
184		2000 FP10	227		2006 SY217
185		(163023) 2001 XU1	228		2008 EJ85
186		2011 EB74	229		(138359) 2000 GX127
187		(11885) Summanus	230		2011 CA7
188		2010 VZ139	231		2011 XZ2
189		2011 YA29	232		(173561) 2000 YV137
190		(180050) 2003 BR21	233		1994 GL
191		2009 WQ6	234		2003 UG22
192		1990 SM	235		(307070) 2002 AV31
193		2001 TC45	236		2007 RZ19
194		2004 TD18	237		2003 OE11
195		(30997) 1995 UO5	238		2011 BE24
196		2007 UC6	239		2005 TF49
197		2009 SU171	240		2007 EG88
198		2006 FH36	241		2006 FK
199		2010 TN167	242		(350964) 2003 BT35

continued

Rank	Phaethon case	Itokawa case
243		2008 NS1
244		2008 EJ1
245		2013 PY38
246		(154658) 2004 FA18
247		2011 CG2
248		2005 FJ
249		2009 FJ
250		2010 XA24
251		2008 TF
252		2012 CN2
253		2003 OA3
254		(276891) 2004 RH340
255		2008 WN2
256		2008 SH82

Table F.2: Asteroid selection IDs from chapter 6

Rank	Earth-to-Phaethon leg	Phaethon-to-Earth leg	Rank	Earth-to-Phaethon leg	Phaethon-to-Earth leg
1	1999 FR19	2011 SO189	26	2011 EK	2013 ER4
2	2010 VB99	2008 GM2	27	2007 XA23	2002 SP
3	2003 YN1	2009 FU23	28	2012 VK76	2013 FW13
4	2013 CZ87	2012 HG2	29	2009 TQ	2004 NK8
5	2005 VY3	(162385) 2000 BM19	30	2004 JO20	2013 SR19
6	2013 SM24	2010 WH1	31	2012 EK8	2011 YU74
7	2004 QG13	2004 XN14	32	2007 UT	2007 VU6
8	2004 ER21	1993 DA	33	(143649) 2003 QQ47	2002 LT38
9	2011 EO11	2007 JZ2	34	2012 VU76	2011 CX46
10	2006 UY64	2008 YC3	35	(310442) 2000 CH59	2003 HG2
11	2004 TD10	2012 KE25	36	2011 GM44	1997 AC11
12	2000 ED14	2010 VQ98	37	2003 TL4	2003 WT153
13	2012 BC62	2010 RO80	38	2011 TP6	2012 FC71
14	2010 RQ64	2006 PY17	39	2010 TN167	2010 SO16
15	2010 EG21	2006 BQ6	40	2007 EZ	(281375) 2008 JV19
16	2011 AA37	2013 JP4	41	2005 NB56	2002 VZ91
17	2009 UD	2010 XL	42	2007 DJ	2009 HE60
18	2011 SS25	2000 BE19	43	2004 FH29	2008 SJ148
19	2007 BC8	2007 XB23	44	2006 WL3	2006 WX1
20	2012 WQ10	2003 EW59	45	1995 DW1	2012 WR10
21	2011 UX275	2007 EV	46	2010 RD	2013 ED68
22	2012 AT22	2005 VE7	47	2011 FS2	2005 ER70
23	2005 EU2	1998 FF14	48	2009 OW6	2012 AF3
24	2004 HL	2002 XS90	49	2005 EJ225	2012 KX41
25	(180186) 2003 QZ30	2013 BR27	50	2008 CC175	2005 CN

continued

Rank	Earth-to-Phaethon leg	Phaethon-to-Earth leg	Rank	Earth-to-Phaethon leg	Phaethon-to-Earth leg
51	2007 EF	2010 JA35	94	2002 CR11	(329275) 1999 VP6
52	2008 SD85	2009 WB54	95	2005 TA	(138127) 2000 EE14
53	2007 XB23	1999 VX25	96	2010 FT9	2012 BB14
54	2008 CX118	2007 WV3	97	1998 FN9	2013 GU66
55	2003 QW30	2013 RL43	98	2002 JW15	2012 UC34
56	1992 YD3	2008 WM	99	2006 QJ65	1998 DK36
57	2010 VQ98	2009 WK6	100	2008 EF32	2008 EP6
58	2010 FX9	2011 UR63	101	2010 SJ	2012 BT1
59	2001 SZ169	2010 SE	102	2008 EJ85	2009 BK2
60	2007 TH71	2000 BO28	103	(303933) 2005 VQ	2000 YS134
61	2004 BB	2001 VC76	104	2011 ER74	2011 AM24
62	2012 UF	2008 UA202	105	2002 PR1	2010 WF3
63	2004 FE4	(354182) 2002 DU3	106	1997 CD17	2003 QC10
64	1992 BC	2001 SQ3	107	2010 TK55	2004 XD51
65	2006 OT9	2013 BC74	108	(315098) 2007 EX	2001 YM2
66	2011 PK10	2012 EO3	109	2006 UL	2009 BW2
67	2010 TE	2011 YW10	110	2010 XO10	2002 VR14
68	2006 VQ13	2002 XT90	111	2010 JR34	2006 YM
69	2009 QJ2	2001 TD	112	2011 SC16	2004 HM
70	2013 NX	2011 UP63	113	2003 BN4	2004 XJ29
71	2009 ET	2006 OC5	114	(309662) 2008 EE	(337075) 1998 QC1
72	2007 EY25	(12538) 1998 OH	115	2003 SW130	2011 GD3
73	2003 WP7	2007 SQ6	116	2007 BY48	2010 VD72
74	2013 SQ19	2008 EE85	117	2011 GJ44	2003 DW10
75	2008 UE7	2012 GE	118	2004 TA1	2006 HE2
76	2003 XV	2006 QQ23	119	2013 JF1	(303450) 2005 BY2
77	2010 AO60	2010 NM	120	2007 TD	2008 JP24
78	2011 SE25	2009 QJ6	121	(199003) 2005 WJ56	(357022) 1999 YG3
79	2013 ER89	1996 TD9	122	2010 NM	2009 WR25
80	2009 WS25	2006 WE4	123	2013 SK20	2011 EC
81	2008 UA92	2011 BP40	124	2003 QK5	2010 WT8
82	2011 SL173	2008 YZ28	125	2010 TD55	2008 UE7
83	2012 HB2	(267940) 2004 EM20	126	2007 HC	2012 RJ15
84	2010 TB54	(309662) 2008 EE	127	2002 TB70	2011 GP44
85	2010 CN	2010 LR33	128	2013 AE53	2009 BG11
86	2009 SX17	1998 MV5	129	2011 DW	2001 FA58
87	2013 FM9	2009 RH	130	2012 LU	2007 WZ4
88	2004 RX164	1998 XN2	131	2007 UB2	2013 JH14
89	2008 AU28	2009 JR5	132	(137199) 1999 KX4	2012 VU76
90	2003 SM84	2013 TV132	133	1996 FT1	2010 VK
91	2012 FC71	2013 AB32	134	2012 FS35	2004 AD1
92	2013 TG135	2009 KN4	135	2013 TK4	2007 TL15
93	2007 SQ6	(162463) 2000 JH5	136	2012 WR3	(308242) 2005 GO21

continued

Rank	Earth-to-Phaethon leg	Phaethon-to-Earth leg	Rank	Earth-to-Phaethon leg	Phaethon-to-Earth leg
137	1997 WB21	(322756) 2001 CK32	180	(235756) 2004 VC	2012 SR56
138	2007 VR183	2010 GX23	181	2007 TF68	2004 FX1
139	2008 UA202	2005 SO1	182	2004 DK1	2007 RS1
140	2007 TF15	2007 YZ	183	2009 VN1	2006 TB7
141	2012 PB20	2010 RF31	184	2009 VA26	2010 CD55
142	2009 DS43	(192563) 1998 WZ6	185	2002 VX91	2005 TS15
143	2009 DC1	(90403) 2003 YE45	186	2012 FX13	2013 RY5
144	2011 WL2	(206910) 2004 NL8	187	1999 KL1	(323300) 2003 UD22
145	2007 BX48	2010 XR69	188	2005 CN	2012 TP231
146	2013 FQ10	2002 GR	189	2002 AO11	2006 WP3
147	(141593) 2002 HK12	2004 YC	190	2001 LD	2009 EU
148	(155110) 2005 TB	2010 CK19	191	2009 HE60	2011 HC36
149	2013 FD8	2011 MQ3	192	2001 YC1	2001 SZ169
150	2012 EA12	2010 LE15	193	(308242) 2005 GO21	2002 HP11
151	2012 SZ2	2013 RO5	194	2012 DY32	2005 TH50
152	2009 UL20	2008 AF3	195	2000 TU28	2011 WB39
153	(137158) 1999 FB	2007 FA	196	2006 WX3	2007 RN133
154	2008 YF3	2002 XY38	197	2012 FR1	2012 HN
155	1999 NW2	2010 OA1	198	1998 FL5	2013 CZ87
156	2012 TY52	2009 JR	199	2012 FU35	2006 SY5
157	2013 EO20	(277830) 2006 HR29	200	2006 SP131	2010 XK
158	2009 UR5	2006 UN	201	2000 EZ106	2012 BZ1
159	2009 FJ1	2008 TN26	202	2005 TK50	2007 EF
160	2007 VZ137	2006 DQ14	203	2013 EB	2011 OR15
161	2010 EB43	2005 QP87	204	2011 SK189	2012 RR16
162	2010 XO	2008 QU3	205	1999 TT16	2002 MN
163	2010 GP67	(367789) 2011 AG5	206	2005 BO1	2010 RM82
164	2011 GC3	2004 OW10	207	2010 AF30	2008 PW4
165	2013 EQ	(163067) 2002 AP3	208	2006 EC	2013 TG
166	2007 VW7	2011 TH5	209	2008 CJ	2008 CE119
167	2007 YF	2012 XA133	210	2007 VU6	2009 HZ67
168	2004 QJ7	2007 EK	211	2013 AR27	2010 FK
169	2008 CC71	(172034) 2001 WR1	212	2006 YF13	2013 TQ5
170	2012 CP46	2009 DO111	213	(152754) 1999 GS6	2009 HV2
171	2011 PS	2012 VR76	214	2011 GE62	2012 TP20
172	2004 YR	2006 WV1	215	2011 FV9	2009 KT4
173	2010 CJ18	2005 OE3	216	2001 WW1	2004 FK2
174	2006 CT9	2011 AB37	217	2005 YS165	2008 WN2
175	2002 XS40	2004 US1	218	2009 DO111	2007 AA2
176	2011 AK5	2013 ER89	219	2012 VQ6	2012 UX27
177	2008 GW20	2011 FS2	220	2010 TS149	2008 HU4
178	2007 DM41	2005 CL7	221	2011 EB12	2010 DW1
179	2011 YC29	2004 QO5	222	2004 QZ1	(99907) 1989 VA

continued

Rank	Earth-to-Phaethon leg	Phaethon-to-Earth leg	Rank	Earth-to-Phaethon leg	Phaethon-to-Earth leg
223	2011 SA25	2012 XP134	266		2012 FP52
224	2011 FV6	(341843) 2008 EV5	267		2009 PQ1
225	2008 YV32	2011 AR26	268		2013 JF1
226	2008 EY68	2009 UU1	269		2009 BA11
227	2000 JZ8	2005 ND63	270		1998 WP7
228	(164121) 2003 YT1	2007 VB138	271		2011 UT63
229	2002 VR14	(329437) 2002 OA22	272		2002 PY39
230	2009 TB	2013 AX60	273		2009 DJ46
231	2001 QE71	2002 VX91	274		(163364) 2002 OD20
232	(367248) 2007 MK13	2009 HE	275		2002 GO5
233	2005 BU	2009 UG	276		2009 RZ3
234	2009 SG2	2009 WM6	277		2011 UT91
235	2013 GQ38	2002 FB	278		2006 BL8
236	2012 HP13	1999 SH10	279		2005 BM1
237	2008 CK119	2012 ML6	280		2009 SJ
238	2008 HD3	2008 HB38	281		2005 LQ40
239	2011 PU1	2005 GB120	282		2008 DC
240	2011 YJ6	(367248) 2007 MK13	283		2001 RU17
241	2006 FL10	2007 VV83	284		2010 GV23
242	2007 LE	2011 YH40	285		2005 NB7
243	2007 GU4	2013 GH66	286		2012 HN1
244	2001 TC45	2005 TD	287		2007 BG
245	2007 CT26	2008 CD70	288		2009 VN1
246	2001 YR3	(10115) 1992 SK	289		2004 YG1
247	2009 DT43	2012 SJ58	290		2010 UJ
248	2003 MS2	2007 RF1	291		2000 WQ148
249	2013 RB6	2007 UD6	292		2011 YE40
250	2012 AC3	2009 WM105	293		2013 RO30
251	2011 EH17	2007 HD15	294		2006 QB31
252	2009 HM82	2010 RY3	295		2013 RM43
253	2012 FU62	2003 FY6	296		2011 SC16
254		2005 LD	297		2008 FW6
255		(301844) 1990 UA	298		2011 CK50
256		1996 BG1	299		(162694) 2000 UH11
257		2010 AB78	300		2012 TR5
258		2009 FX4	301		(68950) 2002 QF15
259		2013 TF6	302		2007 GF
260		(68267) 2001 EA16	303		2010 VU98
261		2013 QF11	304		2006 YC13
262		2003 BS35	305		2007 XA23
263		2012 DL4	306		2004 ST2
264		2005 YU128	307		2007 YQ56
265		2013 TR5	308		2005 GP21

continued

Rank	Earth-to-Phaethon leg	Phaethon-to-Earth leg	Rank	Earth-to-Phaethon leg	Phaethon-to-Earth leg
309		2007 CM26	352		2006 SF281
310		2010 SU15	353		2011 UB276
311		(138258) 2000 GD2	354		2008 UV5
312		2012 HD20	355		2011 ON24
313		2011 GP65	356		2013 NX
314		(189040) 2000 MU1	357		2007 YJ
315		2009 SS	358		2013 EX89
316		2010 NK1	359		2010 MB
317		2012 EB	360		2005 UO
318		2009 SJ18	361		2010 PJ9
319		(162080) 1998 DG16	362		2012 RG15
320		2012 BS23	363		2011 SC108
321		2012 SL50	364		2012 EA12
322		2012 XQ2	365		2010 SD
323		2010 GD35	366		2011 GE3
324		2008 UB92	367		2007 RQ133
325		2006 GC1	368		(326388) 2001 QD96
326		2005 CN61	369		2008 LW16
327		2012 EB2	370		2011 GD
328		2009 CP5	371		1999 RJ33
329		2010 XZ72	372		2007 FB
330		2011 OB26	373		2011 DS
331		2012 TF79	374		2008 YQ27
332		2002 AN129	375		2010 KV7
333		2010 RA12	376		(258325) 2001 VB2
334		2011 SG5	377		2008 BD15
335		1994 XL1	378		2013 FK
336		2012 BW13	379		2011 UC292
337		2013 EV89	380		2004 XG29
338		2013 SM20	381		2009 DE1
339		2000 UR16	382		2013 RG74
340		(162679) 2000 TK1	383		2013 JK22
341		2012 QG42	384		2007 XH16
342		2009 VQ	385		2011 EC12
343		2004 SB56	386		2011 CD66
344		2013 TN4	387		2007 RY19
345		2012 DZ13	388		2002 FS6
346		2008 DF5	389		2009 ME9
347		2012 BA62	390		2007 SV1
348		2012 DQ8	391		2005 GQ33
349		2011 UX275	392		2005 EA
350		(164211) 2004 JA27	393		(89958) 2002 LY45
351		2004 FU162	394		2002 TA67

continued

Rank	Earth-to-Phaethon leg	Phaethon-to-Earth leg	Rank	Earth-to-Phaethon leg	Phaethon-to-Earth leg
395		2008 OV2	438		2007 RX8
396		2005 ER95	439		2010 XA24
397		2011 GM44	440		2005 SY70
398		2006 BJ55	441		2004 CO49
399		2011 JY1	442		2007 LS
400		2013 EY27	443		2010 VO21
401		2013 EQ4	444		2002 EV
402		2009 AC16	445		2011 GL44
403		2011 ES4	446		2009 SH15
404		2011 DD5	447		2011 GE2
405		2011 YT62	448		2008 WP2
406		2002 JR100	449		2010 MY112
407		1995 DW1	450		2005 ES1
408		1999 VW25	451		2010 CD19
409		2005 WD	452		2009 TS7
410		2013 TT5	453		2010 CM19
411		(302830) 2003 FB	454		2013 BS15
412		2010 DA	455		2001 RB12
413		2013 FD8	456		2010 HX107
414		2011 CQ1	457		2009 CD2
415		2000 HO40	458		2008 GE128
416		2012 WG	459		2013 QP48
417		2012 BD14	460		2002 NX
418		2007 UT3	461		2005 KA
419		(189008) 1996 FR3	462		(137170) 1999 HF1
420		1994 AW1	463		2013 QE16
421		2006 EY	464		2006 KL21
422		2005 VL1	465		2011 SK16
423		2009 AM15	466		2013 AJ91
424		2006 AN	467		2004 RO111
425		1993 HC	468		2010 XO56
426		2007 UH	469		2002 LE31
427		2007 JX2	470		2010 BB
428		2001 QM163	471		2012 XM55
429		2010 XC25	472		2008 TE2
430		2010 TK	473		2001 OT
431		2010 CO1	474		2008 DL4
432		2006 UA216	475		(141079) 2001 XS30
433		(311554) 2006 BQ147	476		(357622) 2005 EY95
434		2007 TJ15	477		1994 UG
435		2008 YH30	478		2012 UY68
436		2007 RS146	479		2003 JO14
437		2001 SY269	480		2003 QW30

continued

Rank	Earth-to-Phaethon leg	Phaethon-to-Earth leg	Rank	Earth-to-Phaethon leg	Phaethon-to-Earth leg
481		1994 GL	524		2007 FY20
482		2010 VT21	525		2009 JO2
483		2009 SJ1	526		2013 TG135
484		2005 UQ64	527		2002 AY1
485		2004 PU42	528		2005 EG169
486		2013 LB	529		2002 RR25
487		2011 UQ20	530		2003 QH5
488		2009 FW25	531		2008 UN3
489		2005 HD4	532		2011 AN4
490		2008 VF	533		2008 TB2
491		1999 TY2	534		2012 XL16
492		2005 NB56	535		2010 DG1
493		2003 YN1	536		2013 HM11
494		2012 XO55	537		2005 RB3
495		2009 HC	538		2011 SC25
496		2012 SW2	539		2011 WU74
497		2012 RH10	540		2009 EF1
498		(301011) 2008 JO	541		2003 CO20
499		1998 SD9	542		2006 QN111
500		2007 MC4	543		2008 UT95
501		2012 CR45	544		1993 UD
502		1999 SJ10	545		2007 EN26
503		2009 WS52	546		2012 BC77
504		(254417) 2004 VV	547		2008 TF2
505		2013 NJ10	548		2013 FX7
506		2004 SS26	549		2003 TR9
507		2008 FO	550		2011 EW73
508		2013 RE36	551		(162269) 1999 VO6
509		2010 XA73	552		2004 MO3
510		2001 ED18	553		2013 GF23
511		2004 SU55	554		2005 VE
512		2008 ST7	555		(138359) 2000 GX127
513		1998 SU4	556		2005 ET95
514		2007 VB188	557		2009 WM8
515		2002 NW16	558		2009 FD
516		2008 LC2	559		2008 WH96
517		2004 LO2	560		2010 EN44
518		2004 PB97	561		2007 DE8
519		2013 KP1	562		2008 KA6
520		2012 TS5	563		2011 MB2
521		2013 BR18	564		2005 QA5
522		2010 XO	565		2012 UU158
523		2005 EV95	566		2009 WZ104

continued

Rank	Earth-to-Phaethon leg	Phaethon-to-Earth leg	Rank	Earth-to-Phaethon leg	Phaethon-to-Earth leg
567		2000 SZ162	610		2004 FY15
568		2012 FQ35	611		2010 QN1
569		2009 TD8	612		2012 VN82
570		2009 TJ4	613		2012 BL11
571		2005 EZ223	614		(192559) 1998 VO
572		2009 SO98	615		2007 RO17
573		1999 FP19	616		2010 TV54
574		2010 VM65	617		2004 SW26
575		1998 VD32	618		2001 QC34
576		2013 EL89	619		2012 SL8
577		2011 SE25	620		2009 WC54
578		2004 KB	621		2011 LT17
579		2012 YD7	622		2012 DJ61
580		2010 TL167	623		2008 LH2
581		2012 AB11	624		2008 CT1
582		2007 CB27	625		2003 FB5
583		2004 FJ29	626		2004 CQ
584		2007 RJ1	627		2013 QB11
585		2008 OM8	628		2013 EU9
586		2003 AS42	629		(278381) 2007 MR
587		2009 SR171	630		2006 VQ13
588		2011 GP59	631		2010 GA7
589		2008 EP	632		2005 EJ225
590		2008 CM20	633		2008 SG148
591		(242708) 2005 UK1	634		2007 EC
592		2004 BG86	635		(154269) 2002 SM
593		(136818) Selqet	636		2011 EB12
594		2012 BG11	637		2010 RE
595		(4544) Xanthus	638		2012 FX35
596		(1943) Anteros	639		2011 CR1
597		1999 PS3	640		2012 PB20
598		2012 DO	641		2011 GZ2
599		2009 UD	642		2002 VV17
600		2004 JX20	643		2012 FX13
601		(163697) 2003 EF54	644		2012 DM4
602		(159402) 1999 AP10	645		2007 HA
603		(260277) 2004 TR12	646		2012 CM2
604		2005 ES70	647		2008 YK2
605		2013 AX52	648		2004 LB1
606		2013 EA	649		2009 ST104
607		2013 SE21	650		2004 BE86
608		2009 WG54	651		2011 EU73
609		2013 SR	652		2008 UV

continued

Rank	Earth-to-Phaethon leg	Phaethon-to-Earth leg
653		2010 UL8
654		2013 EP89
655		2011 UY114
656		2004 FM17
657		2009 BD
658		2010 TK7
659		2008 XL1
660		2012 RN15
661		2012 FV35
662		2008 UG7
663		2009 QZ34
664		2006 YF
665		2012 PC20
666		2010 AC3
667		2012 QO10
668		2013 GT66
669		2009 SN
670		2009 WF104
671		2007 RY8
672		2006 EK53
673		(101955) Bennu
674		2011 BN24
675		2012 BO123
676		2005 JU81
677		(238063) 2003 EG
678		2005 BT1
679		2002 LW
680		(235700) 2004 TR13
681		2012 EH5
682		2012 FY13
683		2005 ET2
684		2000 WM63
685		2008 DL5
686		(13651) 1997 BR
687		1998 SB15
688		(53550) 2000 BF19
689		2012 DO8